

The s-Process in Low Metallicity Stars.

II. Interpretation of High-Resolution Spectroscopic Observations with AGB models.

S. Bisterzo^{1*}, R. Gallino^{1,2}, O. Straniero², S. Cristallo³ and F. Käppeler⁴

¹*Dipartimento di Fisica Generale, Università di Torino, Via P. Giuria 1, 10125 Torino, Italy*

²*INAF Osservatorio Astronomico di Collurania, via M. Maggini, 64100 Teramo, Italy*

³*Departamento de Física Teórica y del Cosmos, Universidad de Granada, Campus de Fuentenueva, 18071 Granada, Spain*

⁴*Karlsruhe Institute of Technology, Campus Nord, Institut für Kernphysik, D-76021 Karlsruhe, Germany*

Accepted 1988 December 15. Received 1988 December 14; in original form 1988 October 11

ABSTRACT

High-resolution spectroscopic observations of a hundred metal-poor Carbon and *s*-rich stars (CEMP-*s*) collected from the literature are compared with the theoretical nucleosynthesis models of asymptotic giant branch (AGB) presented in Paper I ($M_{\text{ini}}^{\text{AGB}} = 1.3, 1.4, 1.5, 2 M_{\odot}$, $-3.6 \lesssim [\text{Fe}/\text{H}] \lesssim -1.5$). The *s*-process enhancement detected in these objects is associated to binary systems: the more massive companion evolved faster through the thermally pulsing AGB phase (TP-AGB), synthesising in the inner He-intershell the *s*-elements, which are partly dredged-up to the surface during the third dredge-up (TDU) episode. The secondary observed low mass companion became CEMP-*s* by mass transfer of C and *s*-rich material from the primary AGB.

We analyse the light elements as C, N, O, Na and Mg, as well as the two *s*-process indicators, $[\text{hs}/\text{ls}]$ (where $\text{ls} = \langle \text{Y}, \text{Zr} \rangle$ is the light-*s* peak at $N = 50$ and $\text{hs} = \langle \text{La}, \text{Nd}, \text{Sm} \rangle$ the heavy-*s* peak at $N = 82$), and $[\text{Pb}/\text{hs}]$. We distinguish between CEMP-*s* with high *s*-process enhancement, $[\text{hs}/\text{Fe}] \gtrsim 1.5$ (CEMP-*s*II), and mild *s*-process enhanced stars, $[\text{hs}/\text{Fe}] < 1.5$ (CEMP-*s*I). To interpret the observations, a range of *s*-process efficiencies at any given metallicity is necessary. This is confirmed by the high spread observed in $[\text{Pb}/\text{hs}]$ (~ 2 dex). A degeneration of solutions is found with some exceptions: most main-sequence CEMP-*s*II stars with low $[\text{Na}/\text{Fe}]$ can only be interpreted with $M_{\text{ini}}^{\text{AGB}} = 1.3 - 1.4 M_{\odot}$. Giants having suffered the first dredge-up (FDU) need a dilution $\gtrsim 1$ dex (dil is defined as the mass of the convective envelope of the observed star, M_{\star}^{obs} , over the material transferred from the AGB to the companion, $M_{\text{AGB}}^{\text{trans}}$). Then, AGB models with higher AGB initial masses ($M_{\text{ini}}^{\text{AGB}} = 1.5 - 2 M_{\odot}$) are adopted to interpret CEMP-*s*II giants. In general, solutions with AGB models in the mass range $M_{\text{ini}}^{\text{AGB}} = 1.3 - 2 M_{\odot}$ and different dilution factors are found for CEMP-*s*I stars.

About half of the CEMP-*s* stars with europium measurements show a high *r*-process enhancement (CEMP-*s/r*). The scenario for the origin of CEMP-*s/r* stars is a debated issue. We propose that the molecular cloud, from which the binary system formed, was previously enriched in *r*-process elements, most likely by local SN II pollution. This initial *r*-enrichment does not affect the *s*-process nucleosynthesis. However, for a high *r*-process enrichment ($[\text{r}/\text{Fe}]^{\text{ini}} = 2$), the *r*-process contributions to solar La, Nd and Sm (30%, 40%, 70%) have to be considered. This increases the maximum $[\text{hs}/\text{ls}]$ up to ~ 0.3 dex. CEMP-*s/r* stars reflect this behaviour, showing higher $[\text{hs}/\text{ls}]$ than observed in CEMP-*s* on average.

Detailed analyses for individual stars will be provided in Paper III.

Key words: Stars: AGB – Stars: carbon – Stars: Population II – nucleosynthesis

1 INTRODUCTION

The chemical compositions observed in metal-poor stars are a test of stellar models of nucleosynthesis. Recent high-resolution spectroscopic surveys¹ have identified a sizeable number of metal-poor stars with carbon enhancement (CEMP). Following the classification by Beers & Christlieb (2005), we may distinguish CEMP stars in: CEMP-*s*, CEMP-*s/r*, CEMP-*r*, CEMP-no. Stars with enhancement in *s*-process elements (CEMP-*s*) are the majority among the CEMP stars ($\sim 80\%$, Aoki et al. 2007). About half of CEMP-*s* stars, for which Eu (a typical *r*-process element) has been detected, are enriched in both *s*- and *r*-elements, the CEMP-*s/r* stars. Starting with the first discoveries of CEMP-*s/r* stars by Barbuy et al. (1997), Hill et al. (2000) and Cohen et al. (2003), one of the most debated issues has begun. Indeed, CEMP-*s/r* stars show in their photosphere a competition between two neutron capture processes of completely different astrophysical origin, the *s*-process and the *r*-process. Finally, CEMP-*r* stars exhibit a strong enhancement in *r*-process elements only, and CEMP-no do not show appreciable abundances of heavy elements.

Aoki et al. (2002b, 2004) identified in CS 29498–043 a further subclass, the CEMP- α stars, which show a large excess of C, N, O, and α -elements. Similar characteristics have been detected in the giant CS 22949–037, previously detected by Norris et al. (2001); Depagne et al. (2002). A few objects, called CEMP-no/*s* (Sivarani et al. 2006), show subsolar Sr and a moderately enhanced Ba (about 1 dex). Other candidates are SDSS J1036+1212 (Behara et al. 2010) and BD $-1^\circ 2582$ (Simmerer et al. 2004; Roederer et al. 2010c).

This paper is focused on the theoretical interpretation of CEMP-*s* and CEMP-*s/r* stars. These are old stars of low initial mass ($M < 0.9 M_\odot$) on the main-sequence or the giant phase. The most plausible explanation of their observed *s*-enhancement is mass transfer by stellar winds in binary systems from a primary companion while on its asymptotic giant branch (AGB) phase (now a white dwarf).

The *s*-process nucleosynthesis is mainly ascribed to AGB stars during their thermally pulsing (TP) phase. After a thermal instability, the bottom of the convective envelope penetrates into the top layers of the region between the H- and He-shells (He-intershell), enriching the surface with freshly synthesised ^{12}C and *s*-process elements. This recurrent phenomenon is called third dredge-up (TDU). The major neutron source is the $^{13}\text{C}(\alpha, n)^{16}\text{O}$ reaction. ^{13}C burns radiatively in a thin layer of the He-intershell, the so-called ^{13}C -pocket, at a temperature of about 0.9×10^8 K (Straniero et al. 1995). During the TDU, a small amount of protons at the base of the convective envelope are assumed to penetrate in the top layers of the He-intershell, and are captured by the primary ^{12}C directly produced by helium

burning during previous TPs via the $^{12}\text{C}(\text{p}, \gamma)^{13}\text{N}(\beta^+ \nu)^{13}\text{C}$ reaction (Iben & Renzini 1983). A second neutron source, partially activated in low mass AGBs ($1.3 \lesssim M/M_\odot < 3$) during TPs, is the $^{22}\text{Ne}(\alpha, n)^{25}\text{Mg}$ reaction, which burns more efficiently in intermediate mass AGBs ($3 \lesssim M/M_\odot \lesssim 8$), where a higher temperature is reached at the bottom of the TP. For a complete discussion on AGB nucleosynthesis the reader may refer to Busso et al. (1999); Straniero et al. (2006); Sneden et al. (2008); Käppeler et al. (2010).

Spectroscopic observations of Galactic disc MS, S, C(N) and Ba stars show a spread in the distribution of the *s*-process elements for a given metallicity (Busso et al. 1995, 2001; Abia et al. 2001, 2002; Gallino et al. 2005; Husti et al. 2009 and references therein), which increases in the halo of CEMP-*s* stars (Sneden et al. 2008). This spread involves the three *s*-peaks at the magic neutron numbers, accumulation points of the *s*-process owing to the low neutron-capture cross sections: light-*s* (ls; Sr, Y, Zr) ($N = 50$), heavy-*s* (hs; Ba, La, Ce, Nd, Sm) ($N = 82$) and Pb ($N = 126$). In the halo, a large amount of lead (^{208}Pb) is produced, because the number of neutrons available per iron seed increases as ^{56}Fe decreases with the metallicity, while the ^{13}C is a primary neutron source directly produced in the star independently of the metallicity (Gallino et al. 1998; Goriely & Mowlavi 2000). Then, the neutron flux overcomes the first two peaks feeding Pb, which covers a range from about thirty times solar to values higher than four thousand times solar (e.g., see HD 189711 by Van Eck et al. 2003 and CS 29497–030 by Ivans et al. 2005). A range of *s*-process efficiencies is required in order to interpret the observations in the halo. Starting from the case ST adopted by Gallino et al. (1998) and Arlandini et al. (1999), which was shown to reproduce the solar main component as the average between AGB models of initial masses 1.5 and $3.0 M_\odot$ at half solar metallicity, we have multiplied or divided the ^{13}C (and ^{14}N) abundance in the pocket by different factors.

Our theoretical results are obtained with a post-process nucleosynthesis method (Gallino et al. 1998), based on full evolutionary FRANEC (Frascati Raphson-Newton Evolutionary Code, Chieffi & Straniero 1989) models, following the prescriptions by Straniero et al. (2003). The AGB models with different initial masses ($1.3 \leq M/M_\odot \leq 2$), metallicities ($-3.6 \leq [\text{Fe}/\text{H}] \leq -1.5$) and *s*-process efficiencies ($\text{ST}/150 \leq ^{13}\text{C}\text{-pocket} \leq \text{ST} \times 2$) have been presented by Bisterzo et al. (2010), hereafter Paper I. Below the minimum choice of the ^{13}C -pocket the *s*-process production is negligible. The case $\text{ST} \times 2$ corresponds to an upper limit, because further proton ingestion leads to the formation of ^{14}N at expenses of ^{13}C . We treat the ^{13}C -pocket as a free parameter, assumed to be constant pulse by pulse. As discussed in Paper I, the formation of the ^{13}C -pocket represents a significative source of uncertainty affecting AGB models because the properties of the physical mechanisms involved are not completely understood. The approximation is adopted to test AGB models through a comparison with spectroscopic observations of different stellar populations. Neutron-capture rates and charged particle reactions are updated to 2010 (KADONIS²,

¹ The ESO Large Program First Stars (Cayrel et al. 2004); the HK-survey (Beers et al. 1992; Cohen et al. 2005; Beers et al. 2007a); the Hamburg/ESO Survey (Christlieb 2003); the SEGUE survey, Sloan Extension for Galactic Exploration and Understanding, the SEGUE Stellar Parameter Pipeline, SSPP (Lee et al. 2008a,b); the Sloan Digital Sky Survey, SDSS (York et al. 2000); the Chemical Abundances of Stars in the Halo (CASH) Projects with the Hobby-Eberly Telescope, HET (Ramsey et al. 1998).

² Karlsruhe Astrophysical Database of Nucleosynthesis in Stars, web address ‘http://www.kadonis.org’ as well as further references given in Appendix A of Paper I.

Dillmann et al. 2006; NACRE³ compilation, Angulo et al. 1999). In the halo, AGB models of initial masses $M = 1.3, 1.4, 1.5$ and $2 M_{\odot}$ suffer 5, 10, 20 and 26 TDUs, respectively. The mass involved in each TDU increases with the AGB initial mass and with decreasing metallicity (Fig. 1 and 2 of Paper I).

An AGB star produces a huge amount of primary ^{12}C by partial He burning in the He-intershell. The stellar envelope becomes progressively enriched in $[\text{C}/\text{Fe}]$ by the effect of recurrent TDUs. An increasing amount of primary ^{22}Ne is also synthesised in the advanced thermal pulses by conversion of primary ^{12}C to primary ^{14}N during H-burning via $^{14}\text{N}(\alpha, \gamma)^{18}\text{F}(\beta^+ \nu)^{18}\text{O}$ and $^{18}\text{O}(\alpha, \gamma)^{22}\text{Ne}$ reactions (Mowlavi et al. 1999; Gallino et al. 2006; Husti et al. 2007). This ^{22}Ne contributes significantly to the primary production of light isotopes, as ^{23}Na (via $^{22}\text{Ne}(\text{n}, \gamma)^{23}\text{Na}$) and $^{24,25,26}\text{Mg}$ (via $^{23}\text{Na}(\text{n}, \gamma)^{24}\text{Mg}$, $^{22}\text{Ne}(\alpha, \text{n})^{25}\text{Mg}$ and $^{22}\text{Ne}(\alpha, \gamma)^{26}\text{Mg}$). ^{22}Ne , together with ^{12}C , ^{16}O and ^{23}Na , is among the major neutron poisons in the ^{13}C -pocket. For higher metallicities this effect decreases and becomes negligible at $[\text{Fe}/\text{H}] \geq -1$ (see also Gallino et al. 2006). Moreover, the neutron capture chain starting from $^{22}\text{Ne}(\text{n}, \gamma)$ extends up to ^{56}Fe , producing seeds for the *s*-process. At halo metallicities and at increasing initial AGB mass (resulting in a corresponding increase of the temperature at the bottom of the thermal pulse), Sr, Y and Zr receive an increasing contribution by the $^{22}\text{Ne}(\alpha, \text{n})^{25}\text{Mg}$ neutron source because of the higher amount of primary ^{22}Ne .

The behaviour of the three *s*-process peaks⁴ ls, hs and Pb with metallicity is not linear, being extremely dependent both on the efficiency of the ^{13}C -pocket and on metallicity. The two *s*-process indexes $[\text{hs}/\text{ls}]$ and $[\text{Pb}/\text{hs}]$ characterise the *s*-process distribution independently of the mixing between the material transferred from the AGB to the observed companion. Once the comparison of the two *s*-process indexes with spectroscopic observations of a given star determines the efficiency of the ^{13}C -pocket, one obtains the dilution factor *dil*, defined as the mass of the convective envelope of the observed star (M_{\star}^{obs}) over the material transferred from the AGB to the companion ($M_{\text{AGB}}^{\text{trans}}$):

$$\text{dil} = \log \left(\frac{M_{\star}^{\text{obs}}}{\Delta M_{\text{AGB}}^{\text{trans}}} \right). \quad (1)$$

The aim of this paper is to interpret the observations in CEMP-*s* stars in order to test the AGB nucleosynthesis models presented in Paper I. In particular, the large sample of CEMP-*s* stars collected from the literature allows us to obtain statistical constraints on theoretical models and to verify the reliability of the models themselves. A general description of the sample is given in Section 2. In the analysis, we consider the spectroscopic observations of *s*-process elements belonging to the three *s*-peaks, light elements as C, N, O, Na and Mg, as well as Eu to investigate possible *r*-process contributions. With the improvement of the high quality spectra, the determination of the

$[\text{La}/\text{Eu}]$ ratio in these stars provides the most precise tool to distinguish the respective *r*- and *s*-contributions and to investigate their origin. Indeed, lanthanum is mainly synthesised by the *s*-process (70% of solar La, Winckler et al. 2006), while europium is an element with a dominant *r*-process contribution (less than 6% of solar Eu comes from *s*-process). In Paper I, we predicted a pure *s*-process ratio $[\text{La}/\text{Eu}]_{\text{s}} = 0.8 - 1.1$. In general, accounting of error bars, observed values in the range $0.0 \lesssim [\text{La}/\text{Eu}] \lesssim 0.5$ indicate CEMP-*s* stars having experienced an important *r*-process contribution (Beers & Christlieb 2005). Different hypotheses have been advanced to interpret CEMP-*s/r* stars. After a brief introduction about recent spectroscopic observations of *r*-process elements in some peculiar low metallicity stars (Section 3.1), a possible CEMP-*s/r* scenario is discussed in Section 3.3.

Subsequently, we perform a general analysis by comparing theoretical AGB models with spectroscopic observations for $[\text{La}/\text{Eu}]$ versus metallicity, $[\text{La}/\text{Fe}]$ versus $[\text{Eu}/\text{Fe}]$, $[\text{hs}/\text{ls}]$ and $[\text{Pb}/\text{hs}]$ versus $[\text{Fe}/\text{H}]$ (Section 4). Then, we discuss three stars with different characteristics, the CEMP-*s* giant HD 196944, the main-sequence CEMP-*s/r* HE 0338–3945, and a CEMP-*s* HE 1135+0139 for which no lead is measured. These stars are used as examples to illustrate the method we adopt for the theoretical interpretation with AGB models (Section 5). A detailed analysis of the individual stars is provided in Paper III. One of the main goals is to highlight possible differences between models and observations, providing starting points of debate in which spectroscopic and theoretical studies may intervene. A summary of the main results is given in Sections 6 and 7.

2 PRESENTATION OF THE SAMPLE

About a hundred CEMP-*s* and CEMP-*s/r* stars have been observed in the last decade with very high resolution spectroscopy ($R \gtrsim 50\,000$) (Aoki et al. 2002a,c,d, 2006, 2007, 2008; Barbuy et al. 2005; Cohen et al. 2003, 2006; Goswami et al. 2006; Goswami & Aoki 2010; Ivans et al. 2005; Ishigaki et al. 2010; Jonsell et al. 2006; Johnson & Bolte 2002, 2004; Lucatello et al. 2003; Lucatello 2004; Masseron et al. 2006, 2010; Pereira & Drake 2009; Preston & Sneden 2001; Schuler et al. 2008; Thompson et al. 2008; Tsangarides 2005; Van Eck et al. 2003; Zhang et al. 2009; Roederer et al. 2008; Roederer et al. 2010a) including spectroscopic data by Barklem et al. (2005) ($R \sim 20\,000$; $S/N = 30 - 80$)⁵; Behara et al. (2010) and Sneden et al. (2003b) ($R \sim 30\,000$). Allen et al. (2010) provided high resolution spectra for a new CEMP-*s* candidate and four new CEMP-*s/r* stars, but at present no data are available for further discussions. Among CEMP-*s* stars we include objects with $[\text{C}/\text{Fe}] > 0.5$. Note that some authors prefer a distinction at $[\text{C}/\text{Fe}] > 1$ (Beers & Christlieb 2005).

Additional stars with a limited number of spectroscopic observations are CEMP-*s* candidates: HE 0322–1504, HE 0507–1430, HE 1045–1434, CS 22947–187, CS 22949–008

³ Web address http://pntpm3.ulb.ac.be/Nacre/barre_database.htm

⁴ We defined ls = $\langle \text{Y}, \text{Zr} \rangle$ and hs = $\langle \text{La}, \text{Nd}, \text{Sm} \rangle$ (see Paper I). Sr is excluded from the ls elements and Ba from the hs elements because their lines are in general affected by higher uncertainties (Busso et al. 2001). Examples in CEMP-*s* stars will be given in Bisterzo et al., submitted, hereafter Paper III.

⁵ The signal-to-noise they obtain is from 30 to 50, with the only exception of HE 0202–2204, for which $S/N = 80$.

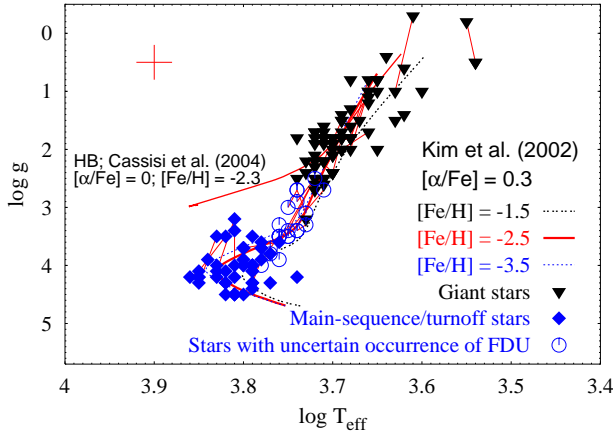


Figure 1. Spectroscopic gravities versus effective temperature of CEMP-s and CEMP-s/r listed in Table 1. Filled circles indicate main-sequence or turnoff stars labelled ‘no’ in column 7; triangles are giants labelled ‘yes’ in column 7. Stars with uncertain occurrence of the FDU are represented with empty circles (see text). Evolutionary tracks by Kim et al. (2002) for stars with $M = 0.8 M_{\odot}$ at 11 Gyr and various metallicities are plotted ($[\text{Fe}/\text{H}] = -1.5$ black line, $[\text{Fe}/\text{H}] = -2.5$ magenta line, $[\text{Fe}/\text{H}] = -3.5$ blue line). The Horizontal Branch (HB) track at $[\text{Fe}/\text{H}] = -2.3$ by Cassisi et al. (2004) is shown with a solid red line. Small changes in the assumed mass have a little effect on the location of the HB. Different observations of the same star are connected by thin solid lines. Typical error bars are shown. (See the electronic edition of the Journal for a colour version of this and the following figures.)

and HD 187216 (Beers et al. 2007a; McWilliam et al. 1995; Rossi et al. 2005; Johnson et al. 2007; Preston 2009; Kipper & Jørgensen 1994). An intense search for very metal-poor candidates is the Galaxy is underway, from which a large number CEMP-s and CEMP-s/r star are to be expected (Beers et al. 2007b).

A radial velocity study by Lucatello et al. (2005) suggests that all CEMP-s stars belong to double (or multiple) systems (see also Tsangarides 2005; Preston 2009). Mass transfer occurs mostly through efficient stellar winds, because the distance between the primary AGB star and the secondary are in general large, with periods $P > 200$ d. Only two CEMP-s with known radial velocities are short amplitude binaries, for which the accretion occurred via Roche-Lobe outflow: HE 0024–2523 (Lucatello et al. 2003) ($P = 3.41$ d), and SDSS 1707+58 (Aoki et al. 2008). When available, radial velocities variations of CEMP-s stars, their period and the relative references are listed in Appendix A, Table A1, online material.

In Table 1, we collect all CEMP-s and CEMP-s/r stars discussed here, with their metallicity, atmospheric parameters, and evolutionary status. In bold are marked the references considered in our analysis (column 2). All stars have metallicities in the range $-3.5 \leq [\text{Fe}/\text{H}] \leq -1.7$, with five exceptions: CS 29503–010 ($[\text{Fe}/\text{H}] = -1.06$; Aoki et al. 2007), HD 26 ($[\text{Fe}/\text{H}] = -1.25, -1.02$; Van Eck et al. 2003; Masseron et al. 2010), HD 206983 ($[\text{Fe}/\text{H}] = -0.99, -1.43$; Junqueira & Pereira 2001; Masseron et al. 2010), HE 0507–1653 ($[\text{Fe}/\text{H}] = -1.38, -1.42$; Aoki et al. 2007; Schuler et al. 2008), HE 1152–0355 ($[\text{Fe}/\text{H}] = -1.27$; Goswami et al. 2006). These stars may be considered as a link between Ba stars and CEMP-s stars, and will be

discussed in a separate Section in Paper III. The most metal-poor stars among CEMP-s and CEMP-s/r are CS 22960–053 (Aoki et al. 2007), CS 30322–023 (Aoki et al. 2007; Masseron et al. 2006), HE 1005–1439 (Aoki et al. 2007; Schuler et al. 2008), HE 1410–0004 (Cohen et al. 2006), SDSS 0126+06 (Aoki et al. 2008), and SDSS J1349–0229 (Behara et al. 2010), with $[\text{Fe}/\text{H}] \lesssim -3$.

In Fig. 1, we plot $\log g$ versus $\log T_{\text{eff}}$ for the stars listed in Table 1. By comparison, we overlap evolutionary tracks of models with initial mass $0.8 M_{\odot}$ at 11 Gyr and three metallicities ($[\text{Fe}/\text{H}] = -1.5, -2.5$ and -3.5) by Kim et al. (2002) and the Horizontal Branch (HB) track at $[\text{Fe}/\text{H}] = -2.3$ by Cassisi et al. (2004). Thirty stars are located on the main-sequence or close to the turnoff. Twenty-one lie on the subgiant phase. All the remaining stars are giants. This distinction is important for the following discussion, in relation to the occurrence of the first dredge-up (FDU) episode. This large mixing between the convective envelope and the inner layers of the star modifies the chemical composition of the surface (see also Section 5.3). In case of binary systems with mass transfer, this mixing also dilutes the C and s-rich material previously transferred from the AGB companion.

Unfortunately, the estimate of the atmospheric parameters at which the FDU occurs, in particular the effective temperature, is uncertain. For $[\text{Fe}/\text{H}] \lesssim -2.0$, a main-sequence star with initial mass of $\sim 0.8 M_{\odot}$ has a very thin convective envelope ($\sim 10^{-3} M_{\odot}$), thus a negligible dilution by convection is expected. After mass accretion, owing to the larger radiative opacity of the C-rich material deposited on the stellar surface, the depth of the convective envelope may eventually increase. However, due to gravitational settling, when the star attains the turnoff, the external layers will be again deprived of heavy elements, so that the convective envelope is even smaller than that at the zero age main-sequence. Indeed, gravitational settling, which acts on time-scales of billions of years (for stars on the main-sequence), depletes the heavy elements from the thin convective envelope of the observed CEMP-s star, which becomes H-rich. For primary stars with a typical initial mass of $1.5 M_{\odot}$, mass transfer occurred about ten billion years ago and the heavy elements accumulated just below the convective envelope (deeper gravitational settling would require longer time-scales). The larger is the mass accreted, the longer is the time required to reach the inner layers of the envelope with a primordial chemical composition. Then, a CEMP-s star at the turnoff would not show s-enhancement if the gravitational settling was efficient during the main-sequence.

Once at the turnoff, the convective envelope starts immediately to advance in depth and recovers what was slowly lost during the previous phase. Consequently, the material transferred from the primary star is progressively diluted. The efficiency of this mixing strongly depends on the amount of mass accreted from the primary. Indeed, the effective temperature on the subgiant branch at which the convective envelope reaches the layers with a primordial chemical composition decreases by increasing the amount of mass transferred. For an extreme case in which the mass accreted is $\sim 0.1 M_{\odot}$, no dilution will be observed at the beginning of the subgiant phase.

Besides gravitational settling, additional processes, as

Table 1. Metallicity, atmospheric parameters and evolutionary state of CEMP-*s* and CEMP-*s/r*. Labels: ‘ms’ means main-sequence, ‘TO’ turnoff, ‘SG’ subgiant and ‘G’ giant; in column 7, the label ‘no’ indicates stars having not suffered the FDU, ‘yes’ is for stars having already suffered the FDU, and ‘no?’ means that the occurrence of the FDU is uncertain (see text). Authors providing data with resolution spectra $R \sim 2000 - 3000$ are indicated with (*). In bold are marked the references considered for further discussions.

Stars (1)	Ref.s ^(a) (2)	[Fe/H] (3)	T_{eff} (4)	$\log g$ (5)	Phase (6)	FDU (7)
BD +04°2466	P09	-1.92	5100	1.8	G	yes
”	I10	-2.10	5065	1.8	”	”
”	Z09	-1.92	5115	1.9	”	”
BS 16080–175	T05	-1.86	6240	3.7	ms/TO	no
BS 17436–058	T05	-1.90	5390	2.2	G	yes
CS 22183–015	JB02	-3.12	5200	2.5	G	yes
”	C06,A07	-2.75	5620	3.4	SG	no?
”	Lai04(*),Lai07(*)	-3.17	5178	2.7	”	yes
”	T05	-3.00	5470	2.9	”	”
CS 22880–074	A02,A07	-1.93	5850	3.8	SG	no?
”	PS01	-1.76	6050	4.0	”	”
CS 22881–036	PS01	-2.06	6200	4.0	ms/TO	no
CS 22887–048	T05	-1.70	6500	3.4	ms/TO	no
”	J07(*)	-2.79	6455	4.0	”	”
CS 22891–171	M10	-2.25	5100	1.6	G	yes
CS 22898–027	A02,A07	-2.26	6250	3.7	ms/TO	no
”	T05	-2.61	6240	3.7	”	”
”	PS01	-2.15	6300	4.0	”	”
”	Lai07(*)	-2.29	5750	3.6	”	”
CS 22942–019	A02	-2.64	5000	2.4	G	yes
”	Sch08	-2.66	”	”	”	”
”	PS01	-2.67	4900	1.8	”	”
”	M10	-2.43	5100	2.5	”	”
CS 22948–27	BB05	-2.47	4800	1.8	G	yes
”	A07	-2.21	5000	1.9	”	”
”	PS01	-2.57	4600	0.8	”	”
”	A02	-2.57	4600	1.0	”	”
CS 22956–28	L04	-1.91	7038	4.3	ms	no
”	S03	-2.08	6900	3.9	”	”
”	M10	-2.33	6700	3.5	ms/TO	”
CS 22960–053	A07	-3.14	5200	2.1	G	yes
”	J07(*)	-3.08	5061	2.4	”	”
CS 22964–161A/B	T08	-2.39	6050	3.7	ms/TO	no
CS 22967–07	L04	-1.81	6479	4.2	ms	no
CS 29495–42	L04	-1.88	5544	3.4	SG	no?
”	J07(*)	-2.30	5400	3.3	”	yes
CS 29497–030	I05	-2.57	7000	4.1	ms	no
”	S03	-2.16	7050	4.2	”	”
”	S04	-2.77	6650	3.5	”	”
”	J07(*)	-2.20	7163	4.2	”	”
CS 29497–34	BB05	-2.90	4800	1.8	G	yes
”	A07	-2.91	4900	1.5	”	”
”	L04	-2.57	4983	2.1	”	”
CS 29503–010	A07	-1.06	6500	4.5	ms	no
CS 29509–027	S03	-2.02	7050	4.2	ms	no
CS 29513–032	R10	-2.08	5810	3.3	SG	no?
CS 29526–110	A02,A07	-2.38	6500	3.2	ms/TO	no
”	A08	-2.06	6800	4.1	”	”
CS 29528–028	A07	-2.86	6800	4.0	ms	no
CS 30301–015	A02,A07	-2.64	4750	0.8	G	yes
CS 30315–91	L04	-1.68	5536	3.4	SG	no?
CS 30322–023	M06	-3.50	4100	-0.3	G	yes
”	A07	-3.25	4300	1.0	”	”
”	M10	-3.39	4100	-0.3	”	”
CS 30323–107	L04	-1.75	6126	4.4	ms	no
CS 30338–089	A07	-2.45	5000	2.1	G	yes
”	L04	-1.75	5202	2.6	”	”
CS 31062–012	A02,A07	-2.55	6250	4.5	ms	no
”	A08	-2.53	6200	4.3	”	”
”	I01	-2.81	6090	3.9	ms/TO	”
CS 31062–050	JB04	-2.42	5500	2.7	SG/G	yes
”	A02,A06,A07	-2.31	5600	3.0	SG	no?
”	Lai07(*)	-2.65	5313	3.1	SG/G	yes
HD 26	VE03	-1.25	5170	2.2	G	yes
”	M10	-1.02	4900	1.5	”	”
HD 5223	G06	-2.06	4500	1.0	G	yes
HD 187861	VE03	-2.30	5320	2.4	G	yes
”	M10	-2.36	4600	1.7	”	”
HD 189711	VE03	-1.80	3500	0.5	G	yes
HD 196944	A02,A07	-2.25	5250	1.8	G	yes
”	J05	-2.23	5250	1.7	”	”

Table 1 (Continue)

Stars (1)	Ref.s ^(a) (2)	[Fe/H] (3)	T_{eff} (4)	$\log g$ (5)	Phase (6)	FDU (7)
"	VE03	-2.40	5250	1.7	"	"
"	M10	-2.19	5250	1.7	"	"
"	R08B	-2.46	5170	1.8	"	"
G 18-24	I10	-1.62	5447	4.2	ms	no
HD 198269	VE03	-2.20	4800	1.3	G	yes
HD 201626	VE03	-2.10	5190	2.3	G	yes
HD 206983	M10	-0.99	4200	0.6	G	yes
"	JP01	-1.43	4200	1.4	"	"
"	DP08	"	"	"	"	"
HD 209621	GA10	-1.93	4500	2.0	G	yes
HD 224959	VE03	-2.20	5200	1.9	G	yes
"	M10	-2.06	4900	2.0	"	"
HE 0012-1441	C06	-2.52	5730	3.5	SG	no?
HE 0024-2523	L03,C04	-2.72	6625	4.3	ms	no
HE 0131-3953	B05	-2.71	5928	3.8	TO/SG	no
HE 0143-0441	C06	-2.31	6240	3.7	ms/TO	no
HE 0202-2204	B05	-1.98	5280	1.7	G	yes
HE 0206-1916	A07	-2.09	5200	2.7	SG	yes
HE 0212-0557	C06	-2.27	5075	2.2	G	yes
HE 0231-4016	B05	-2.08	5972	3.6	SG	no
HE 0322-1504	Beers07(*)	-2.00	4460	0.8	G/HB?	yes
HE 0336+0113	C06	-2.68	5700	3.5	SG	no?
"	L04	-2.41	5947	3.7	"	"
HE 0338-3945	J06	-2.42	6160	4.1	ms/TO	no
"	B05	-2.41	6162	4.1	"	"
HE 0400-2030	A07	-1.73	5600	3.5	SG	no?
HE 0430-4404	B05	-2.07	6214	4.3	ms	no
HE 0441-0652	A07	-2.47	4900	1.4	G	yes
HE 0507-1430	Beers07(*)	-2.40	4560	1.2	G	yes
HE 0507-1653	A07	-1.38	5000	2.4	G	yes
"	Sch08	-1.42	"	"	"	"
HE 0534-4548	Beers07(*)	-1.80	4250	1.5	G	yes
HE 1001-0243	M10	-2.88	5000	2.0	G	yes
HE 1005-1439	A07	-3.17	5000	1.9	G	yes
"	Sch08	-3.08	"	"	"	"
HE 1031-0020	C06	-2.86	5080	2.2	G	yes
HE 1045-1434	Beers07(*)	-2.50	4950	1.8	G	yes
HE 1105+0027	B05	-2.42	6132	3.5	ms/TO	no
HE 1135+0139	B05	-2.33	5487	1.8	G	yes
HE 1152-0355	G06	-1.27	4000	1.0	G	yes
HE 1157-0518	A07	-2.34	4900	2.0	G	yes
HE 1305+0007	G06	-2.03	4750	2.0	G	yes
"	Beers07(*)	-2.50	4560	1.0	"	"
HE 1305+0132	Sch07	-2.50	4462	0.8	G/HB?	yes
"	Sch08	-1.92	"	"	"	"
HE 1319-1935	A07	-1.74	4600	1.1	G	yes
HE 1410-0004	C06	-3.02	5605	3.5	SG	no?
HE 1419-1324	M10	-3.05	4900	1.8	G	yes
HE 1429-0551	A07	-2.47	4700	1.5	G	yes
HE 1430-1123	B05	-2.71	5915	3.8	SG	no
HE 1434-1442	C06	-2.39	5420	3.2	SG	yes
HE 1443+0113	C06	-2.07	4945	2.0	G	yes
HE 1447+0102	A07	-2.47	5100	1.7	G	yes
HE 1509-0806	C06	-2.91	5185	2.5	G	yes
HE 1523-1155	A07	-2.15	4800	1.6	G	yes
HE 1528-0409	A07	-2.61	5000	1.8	G	yes
HE 2148-1247	C03,C04	-2.30	6380	3.9	ms/TO	no
HE 2150-0825	B05	-1.98	5960	3.7	SG	no
HE 2158-0348	C06	-2.70	5215	2.5	G	yes
HE 2221-0453	A07	-2.22	4400	0.4	G	yes
HE 2227-4044	B05	-2.32	5811	3.9	SG	no?
HE 2228-0706	A07	-2.41	5100	2.6	G	yes
HE 2232-0603	C06	-1.85	5750	3.5	SG	no?
HE 2240-0412	B05	-2.20	5852	4.3	SG	no
HE 2330-0555	A07	-2.78	4900	1.7	G	yes
HK II 17435-00532	R08	-2.23	5200	2.2	G	yes
LP 625-44	A02,A06	-2.70	5500	2.5	G	yes
V Ari	VE03	-2.40	3580	-0.2	G	yes
"	Beers07(*)	-2.50	3500	0.5	"	"
SDSS 0126+06	A08	-3.11	6600	4.1	ms	no
SDSS 0817+26	A08	-3.16	6300	4.0	ms	no

Table 1 (Continue)

Stars (1)	Ref.s ^(a) (2)	[Fe/H] (3)	T_{eff} (4)	$\log g$ (5)	Phase (6)	FDU (7)
SDSS 0924+40	A08	-2.51	6200	4.0	ms	no
SDSS 1707+58	A08	-2.52	6700	4.2	ms	no
SDSS 2047+00	A08	-2.05	6600	4.5	ms	no
SDSS J0912+0216	B10	-2.50	6500	4.5	ms	no
SDSS J1349-0229	B10	-3.00	6200	4.0	ms	no

^(a)References are Aoki et al. (2002a,c,d, 2006, 2007, 2008), A02a, A02c, A02d, A06, A07, A08; Barbuy et al. (2005), BB05; Barklem et al. (2005), B05; Beers et al. (2007a), Beers07; Behara et al. (2010), B10; Cohen et al. (2003, 2004, 2006), C03, C04, C06; Drake & Pereira (2008), DP08; Goswami et al. (2006), G06; Goswami & Aoki (2010), GA10; Ivans et al. (2005), I05; Ishigaki et al. (2010), I10; Israelian et al. (2001), I01; Jonsell et al. (2005, 2006), J05,J06; Johnson & Bolte (2002, 2004), JB02, JB04; Johnson et al. (2007), J07; Lai et al. (2007), Lai07; Lai et al. (2004), Lai04; Lucatello et al. (2003), L03; Lucatello (2004), L04; Masseron et al. (2006, 2010), M06, M10; Pereira & Drake (2009), P09; Preston & Sneden (2001), PS01; Roederer et al. (2008a, 2010a), R08, R08B, R10; Schuler et al. (2007, 2008), Sch07, Sch08; Sivarani et al. (2004), S04; Sneden et al. (2003b), S03; Thompson et al. (2008), T08; Tsangarides (2005), T05; Van Eck et al. (2003), VE03; Zhang et al. (2009), Z09.

radiative acceleration and thermohaline mixing, should be included in the analysis. Radiative acceleration may impede gravitational settling (see e.g., Richard et al. 2002). Instead, mixing induced by thermohaline instabilities may reach deep layers in a shorter time scale (\sim millions of years; see e.g., Stancliffe et al. 2007) if not prevented by the other two processes.

The resulting efficiency of all these mixing is very difficult to estimate (Vauclair 2004; Eggleton et al. 2006; Charbonnel & Zahn 2007; Charbonnel & Lagarde 2010; Stancliffe & Glebbeek 2008; Stancliffe 2010; Denissenkov & Pinsonneault 2008; Denissenkov et al. 2009; Denissenkov 2010; Cantiello & Langer 2010; Thompson et al. 2008; Angelou et al. 2011). It is even more problematic if rotation or magnetic fields are included in the analysis. In conclusion, the depth of the mixing after the turnoff phase can not be clearly established: consequently, we can not theoretically establish the dilution for CEMP-*s* stars with effective temperature in the range $T_{\text{eff}} \sim (5700 \pm 150)$ K, because we do not know the level of depth of the convective envelope. In these cases, CEMP-*s* stars are labelled as ‘no?’ in Table 1. The FDU is technically defined as the point of the maximum sinking of the convective envelope during the subgiant phase. The FDU involves about 80% of the mass of the star, and erases all processes occurred during the previous phases. Therefore, CEMP-*s* having suffered the FDU ($T_{\text{eff}} \lesssim 5500$ K) need a dilution of the order of 1 dex or more. These giants are labelled ‘yes’ in column 7 of Table 1 (triangles in Fig. 1). Main-sequence or turnoff stars having not suffered the FDU are labeled ‘no’ in column 7 of Table 1 (filled circles in Fig. 1). The possible need of dilution in order to interpret observations of main-sequence/turnoff stars suggests that mixing (as thermohaline) were at play. Note that the relative ratio of two elements $[El_1/El_2]$ is not affected by the dilution and will be adopted as useful constraint for AGB models (Section 4).

The stars are divided into two groups. CEMP-*s* and CEMP-*s/r* stars with several observed *s*-element are listed

in Table 2. If a limited number of elements is measured, in particular only Sr among ls or Ba among hs, the star is listed in Table 3. This distinction is made because, in general, Sr and Ba are affected by higher uncertainties with respect to the other *s*-elements (Mashonkina et al. 2008; Andrievsky et al. 2009; Short & Hauschildt 2006). When available, in Tables 2 and 3 we report $[Na/Fe]$, $[Mg/Fe]$, $[ls/Fe]$, $[hs/Fe]$ and $[Pb/Fe]$, the *s*-process indicators $[hs/ls]$ and $[Pb/hs]$, as well as $[La/Fe]$, $[Eu/Fe]$, $[La/Eu]$. References and labels in columns 2 and 3 are the same as in Table 1. In both Tables, we further distinguish between different classes of stars, following their abundance pattern:

- CEMP-*s*II are stars with a high *s*-process enhancement, $[hs/Fe] \gtrsim 1.5$ (labeled as ‘sII’ in column 15);
- CEMP-*s*II also showing an *r*-enhancement are called CEMP-*s*II/*r* (in general with $[La/Eu]_{\text{obs}} \sim 0.0 \div 0.5$). Similarly to the classification based on the *s*-process enhancement, we may distinguish between:
 - CEMP-*s*II/*r*II with $[r/Fe]^{\text{ini}} \sim 1.5 \div 2.0$ (labelled as ‘sII/rII’ in column 15) and
 - CEMP-*s*II/*r*I with $[r/Fe]^{\text{ini}} \sim 1.0$ (labelled as ‘sII/rI’ in column 15),
 following our definition of the *r*-process enhancement based on AGB model predictions, as we will discuss in Section 3.3;
- CEMP-*s*I are stars with a mild *s* enrichment, $[hs/Fe] < 1.5$ (labeled as ‘sI’ in column 15⁶).

An additional class of CEMP-*s*I stars with mild *r*-process contribution would be expected, the CEMP-*s*I/*r* stars. None of the stars of our sample belong to this category, likely because of our definition of CEMP-*s/r* stars, which considers *r*-rich those stars having $[r/Fe]^{\text{ini}} \geq 1$ (see Section 3.3). Moreover, we classify stars without Eu measurements as CEMP-*s*I/– or CEMP-*s*II/– (labeled ‘sI/–’ or ‘sII/–’ in column 15). The degree of the *s*-enhancement may depend on different factors: firstly it is affected by the *s*-process efficiency and by the initial mass of the primary AGB; afterwards, the orbital parameters of the binary system (e.g., the distance between the two stars), the efficiency of the stellar winds and the degree of mixing with the envelope of the observed companion influence the final *s*-distribution. At the end of Tables 2 and 3 we report the range covered by the observations. The number of stars belonging to different classes is given in Table 4, where stars from Tables 2 and 3 are considered in columns 2 and 3, respectively. As in Table 1, we distinguish between stars before or after the FDU (‘no’ or ‘yes’, respectively).

Sodium is measured in 53 CEMP-*s* and CEMP-*s/r* stars (column 5), 23 of them have been studied by Aoki et al. (2007). $[Na/Fe]$ is very high in some CEMP-*s* stars (CS 29528-028 by Aoki et al. 2007 has $[Na/Fe] = 2.3$; SDSS

⁶ Barklem et al. (2005) first called ‘s-II’ stars three CEMP-*s* stars with high *s*-enhancement: HE 0131-3953, HE 0338-3945, afterwards studied by Jonsell et al. (2006), and HE 1105+0027. Another distinction is provided by Masseron et al. (2010), who used ‘CEMP-low-*s*’ to denote stars with a low Ba enhancement, but with $[Ba/Eu]$ showing evidence of contamination by *s*-process material. They found four CEMP-low-*s* stars, all discussed here as CEMP-*s*I stars: CS 30322-023 by Masseron et al. (2006), HK II 17435-00532 by Roederer et al. (2008), HE 1001-0243 and HE 1419-1324.

Table 2. Observed [Na/Fe], [Mg/Fe], [ls/Fe], [hs/Fe], [Pb/Fe], their *s*-process indicators [hs/ls] and [Pb/hs], as well as [La/Fe], [Eu/Fe] and [La/Eu] are listed for CEMP-*s* and CEMP-*s/r* stars with a major number of observations. References and labels in columns 2 and 3 are the same given in Table 1. We distinguish between stars with high *s*-process enhancement, [hs/Fe] $\gtrsim 1.5$, called CEMP-sII (or CEMP-sII/rII and CEMP-sII/rI depending on the *r*-process enhancement; see text and Section 3.3), and stars with a mild *s* enrichment, [hs/Fe] < 1.5 , called CEMP-sI. In column 15 the two classes are labeled with ‘sII’ (or ‘sII/rII’ and ‘sII/rI’) and ‘sI’. The labels ‘sI/–’ and ‘sII/–’ stay for stars without europium detection.

Star (1)	Ref. (2)	FDU (3)	[Fe/H] (4)	[Na/Fe] (5)	[Mg/Fe] (6)	[ls/Fe] (7)	[hs/Fe] (8)	[hs/ls] (9)	[Pb/Fe] (10)	[Pb/hs] (11)	[La/Fe] (12)	[Eu/Fe] (13)	[La/Eu] (14)	Type (15)
BD +04°2466	P09,I10	yes	-1.92,-2.10	-0.04	0.25,0.44	0.60	1.20	0.60	1.92	0.72	1.20	-	-	sI/–
BS 16080–175	T05	no	-1.86	-	-	1.20	1.62	0.42	2.60	0.98	1.65	1.05	0.60	sII
BS 17436–058	T05	yes	-1.90	-	-	0.75	1.35	0.60	2.11	0.76	1.39	0.93	0.46	sI
CS 22183–015	C06,A07	no?	-2.75	0.11	0.54	0.55	1.76	1.21	2.79	1.03	1.70	1.70	0.00	sII/rII
”	JB02	yes	-3.12	-	-	0.48	1.61	1.13	3.17	1.56	1.59	1.39	0.20	”
CS 22880–074	A02d,A07	no?	-1.93	-0.09	0.46	0.26	1.10	0.84	1.90	0.80	1.07	0.50	0.57	sI
CS 22881–036	PS01	no	-2.06	0.16	0.40	0.99	1.75	0.76	-	-	1.59	1.00	0.59	sII
CS 22887–048	T05	no	-1.70	-	-	1.11	1.91	0.80	3.40	1.49	1.73	1.49	0.24	sII/rI
CS 22898–027	A02d,A07	no	-2.26	0.33	0.41	0.87	2.17	1.30	2.84	0.67	2.13	1.88	0.25	sII/rII
CS 22942–019	A02d,PS01	yes	-2.64	1.44	0.58	1.65	1.29	-0.36	≤ 1.6	≤ 0.31	1.20	0.79	0.41	sI
CS 22948–27	BB05,A07	yes	-2.47,-2.21	0.52	0.31,0.55	1.23	2.16	0.93	2.72	0.56	2.32	1.88	0.44	sII/rII
CS 22964–161	T08	no	-2.39	0.00	0.36	0.39	1.04	0.65	2.19	1.15	1.07	0.69	0.38	sI
CS 29497–030	I05	no	-2.57	0.58	0.44	1.17	2.19	1.02	3.65	1.46	2.22	1.99	0.23	sII/rII
CS 29497–34	BB05,A07	yes	-2.90	1.37	0.72,1.31	1.21	2.02	0.81	2.95	0.93	2.12	1.80	0.32	sII/rII
CS 29513–032	R10	no?	-2.08	0.15	0.52	0.07	0.52	0.45	1.81	1.29	0.39	0.39	0.00	sI
CS 29526–110	A02c,A07	no	-2.38	-0.07	0.30	1.00	1.88	0.88	3.30	1.42	1.69	1.73	-0.04	sII/rII
CS 29528–028	A07	no	-2.86	2.33	1.69	2.23	2.85	0.62	-	-	2.93	-	-	sII/–
CS 30301–015	A02d,A07	yes	-2.64	1.09	0.86	0.53	0.98	0.45	1.70	0.72	0.84	-0.2	-0.64	sI
CS 30322–023	M06,A07	yes	-3.25	1.04	0.80,0.54	-0.13	0.53	0.66	1.49	0.96	0.48	-0.51	0.99	sI
CS 31062–012	A02d,A07	no	-2.55	0.60	0.45	1.06	1.92	0.86	2.40	0.48	2.02	1.62	0.40	sII/rII
CS 31062–050	JB04,A06,A07	no?	-2.42	0.34	0.84,0.60	0.62	2.02	1.40	2.81	0.79	2.12	1.79	0.33	sII/rII
HD 26 ^a	V03,M10	yes	-1.25,-1.02	-	0.93	0.83	1.33	0.50	2.02	0.69	1.39	0.75	0.64	sII
HD 5223	G06	yes	-2.06	0.46	0.58	1.10	1.66	0.56	≤ 2.21	≤ 0.55	1.76	-	-	sII/–
HD 187861	V03	yes	-2.30	-	-	1.16	1.97	0.81	3.30	1.33	2.0	-	-	sII/–
”	M10	yes	-2.36	-	0.37	-	1.58	-	2.86	1.28	1.73	1.34	0.39	sII/rI
HD 189711	V03	yes	-1.80	-	-	1.18	1.32	0.15	0.90	-0.42	1.20	-	-	sI/–
HD 196944	A02d,A07	yes	-2.25	0.86	0.42	0.61	0.86	0.25	1.90	1.04	0.91	0.17	0.74	sI
HD 198269	V03	yes	-2.20	-	-	0.39	1.33	0.94	2.40	1.07	1.60	-	-	sI/–
HD 201626	V03	yes	-2.10	-	-	0.87	1.60	0.73	2.60	1.00	1.90	-	-	sII/–
HD 206983 ^a	M10,JP01	yes	-0.99,-1.43	0.42,-	0.25,0.61	0.44	0.82	0.38	1.49	0.67	1.04	0.73	0.31	sI
HD 209621	GA10	yes	-1.93	0.01	0.17	1.08	1.91	0.83	1.88	-0.03	2.41	1.35	1.06	sII/rI
HD 224959	V03,M10	yes	-2.20,-2.06	-	0.76	0.95	2.07	1.12	3.10	1.03	2.03	1.74	0.29	sII/rII
HE 0143–0441	C06	no	-2.31	-	0.63	0.74	1.86	1.12	3.11	1.25	1.78	1.46	0.32	sII/rI
HE 0202–2204	B05	yes	-1.98	-	-0.01	0.43	1.10	0.67	-	-	1.36	0.49	0.87	sI
HE 0212–0557	C06	yes	-2.27	-	0.04	1.03	2.05	1.02	-	-	2.28	-	-	sII/–
HE 0231–4016	B05	no	-2.08	-	0.22	0.79	1.26	0.47	-	-	1.22	-	-	sI/–
HE 0336+0113	C06	no?	-2.68	-	1.04	1.68	1.89	0.21	≤ 2.28	≤ 0.39	1.93	1.18	0.75	sII
HE 0338–3945	J06	no	-2.42	0.36	0.30	1.05	2.29	1.24	3.10	0.81	2.28	1.94	0.34	sII/rII
HE 0430–4404	B05	no	-2.07	-	0.29	0.69	1.34	0.65	-	-	1.41	-	-	sI/–
HE 1031–0020	C06	yes	-2.86	-	0.50	0.35	1.29	0.94	2.66	1.37	1.16	≤ 0.87	≥ 0.29	sI/–
HE 1105+0027	B05	no	-2.42	-	0.47	0.91	2.06	1.15	-	-	2.10	1.81	0.29	sII/rII
HE 1135+0139	B05	yes	-2.33	-	0.33	0.39	0.87	0.48	-	-	0.93	0.33	0.60	sI
HE 1152–0355 ^a	G06	yes	-1.27	-	-0.01	0.07	0.96	0.89	-	-	1.57	-	-	sI/–
HE 1305+0007	G06	yes	-2.03	0.26	0.25	1.41	2.58	1.17	2.37	-0.21	2.56	1.97	0.59	sII/rII
HE 1430–1123	B05	no	-2.71	-	0.35	0.73	1.67	0.94	-	-	-	-	-	sII/–
HE 1434–1442	C06	yes	-2.39	0.03	0.30	0.52	1.41	0.89	2.18	0.77	-	-	-	sI/–
HE 1509–0806	C06	yes	-2.91	-	0.64	1.08	1.78	0.70	2.61	0.83	1.67	≤ 0.93	≥ 0.74	sII/(–)
HE 2148–1247	C03	no	-2.30	-	0.50	1.07	2.28	1.21	3.12	0.84	2.38	1.98	0.40	sII/rII
HE 2150–0825	B05	no	-1.98	-	0.36	0.89	1.39	0.50	-	-	1.41	-	-	sI/–
HE 2158–0348	C06	yes	-2.70	-	0.68	1.22	1.47	0.25	2.60	1.13	1.55	0.80	0.75	sII
HE 2232–0603	C06	no?	-1.85	-	0.85	0.62	1.15	0.53	1.55	0.40	1.23	-	-	sI/–
HK II 17435–00532	R08	yes	-2.23	0.69	0.42	0.37	0.92	0.55	-	-	0.78	0.48	0.30	sI
LP 625–44	A02a,A02d,A06	yes	-2.70	1.75	1.12	1.28	2.21	0.93	2.67	0.46	2.50	1.76	0.74	sII/rII
V Ari	V03	yes	-2.40	-	-	1.21	1.42	0.21	1.20	-0.22	1.30	-	-	sI/–
SDSS 0126+06	A08	no	-3.11	0.69	0.61	1.75	2.33	0.58	3.41	1.08	2.46	-	-	sII/–
SDSSJ 0912+0216	B10	no	-2.50	0.38	0.21	0.85	1.69	0.84	2.33	0.64	1.35	1.20	0.15	sII/rI
SDSSJ 1349-0229	B10	no	-3.00	1.49	0.57	1.43	2.00	0.57	3.09	1.09	1.74	1.62	0.12	sII/rII
Range	-	-	-1.0 \div -3.3	-0.1 \div 2.3	0.0 \div 1.7	-0.1 \div 2.2	0.5 \div 2.9	-0.4 \div 1.4	0.9 \div 3.7	-0.4 \div 1.6	0.4 \div 2.9	-0.5 \div 2.0	0.0 \div 1.1	-

^a The three disc stars, HD 26 ([Fe/H] = –1.0), HD 206983 ([Fe/H] = –1.0) and HE 1152–0355 ([Fe/H] = –1.3), will be discussed in Paper III.

1707+58 by Aoki et al. 2008 has [Na/Fe] = 2.7). As recalled in Section 1, Na is synthesised via neutron capture starting from the large amount of primary ^{22}Ne produced at low metallicities ($^{22}\text{Ne}(n, \gamma)^{23}\text{Ne}(\beta^- \nu)^{23}\text{Na}$). Therefore, [Na/Fe] increases with the number of TPs, providing an important constraint of the AGB initial mass in CEMP-*s* stars. Unfortunately, in very metal-poor stars Na may be affected by strong uncertainties due to non-local thermodynamic equilibrium (NLTE) corrections or three-dimensional (3D) hydrodynamical model atmospheres. Recent studies by Andrievsky et al. (2007) show that the NLTE effects may decrease [Na/Fe] by 0.7 dex (see also Barbuy et al. 2005 and Aoki et al. 2007). Most of the [Na/Fe] measurements in Tables 2 and 3 account of NLTE corrections or they are

provided by using two subordinate lines (5682 and 5688 Å), which are weak and exhibit small NLTE corrections (Takeda et al. 2003).

Magnesium is detected in several stars, covering a range from solar up to [Mg/Fe] ~ 1.7 dex. NLTE corrections may increase the final [Mg/Fe] by about 0.3 dex (Andrievsky et al. 2010). In most stars, [Mg/Fe] agrees with observations in field stars (Andrievsky et al. 2010; Mashonkina et al. 2003; Gehren et al. 2006), $0.2 \lesssim [\text{Mg/Fe}] \lesssim 0.6$. The only exceptions are CS 29497–34, CS 29528–028, LP 625–44, SDSS 1707+58 with [Mg/Fe] > 1.0 . In these stars, [Na/Fe] is enhanced as well, supporting the hypothesis that Mg is produced starting from the primary ^{22}Ne through $^{22}\text{Ne}(n, \gamma)^{23}\text{Ne}(\beta^- \nu)^{23}\text{Na}(n, \gamma)^{24}\text{Na}(\beta^- \nu)^{24}\text{Mg}$. In

Table 3. The same as Table 2, but for CEMP-*s* and CEMP-*s/r* stars with a limited number of spectroscopic observations among the characteristic *s*-process elements. Labels ‘sI/–’ or ‘sII/–’ between brackets mean a low upper limit detected for Eu. $[\text{lsf}/\text{Fe}] = [\text{Sr}/\text{Fe}]$ in all these stars, with only one exception, SDSS 2047+00, for which Y and Zr are detected. $[\text{hsf}/\text{Fe}] = [\text{Ba}/\text{Fe}]$, with the exception of those stars with La measurement (column 12), and for HE 0131–3953 for which both La and Nd have been detected. The two disc stars mentioned here, CS 29503–010 ($[\text{Fe}/\text{H}] = -1.1$) and HE 0507–1653 ($[\text{Fe}/\text{H}] = -1.4$), will be discussed in a separate Section in Paper III.

Star (1)	Ref. (2)	FDU (3)	[Fe/H] (4)	[Na/Fe] (5)	[Mg/Fe] (6)	[lsf/Fe] (7)	[hsf/Fe] (8)	[hsf/lsf] (9)	[Pb/Fe] (10)	[Pb/hsf] (11)	[La/Fe] (12)	[Eu/Fe] (13)	[La/Eu] (14)	Type (15)
CS 22891–171	M10	yes	-2.25	-	0.70	-	2.22	-	1.85	-0.37	2.12	1.73	0.39	sII/rII
CS 22956–28	S03	no	-2.08	-	-	1.38	0.42	-0.96	-	-	-	-	-	sI/–
"	M10	"	-2.33	-	-	-	0.51	-	<1.33	<0.82	<0.50	<0.91	-	"
CS 22960–053	A07	yes	-3.14	-	0.65	-	0.86	-	-	-	-	-	-	sI/–
CS 22967–07	L04	no	-1.81	0.14	0.64	0.93	1.77	0.84	2.80	1.03	1.50	0.80	0.70	sII
CS 29495–42	L04	no?	-1.88	-0.05	0.80	0.20	1.54	1.34	1.30	-0.24	1.30	0.80	0.50	sI
CS 29503–010 ^a	A07	no	-1.06	0.16	0.36	-	1.50	-	-	-	-	-	-	s(II)/–
CS 29509–027	S03	no	-2.02	-	-	0.82	1.33	0.51	-	-	-	-	-	sI/–
CS 30315–91	L04	no?	-1.68	0.21	0.77	0.26	1.23	0.97	1.90	0.67	0.90	≤0.4	≥0.5	sI(–)
CS 30323–107	L04	no	-1.75	-0.50	0.65	0.46	1.47	1.01	2.50	1.03	1.10	≤0.6	≥0.5	sII(–)
CS 30338–089	A07	yes	-2.45	0.46	0.48	-	2.22	-	-	-	-	-	-	sII/–
"	L04	"	-1.75	0.20	0.35	0.61	1.71	1.10	3.70	1.99	1.60	1.80	-0.20	sII(rII)
G 18–24	I10	no	-1.62	-0.30	0.23	0.58	1.17	0.59	-	-	-	-	-	sI/–
HE 0012–1441	C06	no?	-2.52	-	0.91	-	1.15	-	≤1.92	≤0.77	-	-	-	sI/–
HE 0024–2523	L03	no	-2.70	0.17	0.73	0.34	1.63	1.29	3.30	1.67	1.80	≤1.10	≥0.7	sII(–)
HE 0131–3953	B05	no	-2.71	-	0.30	0.46	1.97	1.51	-	-	1.94	1.62	0.32	sII/rII
HE 0206–1916	A07	yes	-2.09	0.34	0.52	-	1.97	-	-	-	-	-	-	sII/–
HE 0400–2030	A07	no?	-1.73	0.51	0.62	-	1.64	-	-	-	-	-	-	sII/–
HE 0441–0652	A07	yes	-2.47	0.32	0.35	-	1.11	-	-	-	-	-	-	sI/–
HE 0507–1653 ^a	A07	yes	-1.38	0.23	0.19	-	1.89	-	-	-	-	-	-	sII/–
HE 1001–0243	M10	yes	-2.88	-	0.37	-	0.59	-	≤1.38	≤0.79	0.55	-0.04	0.59	sI
HE 1005–1439	A07	yes	-3.17	0.79	0.60	-	1.06	-	-	-	-	-	-	sI/–
HE 1157–0518	A07	yes	-2.34	0.34	0.50	-	2.14	-	-	-	-	-	-	sII/–
HE 1305+0132	Sch08	yes	-1.92	-	-	-	0.86	-	-	-	-	-	-	sI/–
HE 1319–1935	A07	yes	-1.74	-	0.47	-	1.89	-	-	-	-	-	-	sII/–
HE 1410–0004	C06	no?	-3.02	0.48	0.58	0.18	1.06	0.88	≤3.17	≤2.11	-	≤2.40	-	sI/–
HE 1419–1324	M10	yes	-3.05	-	0.53	-	0.84	-	2.15	1.31	0.82	0.53	0.29	sI
HE 1429–0551	A07	yes	-2.47	0.65	0.52	-	1.57	-	-	-	-	-	-	sII/–
HE 1443+0113	C06	yes	-2.07	0.37	0.37	-	1.40	-	-	-	-	-	-	sI/–
HE 1447+0102	A07	yes	-2.47	0.67	1.43	-	2.70	-	-	-	-	-	-	sII/–
HE 1523–1155	A07	yes	-2.15	-	0.62	-	1.72	-	-	-	-	-	-	sII/–
HE 1528–0409	A07	yes	-2.61	0.73	0.83	-	2.30	-	-	-	-	-	-	sII/–
HE 2221–0453	A07	yes	-2.22	-	0.80	-	1.75	-	-	-	-	-	-	sII/–
HE 2227–4044	B05	no?	-2.32	-	0.30	0.41	1.33	0.92	-	-	1.28	-	-	sI/–
HE 2228–0706	A07	yes	-2.41	-	0.67	-	2.50	-	-	-	-	-	-	sII/–
HE 2240–0412	B05	no	-2.20	-	0.28	0.24	1.37	1.13	-	-	-	-	-	sI/–
HE 2330–0555	A07	yes	-2.78	0.58	0.67	-	1.22	-	-	-	-	-	-	sI/–
SDSS 0817+26	A08	no	-3.16	-	0.43	0.14	0.77	0.63	-	-	-	-	-	sI/–
SDSS 0924+40	A08	no	-2.51	1.31	0.52	0.60	1.81	1.21	3.01	1.20	-	-	-	sII/–
SDSS 1707+58	A08	no	-2.52	2.71	1.13	2.25	3.40	1.15	≤3.72	≤0.32	-	-	-	sII/–
SDSS 2047+00	A08	no	-2.05	0.33	0.27	0.88	1.50	0.72	-	-	-	-	-	sII/–
Range	-	-	-1.1÷-3.2	-0.5÷2.7	0.2÷1.4	0.2÷2.3	0.4÷3.4	-1.0÷1.5	1.3÷3.7	-0.4÷2.0	0.6÷2.1	0.0÷1.7	-0.2÷0.7	-

^a The two disc stars CS 29503–010 ($[\text{Fe}/\text{H}] = -1.1$) and HE 0507–1653 ($[\text{Fe}/\text{H}] = -1.4$), will be discussed in Paper III.

Table 4. Number of stars belonging to different categories of CEMP-*s* and CEMP-*s/r*. Stars with high *s*-process enhancement are labeled ‘II’ (CEMP-sII or CEMP-sII/*r*, with $[\text{hs}/\text{Fe}] \geq 1.5 - 2$); stars with a mild *s*-process enhancement are labeled ‘I’ (CEMP-sI or CEMP-sI/*r*I, with $[\text{hs}/\text{Fe}] < 1.5$). Among CEMP-*s* stars showing different *r*-process enhancements we distinguish between CEMP-sII/*r*II and CEMP-sII/*r*I. Stars with no europium measurement are labeled CEMP-sI/– and CEMP-sII/–. We distinguish between stars having or having not suffered the FDU (‘no’ or ‘yes’, respectively). CS 22183–015, for which discrepant atmospheric parameters have been measured by different authors (Cohen et al. 2006; Aoki et al. 2007; Johnson & Bolte 2002; Lai et al. 2007), is labeled with ‘(?)’. Note that none of the stars of the sample is classified as CEMP-sI/*r*I stars, likely because of our definition of CEMP-*s/r* stars (see Section 3.3). We refer to Paper III for a detailed analysis of these stars.

Class (1)	n. stars (2)	n. stars with limited number of data (3)
CEMP-sII	3 no; 3 yes	3 no
CEMP-sI	3 no; 9 yes	2 no; 2 yes
CEMP-sII/ <i>r</i> II with $[\text{r}/\text{Fe}]^{\text{ini}} \sim 2$	5 no; 1 yes	-
CEMP-sII/ <i>r</i> II with $[\text{r}/\text{Fe}]^{\text{ini}} \sim 1.5$	4 no; 5 yes; 1 (?)	1 no; 2 yes
CEMP-sII/ <i>r</i> I with $[\text{r}/\text{Fe}]^{\text{ini}} \sim 1.0$	3 no; 1 yes	-
CEMP-sI/ <i>r</i> I	-	-
CEMP-sII/–	3 no; 3 yes	4 no; 11 yes
CEMP-sI/–	4 no; 7 yes	7 no; 7 yes

addition, $^{25,26}\text{Mg}$ are synthesised via the $^{22}\text{Ne}(\alpha, n)^{25}\text{Mg}$ and $^{22}\text{Ne}(\alpha, \gamma)^{26}\text{Mg}$ reactions.

The ratios $[\text{ls}/\text{Fe}]$ and $[\text{hs}/\text{Fe}]$ are reported in columns 7 and 8. For stars listed in Table 2, if a given element among Y and Zr or among La, Nd and Sm is not observed we adopt the AGB prediction. It means that we consider in the ls and hs average the values of the missing elements estimated with the best theoretical AGB interpretation. The best AGB model that interprets the observations is calibrated on the basis of an accurate analysis, as we will describe in Section 5. Note that, in general, with this method the $[\text{ls}/\text{Fe}]$ and $[\text{hs}/\text{Fe}]$ ratios agree within 0.15 dex with the values provided without including our AGB predictions. Major details on the adopted models (listed in Tables 10 and 11) will be discussed in Paper III for individual stars. When available, $[\text{ls}/\text{Fe}]$ and $[\text{hs}/\text{Fe}]$ account for the number of lines detected for each element. In Table 3, stars with a limited number of s -process observations are listed: in several cases only Sr among ls or Ba among hs are detected. If not differently specified (see caption), we adopt for these stars the different notation $[\text{ls}\dagger/\text{Fe}] = [\text{Sr}/\text{Fe}]$ and $[\text{hs}\dagger/\text{Fe}] = [\text{Ba}/\text{Fe}]$. The s -process indicators $[\text{hs}/\text{ls}]$ and $[\text{Pb}/\text{hs}]$ are reported in columns 9 and 11, respectively. Most stars cover a range between $0.4 \lesssim [\text{hs}/\text{ls}] \lesssim 1.0$. Negative values are observed in two CEMP- s I, CS 22942–019 (Table 2) and CS 22956–28 (Table 3). Excluding the upper limits, the range of $[\text{Pb}/\text{hs}]$ covers about 2 dex. Five stars have negative $[\text{Pb}/\text{hs}]$ (HD 189711, HE 1305+0007 and V Ari from Table 2; CS 22891–171 and CS 29495–42 from Table 3).

The observed $[\text{La}/\text{Fe}]$, $[\text{Eu}/\text{Fe}]$ and their ratio $[\text{La}/\text{Eu}]$ (columns 11 to 13) provide, in general, a good indicator of the s - and r -process contribution in stars. A detailed discussion about CEMP- s/r stars and their theoretical interpretation will be given in the following Sections. Eu is detected in 38 stars of Table 2; 20 of them are CEMP- s/r with an observed $[\text{La}/\text{Eu}] \sim 0.0 - 0.5$ dex. Few exceptions are listed in Table 2. The three CEMP- s/r HD 209621, HE 1305+0007 and LP 625–44 have $[\text{La}/\text{Eu}] = 1.06, 0.56$ and 0.74 , respectively (column 14). For HD 209621 and LP 625–44, $[\text{La}/\text{Eu}]$ is higher than the other elements belonging to the second s -peak on which we based the r -enhancement. HE 1305+0007 has a high $[\text{La}/\text{Eu}]$ because of its very high $[\text{La}/\text{Fe}] \sim 2.6$. Despite the low $[\text{La}/\text{Eu}]$, the four stars CS 22942–019, CS 22964–161, CS 29513–032, HK II 17435–00532, are classified as CEMP- s I, because the low $[\text{La}/\text{Eu}]$ is a consequence of the low s -process contribution to $[\text{La}/\text{Fe}]$, instead of a high r -process contribution to $[\text{Eu}/\text{Fe}]$. Among the seven CEMP- s with Eu detected in Table 3, only three stars are CEMP- s/r (CS 22891–171 by Masseron et al. 2010, CS 30338–089 by Lucatello 2004 and HE 0131–3953 by Barklem et al. 2005).

3 R-PROCESS ENHANCEMENT IN METAL-POOR STARS

3.1 r -enhanced stars

In the past few decades, several spectroscopic efforts have been dedicated to the study of low metallicity stars showing high r -process enhancements. Sneden et al. (1994, 2003a) firstly analysed the spectrum of a giant with $[\text{Eu}/\text{Fe}] = 1.64$ and $[\text{La}/\text{Eu}] = -0.55$. This star is the prototype of a new

class of peculiar stars, the “pure r -process-enhanced metal-poor” stars. Following the standard classification given by Christlieb et al. (2004) and Beers & Christlieb (2005), r -II stars have $[\text{Eu}/\text{Fe}] \geq 1$ and r -I show $0.3 \leq [\text{Eu}/\text{Fe}] \leq 1$. In both cases $[\text{Ba}/\text{Eu}] < 0$ (or $[\text{La}/\text{Eu}] \leq 0$) to exclude any s -process contribution. Up to date, several r -II stars have been analysed: most noteworthy are CS 31082–001 by (Hill et al. 2002; Plez et al. 2004) ($[\text{Eu}/\text{Fe}] \sim 1.6$), HD 115444 by Westin et al. (2000) ($[\text{Eu}/\text{Fe}] = 0.85$), HE 1523–0901 by Frebel et al. (2007) ($[\text{Eu}/\text{Fe}] \sim 1.8$), CS 29497–004 by Christlieb et al. (2004) ($[\text{Eu}/\text{Fe}] = 1.64$), CS 31078–018 by Lai et al. (2008) ($[\text{Eu}/\text{Fe}] = 1.23$), CS 29491–069 ($[\text{Eu}/\text{Fe}] = 1.0$) and HE 1219–0312 ($[\text{Eu}/\text{Fe}] = 1.4$) by Hayek et al. (2009), CS 22183–031 by Honda et al. (2004) ($[\text{Eu}/\text{Fe}] = 1.2$), CS 22953–003 by François et al. (2007) ($[\text{Eu}/\text{Fe}] = 1.05$). Recently, Mashonkina et al. (2010) discovered the new star HE 2327–5642 ($[\text{Eu}/\text{Fe}] = 0.98$; $[\text{r}/\text{Fe}] = 1.5$) and Aoki et al. (2010) found the r -II stars with the highest $[\text{Eu}/\text{Fe}]$ detected, SDSS J2357–0052 (with $[\text{Fe}/\text{H}] = -3.4$ and $[\text{Eu}/\text{Fe}] = 1.92$ dex). Identified r -I stars are CS 30306–132 by Honda et al. (2004); Aoki et al. (2005), HD 221170 by Ivans et al. (2006), and BD +173248 by Cowan et al. (2002); Roederer et al. (2010b) ($[\text{Eu}/\text{Fe}] \sim 0.8 - 0.9$).

3.2 r -process residual

The r -process is associated with explosive conditions in massive stars, although the astrophysical site is still unknown. From the theoretical point of view, several models have been advanced (Farouqi et al. 2010; Qian & Wasserburg 2008, 2007; Kratz et al. 2007; Wanajo & Ishimaru 2006), but an exhaustive interpretation is still lacking. The mostly adopted estimate of the solar r -process contribution to each isotope were first evaluated by Käppeler et al. (1982) with the *residual method*, $N_r = N_\odot - N_s$. It was successfully adopted to derive the solar s -process abundances as well as to acquire information on the physical conditions during the s -process far from the branching points. Subsequently, this classical approach was replaced by a first generation of stellar s -process models (Gallino et al. 1998; Arlandini et al. 1999, as anticipated in Section 1), avoiding inconsistencies encountered close to the magic neutron numbers due to the use of more accurate cross section measurements. In Table 5 the solar s -process contributions of Arlandini et al. (1999) (column 4 in N_s ; column 6 in percentages) are compared to the updated results of 2010 (column 5 in N_s ; column 7 in percentages) for isotopes from ^{63}Cu up to ^{209}Bi . N_r values of each isotope obtained with the residual method are listed in column 8. However, the solar s abundances should include the contributions of all stellar generations over the Galactic history. In particular, low metallicity stars of low initial mass produce a huge amount of Pb and Bi (the so-called strong s -process component; Section 1), while only about 50% of solar Pb and 6% of solar Bi are synthesised by the main component (see columns 6 and 8). For this reason, an appropriate evaluation of the s -contributions at the end of the s -path is provided by a Galactic Chemical Evolution model as described by Travaglio et al. (1999, 2004) (updated by Serminato et al. 2009): $N_s^{\text{GCE}}(\text{Pb}) = 87\%$, $N_s^{\text{GCE}}(\text{Bi}) = 26\%$. These values are reported between brackets in column 6; the resulting r -process percentages for Pb and Bi are listed in column 8. Comparison between observations of elements from Ba to Bi

Table 5. Solar *s*-process contribution (N_s) and residuals (N_r) for isotopes from Cu to Bi. In column 2 and 3 the solar abundances by Anders & Grevesse (1989), AG89, and Lodders, Palme & Gail (2009), L09, are listed, respectively. Values are normalised to the number of silicon atoms of $N(\text{Si}) = 10^6$. N_s by Arlandini et al. (1999) stellar model, A99, (column 4) are compared with updated results (column 6) accounting for recent neutron capture cross sections, normalised to solar abundances by L09. The *s* contributions are normalised to ^{150}Sm . In columns 5 and 7 we report the percentages of the *s*-process solar contributions from A99 and from updated models, respectively. The residual *r*-process percentages are listed in column 8 for isotopes from Ba to Bi.

Isotope	Solar Abb. AG89	Solar Abb. L09	N_s A99	<i>s</i> (%)	N_s Updated	<i>s</i> (%) Updated ^(a)	<i>r</i> (%) Updated
(1)	(2)	(3)	(4)	(5)	(6)	(7)	(8)
⁶³ Cu	3.61E+02	3.74E+02	2.95E+00	0.8	2.73E+00	0.7	
⁶⁵ Cu	1.61E+02	1.67E+02	2.04E+00	1.3	3.21E+00	1.9	
Cu				1.0		1.1±0.1	
⁶⁴ Zn	6.13E+02	6.30E+02	9.21E−01	0.2	8.39E−01	0.1	
⁶⁶ Zn	3.52E+02	3.62E+02	3.44E+00	1.0	3.36E+00	0.9	
⁶⁷ Zn	5.17E+01	5.30E+01	7.78E−01	1.5	7.58E−01	1.4	
⁶⁸ Zn	2.36E+02	2.43E+02	6.78E+00	2.9	5.03E+00	2.1	
⁷⁰ Zn	7.80E+00	8.00E+00	2.36E−02	0.3	1.20E−02	0.2	
Zn				0.9		0.8±0.1	
⁶⁹ Ga	2.27E+01	2.20E+01	8.73E−01	3.8	7.71E−01	3.5	
⁷¹ Ga	1.51E+01	1.46E+01	8.35E−01	5.5	8.39E−01	5.7	
Ga				4.5		4.4±0.2	
⁷⁰ Ge	2.44E+01	2.43E+01	1.60E+00	6.6	1.38E+00	5.7	
⁷² Ge	3.26E+01	3.17E+01	2.47E+00	7.6	2.38E+00	7.5	
⁷³ Ge	9.28E+00	8.80E+00	4.68E−01	5.0	6.51E−01	7.4	
⁷⁴ Ge	4.34E+01	4.12E+01	2.62E+00	6.0	3.68E+00	8.9	
⁷⁶ Ge	9.28E+00	8.50E+00	5.52E−03	0.1	5.34E−03	0.1	
Ge				6.0		7.1±0.7	
⁷⁵ As	6.56E+00	6.10E+00	3.02E−01	4.6	3.77E−01	6.2	
As				4.6		6.2±0.6	
⁷⁶ Se	5.60E+00	6.32E+00	8.62E−01	15.4	8.48E−01	13.4	
⁷⁷ Se	4.70E+00	5.15E+00	3.15E−01	6.7	3.35E−01	6.5	
⁷⁸ Se	1.47E+01	1.60E+01	1.57E+00	10.7	2.36E+00	14.7	
⁸⁰ Se	3.09E+01	3.35E+01	2.73E+00	8.8	2.87E+00	8.6	
⁸² Se	5.70E+00	5.89E+00	3.39E−03	0.1	4.03E−03	0.1	
Se				8.9		9.5±0.7	
⁷⁹ Br	5.98E+00	5.43E+00	5.22E−01	8.7	4.65E−01	8.6	
⁸¹ Br	5.82E+00	5.28E+00	5.41E−01	9.3	5.69E−01	10.8	
Br				9.0		9.7±1.5	
⁸⁰ Kr	9.99E−01	1.30E+00	1.17E−01	11.7	1.03E−01	7.9	
⁸² Kr	5.15E+00	6.51E+00	1.91E+00	37.1	1.55E+00	23.8	
⁸³ Kr	5.16E+00	6.45E+00	6.50E−01	12.6	5.81E−01	9.0	
⁸⁴ Kr	2.57E+01	3.18E+01	3.54E+00	13.8	3.71E+00	11.7	
⁸⁶ Kr	7.84E+00	9.61E+00	2.12E+00	27.0	1.55E+00	16.2	
Kr				19.0		13.4	
⁸⁵ Rb	5.12E+00	5.12E+00	8.36E−01	16.3	9.37E−01	18.3	
⁸⁷ Rb	2.11E+00	2.11E+00	7.46E−01	35.4	6.18E−01	29.3	
Rb				22.0		21.5±1.5	
⁸⁶ Sr	2.32E+00	2.30E+00	1.09E+00	47.0	1.36E+00	59.2	
⁸⁷ Sr	1.51E+00	1.60E+00	7.60E−01	50.3	8.75E−01	54.7	
⁸⁸ Sr	1.94E+01	1.92E+01	1.79E+01	92.2	-	+6.0% ^(b)	
Sr				85.0		97.3±6.8	
⁸⁹ Y	4.64E+00	4.63E+00	4.27E+00	92.0	-	+3.0% ^(b)	
Y				92.0		+3.0%±10.3 ^(b)	
⁹⁰ Zr	5.87E+00	5.55E+00	4.24E+00	72.2	4.70E+00	84.8	
⁹¹ Zr	1.28E+00	1.21E+00	1.23E+00	96.1	-	+5.5% ^(b)	
⁹² Zr	1.96E+00	1.85E+00	1.83E+00	93.4	-	+0.5% ^(b)	
⁹⁴ Zr	1.98E+00	1.87E+00	-	+8.2% ^(b)	-	+25.5% ^(b)	
⁹⁶ Zr	3.20E−01	3.02E−01	1.76E−01	55.0	1.55E−01	51.3	
Zr				83.0		96.0±9.6	
⁹³ Nb	6.98E−01	7.80E−01	5.96E−01	85.4	6.68E−01	85.6	
Nb				85.0		85.6±8.6	
⁹⁴ Mo	2.36E−01	2.33E−01	1.53E−03	0.6	2.00E−03	0.9	
⁹⁵ Mo	4.06E−01	4.04E−01	2.25E−01	55.4	2.81E−01	69.6	
⁹⁶ Mo	4.25E−01	4.25E−01	-	+6.1% ^(b)	-	+19.9% ^(b)	
⁹⁷ Mo	2.44E−01	2.45E−01	1.43E−01	58.6	1.56E−01	63.7	
⁹⁸ Mo	6.15E−01	6.22E−01	4.66E−01	75.8	5.11E−01	82.2	

Table 5 (Continue)

Isotope	Solar Abb. AG89	Solar Abb. L09	N _s A99	s (%) A99	N _s Updated	s (%) Updated ^(a)	r (%) Updated
(1)	(2)	(3)	(4)	(5)	(6)	(7)	(8)
¹⁰⁰ Mo	2.46E-01	2.50E-01	9.42E-03	3.8	1.12E-02	4.5	
Mo				50.0		57.7±5.8	
⁹⁹ Ru	2.36E-01	2.27E-01	6.69E-02	28.3	7.52E-02	33.1	
¹⁰⁰ Ru	2.34E-01	2.24E-01	2.23E-01	95.3	-	+9.9% ^(b)	
¹⁰¹ Ru	3.16E-01	3.04E-01	4.83E-02	15.3	5.38E-02	17.7	
¹⁰² Ru	5.88E-01	5.62E-01	2.53E-01	43.0	2.81E-01	50.0	
¹⁰⁴ Ru	3.48E-01	3.32E-01	9.52E-03	2.7	8.17E-03	2.5	
Ru				32.0		37.3±2.2	
¹⁰³ Rh	3.44E-01	3.70E-01	4.67E-02	13.6	5.64E-02	15.2	
Rh				14.0		15.2±1.5	
¹⁰⁴ Pd	1.55E-01	1.51E-01	-	+5.7% ^(b)	-	+21.6% ^(b)	
¹⁰⁵ Pd	3.10E-01	3.03E-01	4.27E-02	13.8	4.75E-02	15.7	
¹⁰⁶ Pd	3.80E-01	3.71E-01	1.95E-01	51.3	2.17E-01	58.4	
¹⁰⁸ Pd	3.68E-01	3.59E-01	2.40E-01	65.2	2.68E-01	74.6	
¹¹⁰ Pd	1.63E-01	1.59E-01	5.93E-03	3.6	4.73E-03	3.0	
Pd				46.0		53.1±2.7	
¹⁰⁷ Ag	2.52E-01	2.54E-01	3.77E-02	15.0	4.21E-02	16.6	
¹⁰⁹ Ag	2.34E-01	2.36E-01	5.86E-02	25.0	6.64E-02	28.1	
Ag				20.0		22.1±1.1	
¹⁰⁸ Cd	1.43E-02	1.40E-02	1.61E-05	0.1	5.34E-05	0.4	
¹¹⁰ Cd	2.01E-01	1.97E-01	1.95E-01	97.0	-	+15.1% ^(b)	
¹¹¹ Cd	2.06E-01	2.01E-01	4.87E-02	23.6	7.65E-02	38.0	
¹¹² Cd	3.88E-01	3.80E-01	2.05E-01	52.8	2.84E-01	74.8	
¹¹³ Cd	1.97E-01	1.92E-01	6.85E-02	34.8	8.30E-02	43.2	
¹¹⁴ Cd	4.63E-01	4.52E-01	2.95E-01	63.7	4.06E-01	89.8	
¹¹⁶ Cd	1.21E-01	1.18E-01	2.13E-02	17.6	2.00E-02	17.0	
Cd				52.0		69.6±4.9	
¹¹³ In	7.90E-03	8.00E-03	5.59E-08	0.0	5.96E-08	0.0	
¹¹⁵ In	1.76E-01	1.70E-01	6.43E-02	36.5	7.53E-02	44.3	
In				35.0		42.4±3.0	
¹¹⁴ Sn	2.52E-02	2.40E-02	4.75E-06	0.0	5.14E-06	0.0	
¹¹⁵ Sn	1.29E-02	1.20E-02	3.06E-04	2.4	3.41E-04	2.8	
¹¹⁶ Sn	5.55E-01	5.24E-01	4.76E-01	85.8	5.04E-01	96.2	
¹¹⁷ Sn	2.93E-01	2.77E-01	1.41E-01	48.1	1.58E-01	56.9	
¹¹⁸ Sn	9.25E-01	8.73E-01	6.67E-01	72.1	7.04E-01	80.6	
¹¹⁹ Sn	3.28E-01	3.09E-01	1.27E-01	38.7	2.02E-01	65.3	
¹²⁰ Sn	1.25E+00	1.18E+00	9.77E-01	78.5	9.93E-01	84.5	
¹²² Sn	1.77E-01	1.67E-01	7.93E-02	44.8	7.78E-02	46.6	
Sn				65.0		73.2±11.0	
¹²¹ Sb	1.77E-01	1.79E-01	6.78E-02	38.3	7.40E-02	41.4	
¹²³ Sb	1.32E-01	1.34E-01	8.06E-03	6.1	8.66E-03	6.5	
Sb				25.0		26.4±4.0	
¹²² Te	1.24E-01	1.22E-01	1.09E-01	87.9	1.19E-01	97.2	
¹²³ Te	4.28E-02	4.30E-02	3.83E-02	89.5	4.18E-02	97.3	
¹²⁴ Te	2.29E-01	2.26E-01	2.08E-01	90.8	-	+0.3% ^(b)	
¹²⁵ Te	3.42E-01	3.35E-01	6.80E-02	19.9	7.44E-02	22.2	
¹²⁶ Te	9.09E-01	8.89E-01	3.68E-01	40.5	3.99E-01	44.9	
¹²⁸ Te	1.53E+00	1.49E+00	2.47E-02	1.6	5.69E-02	3.8	
Te				17.0		19.6±1.4	
¹²⁷ I	9.00E-01	1.10E+00	4.75E-02	5.3	5.15E-02	4.7	
I				5.3		4.7±1.0	
¹²⁸ Xe	1.03E-01	1.22E-01	8.42E-02	81.7	9.89E-02	81.1	
¹²⁹ Xe	1.28E+00	1.50E+00	4.03E-02	3.1	4.25E-02	2.8	
¹³⁰ Xe	2.05E-01	2.39E-01	1.70E-01	82.9	2.11E-01	88.1	
¹³¹ Xe	1.02E+00	1.19E+00	6.65E-02	6.5	7.92E-02	6.7	
¹³² Xe	1.24E+00	1.44E+00	4.16E-01	33.5	3.89E-01	27.1	
¹³⁴ Xe	4.59E-01	5.27E-01	2.22E-02	4.8	1.91E-02	3.6	
Xe				15.0		15.4	

Table 5 (Continue)

Isotope	Solar Abb. AG89	Solar Abb. L09	N _s A99	s (%) A99	N _s Updated	s (%) Updated ^(a)	r (%) Updated
(1)	(2)	(3)	(4)	(5)	(6)	(7)	(8)
¹³³ Cs	3.72E-01	3.71E-01	5.39E-02	15.0	5.80E-02	15.6	
Cs				15.0		15.6±0.8	
¹³⁴ Ba	1.09E-01	1.08E-01	1.07E-01	98.2	-	+12.5% ^(b)	
¹³⁵ Ba	2.96E-01	2.95E-01	7.75E-02	26.2	8.91E-02	30.2	69.8
¹³⁶ Ba	3.53E-01	3.51E-01	-	+0.3% ^(b)	-	+13.7% ^(b)	
¹³⁷ Ba	5.04E-01	5.02E-01	3.30E-01	65.5	3.38E-01	67.3	32.7
¹³⁸ Ba	3.22E+00	3.21E+00	2.76E+00	85.7	3.02E+00	94.2	5.8
Ba				81.0		88.7±5.3	11.3
¹³⁹ La	4.46E-01	4.57E-01	2.77E-01	62.1	3.25E-01	71.0	28.9
La				62.1		71.1±3.6	28.9
¹⁴⁰ Ce	1.01E+00	1.04E+00	8.36E-01	83.2	9.33E-01	89.5	10.5
¹⁴² Ce	1.26E-01	1.31E-01	2.79E-02	22.1	2.53E-02	19.3	80.7
Ce				77.0		81.3±4.1	18.7
¹⁴¹ Pr	1.67E-01	1.72E-01	8.13E-02	48.7	8.89E-02	51.7	48.3
Pr				49.0		51.7±3.6	48.3
¹⁴² Nd	2.25E-01	2.31E-01	2.08E-01	92.4	2.26E-01	97.6	2.4
¹⁴³ Nd	1.00E-01	1.03E-01	3.16E-02	31.6	3.37E-02	32.7	67.3
¹⁴⁴ Nd	1.97E-01	2.03E-01	1.00E-01	50.8	1.06E-01	52.2	47.8
¹⁴⁵ Nd	6.87E-02	7.50E-02	1.89E-02	27.5	1.97E-02	26.3	73.7
¹⁴⁶ Nd	1.42E-01	1.47E-01	9.11E-02	64.2	9.62E-02	65.5	34.5
¹⁴⁸ Nd	4.77E-02	4.90E-02	9.05E-03	19.0	9.41E-03	19.2	80.8
Nd				56.0		57.3±2.9	42.7
¹⁴⁷ Sm	3.99E-02	4.10E-02	8.25E-03	20.7	1.08E-02	26.2	73.8
¹⁴⁸ Sm	2.92E-02	3.00E-02	2.82E-02	96.6	-	+2.2% ^(b)	
¹⁴⁹ Sm	3.56E-02	3.70E-02	4.45E-03	12.5	4.68E-03	12.6	87.4
¹⁵⁰ Sm	1.91E-02	2.00E-02	1.91E-02	100.0	2.00E-02	100.0	
¹⁵² Sm	6.89E-02	7.10E-02	1.58E-02	22.9	1.64E-02	23.1	76.9
¹⁵⁴ Sm	5.86E-02	6.00E-02	4.69E-04	0.8	1.64E-03	2.7	97.3
Sm				29.0		31.3±1.6	68.7
¹⁵¹ Eu	4.65E-02	4.71E-02	3.04E-03	6.5	2.81E-03	6.0	94.0
¹⁵³ Eu	5.08E-02	5.14E-02	2.58E-03	5.1	3.06E-03	5.9	94.1
Eu				5.8		6.0±0.3	94.0
¹⁵² Gd	6.60E-04	7.00E-04	5.83E-04	88.3	4.94E-04	70.5	29.5
¹⁵⁴ Gd	7.19E-03	7.80E-03	6.85E-03	95.3	6.86E-03	88.0	12.0
¹⁵⁵ Gd	4.88E-02	5.33E-02	2.88E-02	59.0	3.02E-03	5.7	94.3
¹⁵⁶ Gd	6.76E-02	7.36E-02	1.15E-02	17.0	1.24E-02	16.9	83.1
¹⁵⁷ Gd	5.16E-02	5.63E-02	5.53E-03	10.7	5.98E-03	10.6	89.4
¹⁵⁸ Gd	8.20E-02	8.94E-02	2.25E-02	27.4	2.42E-02	27.1	72.9
¹⁶⁰ Gd	7.21E-02	7.87E-02	8.27E-04	1.1	4.87E-04	0.6	99.4
Gd				15.0		13.5±0.7	86.5
¹⁵⁹ Tb	6.03E-02	6.34E-02	4.36E-03	7.2	5.36E-03	8.4	91.6
Tb				7.2		8.4±0.6	91.6
¹⁶⁰ Dy	9.22E-03	9.40E-03	8.06E-03	87.4	8.58E-03	91.3	8.7
¹⁶¹ Dy	7.45E-02	7.62E-02	4.12E-03	5.5	3.95E-03	5.2	94.8
¹⁶² Dy	1.01E-01	1.03E-01	1.64E-02	16.2	1.65E-02	16.0	84.0
¹⁶³ Dy	9.82E-02	1.01E-01	3.52E-03	3.6	4.36E-03	4.3	95.7
¹⁶⁴ Dy	1.11E-01	1.14E-01	2.61E-02	23.5	2.62E-02	23.0	77.0
Dy				15.0		14.8±0.7	85.2
¹⁶⁵ Ho	8.89E-02	9.10E-02	6.95E-03	7.8	7.41E-03	8.1	91.9
Ho				7.8		8.1±0.6	91.9
¹⁶⁴ Er	4.04E-03	4.20E-03	3.34E-03	82.7	3.13E-03	74.5	25.5
¹⁶⁶ Er	8.43E-02	8.80E-02	1.25E-02	14.8	1.40E-02	15.9	84.1
¹⁶⁷ Er	5.76E-02	6.00E-02	4.92E-03	8.5	5.49E-03	9.2	90.8
¹⁶⁸ Er	6.72E-02	7.10E-02	1.90E-02	28.3	2.03E-02	28.6	71.4
¹⁷⁰ Er	3.74E-02	3.90E-02	2.69E-03	7.2	4.81E-03	12.3	87.7
Er				17.0		18.2±0.9	81.8
¹⁶⁹ Tm	3.78E-02	4.06E-02	5.03E-03	13.3	4.96E-03	12.2	87.8

Table 5 (Continue)

Isotope	Solar Abb. AG89	Solar Abb. L09	N_s A99	s (%) A99	N_s Updated	s (%) Updated ^(a)	r (%) Updated
(1)	(2)	(3)	(4)	(5)	(6)	(7)	(8)
Tm				13.3		12.2±0.9	87.8
¹⁷⁰ Yb	7.56E−03	7.60E−03	-	+1.1% ^(b)	6.89E−03	90.6	9.4
¹⁷¹ Yb	3.54E−02	3.61E−02	4.93E−03	13.9	7.54E−03	20.9	79.1
¹⁷² Yb	5.43E−02	5.56E−02	1.65E−02	30.4	2.44E−02	43.9	56.1
¹⁷³ Yb	4.00E−02	4.13E−02	8.57E−03	21.4	1.11E−02	26.9	73.1
¹⁷⁴ Yb	7.88E−02	8.21E−02	3.91E−02	49.6	4.97E−02	60.5	39.5
¹⁷⁶ Yb	3.15E−02	3.33E−02	4.28E−03	13.6	2.73E−03	8.2	91.8
Yb				33.0		39.9±2.0	60.1
¹⁷⁵ Lu	3.57E−02	3.70E−02	6.33E−03	17.7	6.60E−03	17.8	82.2
¹⁷⁶ Lu	1.04E−03	1.10E−03	-	+25.0% ^(b)	-	+1.2% ^(b)	
Lu				20.0		20.2±1.0	79.8
¹⁷⁶ Hf	7.93E−03	8.10E−03	7.65E−03	96.5	7.88E−03	97.3	2.7
¹⁷⁷ Hf	2.87E−02	2.90E−02	5.29E−03	18.4	4.98E−03	17.2	82.8
¹⁷⁸ Hf	4.20E−02	4.25E−02	2.40E−02	57.1	2.49E−02	58.5	41.5
¹⁷⁹ Hf	2.10E−02	2.12E−02	7.74E−03	36.9	8.70E−03	41.0	59.0
¹⁸⁰ Hf	5.41E−02	5.47E−02	4.08E−02	75.4	4.85E−02	88.8	11.2
Hf				56.0		61.0±3.1	39.0
¹⁸⁰ Ta	2.48E−06	2.60E−06	1.21E−06	48.8	1.96E−06	75.5	24.5
¹⁸¹ Ta	2.07E−02	2.10E−02	8.55E−03	41.3	9.77E−03	46.5	53.5
Ta				41.0		46.5±4.7	53.5
¹⁸⁰ W	1.73E−04	2.00E−04	8.02E−06	4.6	1.03E−05	5.1	94.9
¹⁸² W	3.50E−02	3.63E−02	1.60E−02	45.7	2.20E−02	60.6	39.4
¹⁸³ W	1.90E−02	1.96E−02	1.02E−02	53.7	1.13E−02	57.9	42.1
¹⁸⁴ W	4.08E−02	4.20E−02	2.88E−02	70.6	3.27E−02	77.8	22.2
¹⁸⁶ W	3.80E−02	3.90E−02	1.91E−02	50.3	2.28E−02	58.5	41.5
W				56.0		64.8±6.5	35.2
¹⁸⁵ Re	1.93E−02	2.07E−02	4.78E−03	24.8	5.68E−03	27.4	72.6
¹⁸⁷ Re	3.51E−02	3.74E−02	6.65E−05	0.2	3.74E−03	10.0	90.0
Re				8.9		16.2±1.6	83.8
¹⁸⁶ Os	1.07E−02	1.08E−02	1.04E−02	97.2	-	+11.6% ^(b)	
¹⁸⁷ Os	8.07E−03	8.60E−03	6.58E−03	81.5	3.43E−03	39.9	60.1
¹⁸⁸ Os	8.98E−02	9.04E−02	1.72E−02	19.2	2.68E−02	29.6	70.4
¹⁸⁹ Os	1.09E−01	1.10E−01	4.70E−03	4.3	4.93E−03	4.5	95.5
¹⁹⁰ Os	1.78E−01	1.79E−01	2.14E−02	12.0	2.61E−02	14.6	85.4
¹⁹² Os	2.77E−01	2.78E−01	2.86E−03	1.0	9.73E−03	3.5	96.5
Os				9.4		12.3±1.0	87.7
¹⁹¹ Ir	2.47E−01	2.50E−01	4.68E−03	1.9	5.01E−03	2.0	98.0
¹⁹³ Ir	4.14E−01	4.21E−01	4.40E−03	1.1	5.54E−03	1.3	98.7
Ir				1.4		1.6±0.1	98.4
¹⁹² Pt	1.05E−02	1.00E−02	1.03E−02	98.1	8.71E−03	87.1	12.9
¹⁹⁴ Pt	4.41E−01	4.20E−01	1.77E−02	4.0	2.77E−02	6.6	93.4
¹⁹⁵ Pt	4.53E−01	4.31E−01	7.53E−03	1.7	1.11E−02	2.6	97.4
¹⁹⁶ Pt	3.38E−01	3.22E−01	3.30E−02	9.8	4.27E−02	13.2	86.8
¹⁹⁸ Pt	9.63E−02	9.10E−02	2.33E−05	0.0	3.06E−05	0.0	100.0
Pt				5.1		7.1±0.6	92.9
¹⁹⁷ Au	1.87E−01	1.95E−01	1.09E−02	5.8	1.16E−02	5.9	94.1
Au				5.8		5.9±0.6	94.1
¹⁹⁸ Hg	3.39E−02	4.60E−02	-	+2.4% ^(b)	3.80E−02	82.6	17.4
¹⁹⁹ Hg	5.74E−02	7.70E−02	1.52E−02	26.5	1.67E−02	21.7	78.3
²⁰⁰ Hg	7.85E−02	1.06E−01	5.15E−02	65.6	5.55E−02	52.4	47.6
²⁰¹ Hg	4.48E−02	6.00E−02	2.22E−02	49.6	2.38E−02	39.7	60.3
²⁰² Hg	1.02E−01	1.37E−01	8.23E−02	81.1	8.94E−02	65.3	34.7
²⁰⁴ Hg	2.33E−02	3.10E−02	2.07E−03	8.9	2.49E−03	8.0	92.0
Hg				61.0		49.3±9.9	50.7
²⁰³ Tl	5.43E−02	5.40E−02	4.06E−02	74.8	4.49E−02	83.1	16.9
²⁰⁵ Tl	1.30E−01	1.29E−01	9.89E−02	76.3	8.10E−02	62.8	37.2
Tl				76.0		68.8±5.5	31.2

Table 5 (Continue)

Isotope	Solar Abb. AG89	Solar Abb. L09	N_s A99	s (%) A99	N_s Updated	s (%) Updated ^(a)	r (%) Updated
(1)	(2)	(3)	(4)	(5)	(6)	(7)	(8)
²⁰⁴ Pb	6.11E-02	6.60E-02	5.76E-02	94.3	6.38E-02	96.7	
²⁰⁶ Pb	5.93E-01	6.14E-01	3.43E-01	57.8	4.09E-01	66.6	
²⁰⁷ Pb	6.44E-01	6.80E-01	4.10E-01	63.7	3.93E-01	57.8	
²⁰⁸ Pb	1.83E+00	1.95E+00	6.30E-01	34.5	8.10E-01	41.6	
Pb				46.0		50.7±3.6 (87) ^(c)	(13) ^(c)
²⁰⁹ Bi	1.44E-01	1.38E-01	7.07E-03	4.9	8.71E-03	6.3	
Bi				4.9		6.3±0.6 (26) ^(c)	(74) ^(c)

^(a)The uncertainties provided in this column account of the solar abundance accuracy estimated by L09.

^(b)Overabundances with respect to solar (in percentage).

^(c)The values between brackets for Pb and Bi account for the contribution of the strong component (see text).

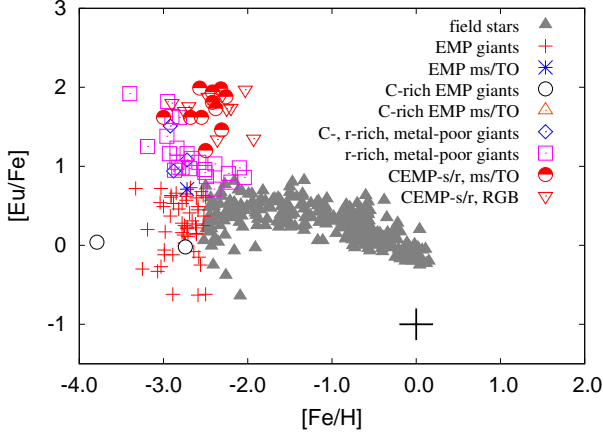


Figure 2. $[\text{Eu}/\text{Fe}]$ abundances collected from the literature using the SAGA database (Suda et al. 2008, 2011), including rII and rI stars listed in Section 3.1. For comparison, CEMP-*s/r* stars discussed here are also shown (see text). Filled triangles are field stars with $[\text{Fe}/\text{H}] \gtrsim 2.5$; plus and asterisks are Extremely Metal-Poor (EMP; $[\text{Fe}/\text{H}] \lesssim 2.5$) giants and ms/TO stars, respectively; filled circles and empty triangles are C-rich EMP giants and ms/TO stars, respectively. Stars showing an *r*-enhancement are: empty diamonds (C-rich, EMP), empty squares (EMP), half empty circles (CEMP-*s/r* ms/TO), empty triangles (CEMP-*s/r* giants). Typical error bars are indicated.

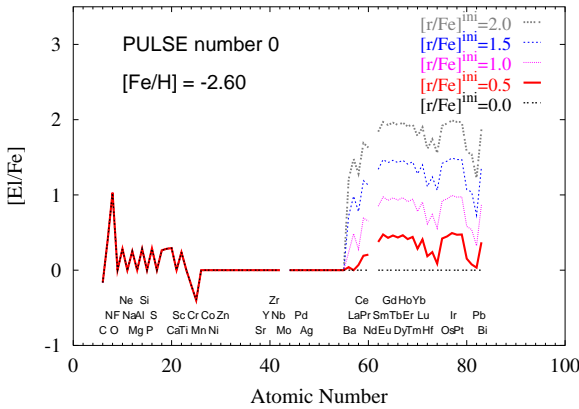


Figure 3. Initial abundances for different initial *r*-process enrichments ($[\text{r}/\text{Fe}]^{\text{ini}} = 0.0, 0.5, 1.0, 1.5$, and 2.0) for elements from Ba to Bi. For neutron capture elements below Ba, a mild initial *r*-process enrichment $[\text{r}/\text{Fe}]^{\text{ini}} \lesssim 1.0$ could be introduced (see discussion in Section 3.1). Note that for elements lighter than $A = 30$, we assumed the initial abundances described in Paper I, Section 2.1.

and the scaled solar-system *r*-element abundance distribution shows remarkable agreement in some *r*-rich stars (CS 22892-052, BD +173248, HD 221170, HD 115444), suggesting a perhaps unique *r*-process component in this range⁷. Instead, neutron capture elements below Ba ($40 < Z <$

⁷ For these four stars the authors provided Th (and U) measurements, also in agreement with the solar-system *r*-element distribution. Other *r*-rich stars (CS 30306-132, CS 31078-018, CS 31082-001 and HE 1219-0312) show an enhanced ratio in the actinide region ($Z \gtrsim 90$) with respect to solar, while elements from

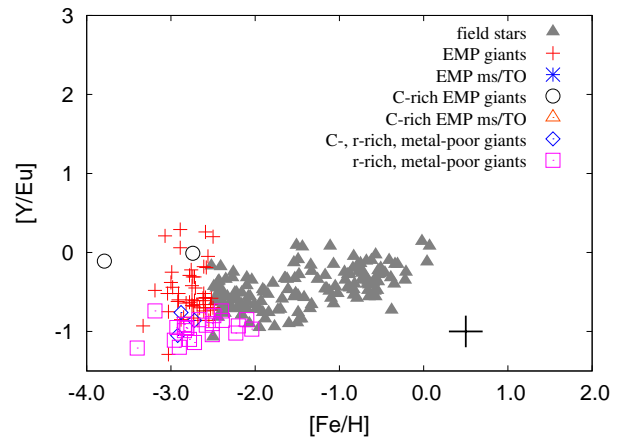
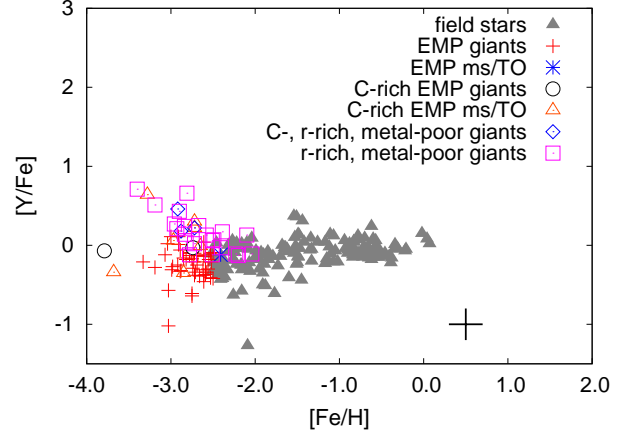


Figure 4. *Top panel:* The same as Fig. 2, but for $[\text{Y}/\text{Fe}]$. Note that CEMP-*s/r* stars have been excluded from this figure because, in these stars, Y is mainly produced by the *s*-process. *Bottom panel:* the same as top panel but for $[\text{Y}/\text{Eu}]$. Typical error bars are indicated.

56) show deviations from the solar *r*-process curve (e.g., Sneden et al. 2003a), in agreement with the hypothesis of multiple *r*-process components.

These considerations make use of the residual method to estimate the *r*-process contribution disputable in the region below Ba. Despite that, the residual method remains a valid approximation in the region between Ba and Bi (see Section 3.3) because of the limited knowledge of the primary *r*-process nucleosynthesis, but it does not exclude different approaches.

3.3 CEMP-*s/r* stars

Among the 45 CEMP-*s* stars with Eu detection listed in Tables 2 and 3, half are CEMP-*s/r*, with $[\text{Eu}/\text{Fe}]$ and $[\text{La}/\text{Eu}]$ incompatible with a pure *s*-process contribution. In some cases, Eu is strongly enhanced ($[\text{Eu}/\text{Fe}] \sim 2$ and $[\text{La}/\text{Eu}] \sim 0$, e.g. CS 29497-030 by Ivans et al. 2005, HE 0338-3945 by Jonsell et al. 2006, HE 1305+0007 by Goswami et al. 2006 and HE 2148-1247 by Cohen et al. 2003), (Section 3.1).

Ba to Bi follow the scaled Solar-system *r*-element abundances (Schatz et al. 2002; Roederer et al. 2009).

Table 6. Theoretical results of [La/Fe], [Eu/Fe] and [La/Eu] predicted in the AGB envelope for models of $M_{\text{AGB}}^{\text{ini}} = 1.3$ and $1.5 M_{\odot}$, [Fe/H] = -2.6 , and three choices of ^{13}C -pocket (ST, ST/12 and ST/75). Different *r*-process enrichments are considered ([r/Fe] $^{\text{ini}} = 0.0, 0.5, 1.0, 1.5, 2$). Results similar to $M = 1.5 M_{\odot}$ are obtained for AGB models of initial mass $M = 2.0 M_{\odot}$.

$M_{\text{AGB}}^{\text{ini}} = 1.3 M_{\odot}; [\text{Fe}/\text{H}] = -2.6$						
Case (1)	Predicted ratios (2)	[r/Fe] $^{\text{ini}} = 0$ (3)	[r/Fe] $^{\text{ini}} = 0.5$ (4)	[r/Fe] $^{\text{ini}} = 1$ (5)	[r/Fe] $^{\text{ini}} = 1.5$ (6)	[r/Fe] $^{\text{ini}} = 2$ (7)
ST	[La/Fe]	0.73	0.73	0.86	1.12	1.51
	[Eu/Fe]	0.17	0.53	0.98	1.47	1.96
	[La/Eu]	0.56	0.20	-0.12	-0.35	-0.42
ST/12	[La/Fe]	1.88	1.88	1.89	1.92	2.01
	[Eu/Fe]	1.06	1.12	1.29	1.59	2.00
	[La/Eu]	0.82	0.76	0.60	0.33	0.01
ST/75	[La/Fe]	1.28	1.28	1.32	1.43	1.66
	[Eu/Fe]	0.29	0.59	1.00	1.47	1.96
	[La/Eu]	0.99	0.69	0.32	-0.04	-0.30
$M_{\text{AGB}}^{\text{ini}} = 1.5 M_{\odot}; [\text{Fe}/\text{H}] = -2.6$						
ST	[La/Fe]	1.98	1.98	1.99	2.01	2.07
	[Eu/Fe]	1.19	1.23	1.35	1.59	1.95
	[La/Eu]	0.79	0.75	0.64	0.42	0.12
ST/12	[La/Fe]	2.69	2.69	2.69	2.69	2.71
	[Eu/Fe]	1.72	1.73	1.77	1.87	2.10
	[La/Eu]	0.97	0.96	0.92	0.82	0.61
ST/75	[La/Fe]	1.50	1.50	1.52	1.58	1.73
	[Eu/Fe]	0.43	0.63	0.97	1.40	1.88
	[La/Eu]	1.07	0.87	0.55	0.18	-0.15

Starting from the pioneering work of Burbidge et al. (1957), it is clear that *s*- and *r*-process have to be ascribed to separate astrophysical sites. As introduced in Section 1, the [La/Eu] ratio is a good indicator of the competition between the two processes. We remember that 70% of solar La is synthesised by the *s*-process and 94% of solar Eu is provided by the *r*-process (see Table 5, column 6). The large enhancement of typical elements of both processes in the envelope of these stars is highly debated. A pure *s*-process predicts $[\text{La}/\text{Eu}]_{\text{s}} \sim 0.8 - 1.1$, depending on the AGB initial mass and metallicity. All isotopes between Ba and Eu have well determined neutron-capture cross sections (Winckler et al. 2006; Käppeler, Beer & Wisshak 1989, <http://www.kadonis.org>). In order to explain a [La/Eu] ratio close to 0 together with a high *s*-process enhancement ($[\text{La}/\text{Fe}] \sim 2$) as observed in some CEMP-*s/r* stars, different scenarios have been proposed in the literature (Jonsell et al. 2006; Cohen et al. 2003 and references therein; Zijlstra 2004; Barbuy et al. 2005).

We discuss here our hypothesis, see also Sneden et al. (2008) and Bisterzo et al. (2009), based on the spread observed in [Eu/Fe] in field halo stars shown in Fig. 2. Spectroscopic data are from McWilliam et al. (1995); Hill et al. (2000); Johnson & Bolte (2001); Mishenina et al. (2001); Mashonkina et al. (2003); Sneden et al. (2003a); Christlieb et al. (2004); Simmerer et al. (2004); Honda et al. (2004); Barklem et al. (2005); François et al. (2007); Frebel et al. (2007); Aoki & Honda (2008); Hayek et al. (2009); Roederer et al. (2010c). For comparison, we added also observations of the CEMP-*s/r* stars

listed in Tables 2 and 3. High [Eu/Fe] enrichments are limited at $[\text{Fe}/\text{H}] < -2$, sustaining the hypothesis that a range of progenitor massive stars contribute to the *r*-process. The spread may be attributed to inhomogeneous mixing of the interstellar medium in the Galaxy (Ishimaru & Wanajo 1999; Travaglio et al. 2001b; Wanajo & Ishimaru 2006)⁸. Note that the spread is not present at disc metallicities; [Eu/Fe] follows the behaviour of [O/Fe], linearly decreasing at $[\text{Fe}/\text{H}] > -1$ owing to a progressively higher contribution to Fe in the interstellar medium from long-lived SNe Ia (Travaglio et al. 1999).

Starting with the spread observed in [Eu/Fe], we can hypothesise different initial *r*-process enhancements within the observed range (~ 2 dex), averaged around ~ 0.5 dex. The *r*-enhancement detected in peculiar stars with very low metallicities may be due to a local SNe II explosions, leading to an *r*-enrichment of molecular clouds from which CEMP-*s/r* stars may have formed. Both stars belonging to the binary system have the same initial *r*-enhancement. The more massive star is supposed to evolve through the TP-AGB phase, synthesising *s*-elements and polluting the observed companion through stellar winds.

Vanhala & Cameron (1998) showed through numerical simulations that supernova ejecta may interact with a

⁸ Recent studies by Carollo et al. (2007, 2010, 2011) show evidence of dichotomy of the Galactic halo, formed from two individual (broadly overlapping) stellar components with different chemical compositions and kinematics.

Table 7. Theoretical results of $[\text{El}/\text{Fe}]$ predicted in the AGB envelope for models of $M_{\text{AGB}}^{\text{ini}} = 1.3$ and $1.5 M_{\odot}$, two different choices of the ^{13}C -pocket (ST in Cols 3 to 6 and ST/12 in Cols 7 to 10), $[\text{Fe}/\text{H}] = -2.6$, and two initial r -process enrichments: $[\text{r}/\text{Fe}]^{\text{ini}} = 0$ and $[\text{r}/\text{Fe}]^{\text{ini}} = 2$. The initial r -enhancement is applied for elements from Ba to Bi (see text). At the end of the Table, $[\text{ls}/\text{Fe}]$, $[\text{hs}/\text{Fe}]$, $[\text{hs}/\text{ls}]$ and $[\text{Pb}/\text{hs}]$ are also reported. Note that, with a pure s -process contribution ($[\text{r}/\text{Fe}]^{\text{ini}} = 0$), AGB models with $M_{\text{AGB}}^{\text{ini}} = 1.3$ and $1.5 M_{\odot}$ predict $[\text{Eu}/\text{Fe}]_{\text{s}} = 0.17$ and 1.19 with case ST and 1.06 and 1.72 with case ST/12, respectively.

Case ST						Case ST/12			
(1)	(2)	(3)	(4)	(5)	(6)	(7)	(8)	(9)	(10)
$[\text{El}/\text{Fe}]$	Z	$M = 1.3 M_{\odot}$ $[\text{r}/\text{Fe}]^{\text{ini}} = 0$	$M = 1.3 M_{\odot}$ $[\text{r}/\text{Fe}]^{\text{ini}} = 2$	$M = 1.5 M_{\odot}$ $[\text{r}/\text{Fe}]^{\text{ini}} = 0$	$M = 1.5 M_{\odot}$ $[\text{r}/\text{Fe}]^{\text{ini}} = 2$	$M = 1.3 M_{\odot}$ $[\text{r}/\text{Fe}]^{\text{ini}} = 0$	$M = 1.3 M_{\odot}$ $[\text{r}/\text{Fe}]^{\text{ini}} = 2$	$M = 1.5 M_{\odot}$ $[\text{r}/\text{Fe}]^{\text{ini}} = 0$	$M = 1.5 M_{\odot}$ $[\text{r}/\text{Fe}]^{\text{ini}} = 2$
Sr	38	0.36	0.36	1.37	1.37	0.64	0.64	2.24	2.24
Y	39	0.35	0.35	1.40	1.40	0.80	0.80	2.41	2.41
Zr	40	0.34	0.34	1.36	1.36	0.89	0.89	2.44	2.44
Ba	56	0.74	1.22	1.96	2.00	1.85	1.91	2.72	2.73
La	57	0.73	1.51	1.98	2.07	1.88	2.01	2.69	2.71
Ce	58	0.82	1.37	2.16	2.20	2.05	2.11	2.76	2.77
Pr	59	0.64	1.70	1.94	2.10	1.85	2.07	2.55	2.59
Nd	60	0.71	1.65	2.04	2.15	1.94	2.10	2.61	2.64
Sm	62	0.58	1.82	1.89	2.11	1.75	2.07	2.43	2.51
Eu	63	0.17	1.96	1.19	1.95	1.06	2.00	1.72	2.10
Gd	64	0.38	1.92	1.62	2.04	1.47	2.04	2.15	2.32
Tb	65	0.25	1.95	1.38	1.98	1.23	2.01	1.90	2.18
Dy	66	0.37	1.92	1.61	2.03	1.45	2.03	2.13	2.30
Ho	67	0.24	1.95	1.37	1.98	1.21	2.01	1.88	2.17
Er	68	0.45	1.90	1.75	2.08	1.56	2.05	2.25	2.38
Tm	69	0.37	1.93	1.60	2.04	1.42	2.04	2.11	2.29
Yb	70	0.70	1.79	2.09	2.23	1.86	2.11	2.57	2.62
Lu	71	0.48	1.90	1.80	2.10	1.57	2.05	2.27	2.40
Hf	72	0.86	1.64	2.27	2.33	2.05	2.17	2.74	2.76
Ta	73	0.75	1.75	2.14	2.26	1.94	2.13	2.61	2.65
W	74	0.86	1.60	2.27	2.33	2.08	2.19	2.74	2.76
Re	75	0.43	1.92	1.71	2.07	1.55	2.06	2.12	2.30
Os	76	0.34	1.93	1.59	2.03	1.41	2.04	2.04	2.25
Ir	77	0.06	1.98	0.77	1.92	0.63	1.99	1.18	1.96
Pt	78	0.23	1.96	1.36	1.98	1.18	2.01	1.79	2.13
Au	79	0.22	1.96	1.33	1.98	1.16	2.01	1.76	2.12
Hg	80	0.92	1.74	2.35	2.42	2.17	2.28	2.77	2.79
Tl	81	0.97	1.58	2.42	2.46	2.22	2.29	2.71	2.73
Pb	82	3.19	3.19	4.06	4.06	2.99	2.99	3.25	3.26
Bi	83	3.06	3.08	3.91	3.91	2.64	2.71	2.95	2.98
$[\text{ls}/\text{Fe}]$	-	0.35	0.35	1.38	1.38	0.85	0.85	2.43	2.43
$[\text{hs}/\text{Fe}]$	-	0.67	1.66	1.97	2.11	1.86	2.06	2.58	2.62
$[\text{hs}/\text{ls}]$	-	0.32	1.31	0.59	0.73	1.01	1.21	0.15	0.19
$[\text{Pb}/\text{hs}]$	-	2.52	1.53	2.09	1.95	1.13	0.93	0.67	0.64

molecular cloud, polluting it with freshly synthesised material, likely triggering the formation of binary systems consisting of stars with low mass. This may explain the high frequency of CEMP- s/r among very metal-poor stars. However, we do not exclude other hypotheses supporting an initial r -process enrichment of the molecular cloud.

The choice of the initial r -enhancement (scaled to Eu) is made adopting the solar isotopic r -process contributions obtained with the residual method. As discussed in Section 3.1, the residual method remains a valid approximation to estimate the r -process contributions for elements from Ba to Bi. We consider as CEMP- s/r those stars that need an initial r -process enhancement in the range between $1 \leq [\text{r}/\text{Fe}]^{\text{ini}} \sim 2$. Note that stars with $[\text{r}/\text{Fe}]^{\text{ini}} \sim 1$ lie at the limit between CEMP- s and CEMP- s/r . As introduced in Section 2, following our definition of CEMP- s/r stars most of the CEMP-sI stars with low r -enhancement are not considered r -rich.

Fig. 3 shows the initial abundances (scaled to europium) adopted for different choices of the initial r -process enrichment $[\text{r}/\text{Fe}]^{\text{ini}} = 0.0, 0.5, 1.0, 1.5$, and 2.0 , for elements from Ba to Bi.

For neutron capture elements lighter than Ba, different initial r -process enrichment could be introduced under the assumption of a multiplicity of the r -process components, as discussed in Section 3.2. Particularly debated is the understanding of the origin of Sr, Y and Zr, for which the hypothesis of an additional primary contribution of unknown origin was advanced by Travaglio et al. (2004) (called LEPP, lighter element primary process, see also Montes et al. 2008). In particular, the same r -process by SNe II that contributes to elements heavier than Ba synthesised only $\sim 10\%$ of solar Sr, Y and Zr (Travaglio et al. 2004). This is sustained by the spread (> 1 dex) shown by $[\text{Sr}, \text{Y}, \text{Zr}/\text{Fe}]$ and $[\text{Sr}, \text{Y}, \text{Zr}/\text{Eu}]$ at $[\text{Fe}/\text{H}] < -2$. As example, we show in Fig. 4, observations of $[\text{Y}/\text{Fe}]$ and $[\text{Y}/\text{Eu}]$ versus $[\text{Fe}/\text{H}]$ for unevolved Galactic stars (top and bottom panels, respectively). Under the hypothesis that about 30% of iron is produced by SNe II, in first approximation, we may assume initial solar-scaled values for the ls elements. Indeed, the $[\text{Sr}, \text{Y}, \text{Zr}/\text{Fe}]$ ratios observed in unevolved halo stars reach maximum values of about 0.5 dex, which has little impact on the $[\text{ls}/\text{Fe}]$ in CEMP- s . This behaviour is confirmed by the recent study by Andrievsky et al. (2011),

who detected Sr in halo stars and accounted of NLTE corrections.

In Table 6, column 3, we reported theoretical results of a pure *s*-process contribution ($[r/Fe]^{ini} = 0$) for $[La/Fe]$, $[Eu/Fe]$ and $[La/Eu]$. AGB models with initial masses $M = 1.3$ and $1.5 M_{\odot}$, $[Fe/H] = -2.6$ and three ^{13}C -pockets (ST, ST/12, ST/75) are adopted. Low $[La/Eu]_s$ ratios (~ 0.5 dex) may be a consequence of the low *s*-process contribution to $[La/Fe]$ (e.g., case ST that overcomes La mainly producing Pb; AGBs with low initial mass, which undergo a limited number of TDUs). Different initial *r*-enrichments are adopted in columns 4 to 7 ($[r/Fe]^{ini} = 0.5, 1.0, 1.5$, and 2.0), reaching $[La/Eu]_{s+r}$ values close to 0. In case of a low *s*-process contribution to $[La/Fe]$ (e.g., an AGB model with initial mass $M = 1.3 M_{\odot}$, case ST), the initial *r*-process enhancement predominates, providing $[La/Eu]_{s+r}$ down to $-0.3 \div -0.4$ for $[r/Fe]^{ini} = 1.5$ or 2.0 . We include these values in the frame of a complete theoretical analysis. However, none of these models can provide theoretical interpretations for CEMP-*s/r* stars: indeed, by definition stars with $[La/Eu] < 0$ belong to a different category of stars, the CEMP-*r* stars (Beers & Christlieb 2005).

In Table 7 $[El/Fe]$ abundances (for Sr, Y, and Zr and for elements from Ba to Bi) are reported for AGB models with initial masses $M = 1.3$ and $1.5 M_{\odot}$ at $[Fe/H] = -2.6$, two ^{13}C -pocket choices (ST in columns 3 to 6 and ST/12 in columns 7 to 10), and two initial *r*-process enrichments: $[r/Fe]^{ini} = 0$ and $[r/Fe]^{ini} = 2$. The ratios $[ls/Fe]$, $[hs/Fe]$, $[hs/ls]$ and $[Pb/hs]$ are also listed at the end of the Table. From Section 3.1, Table 5, we derive that $\sim 70\%$ of solar La, $\sim 60\%$ of solar Nd, and $\sim 30\%$ of solar Sm are synthesised by the *s*-process. Consequently, in presence of a very high *r*-process enrichment, the actual value of $[hs/Fe]$ has also to account of an initial *r*-process contribution: $\sim 30\%$ of solar La, $\sim 40\%$ of solar Nd, and $\sim 70\%$ of solar Sm. Note that the *s*-process nucleosynthesis is not affected by different choices of initial *r*-enrichment. The changes in $[hs/Fe]$ are a consequence of the initial $[hs/Fe]^{ini}$ enhancement assumed molecular cloud by *r*-process contributions. Then, in case of $[r/Fe]^{ini} = 2$, the initial $[hs/Fe]$ of the molecular cloud is averaged among $[La/Fe]^{ini} \sim 1.5$, $[Nd/Fe]^{ini} \sim 1.6$ and $[Sm/Fe]^{ini} \sim 1.8$. In first approximation we assumed a solar-scaled Y and Zr, because the $[Y, Zr/Fe]$ ratios observed in unevolved halo stars reach maximum values of about 0.5 dex, which does not affect the $[ls/Fe]$ ratios much. By comparing AGB models with and without initial *r*-enhancement, the largest differences are shown for low $[hs/Fe]_s$ in the primary AGB, because the final $[hs/Fe]_{s+r}$ value is more sensible to the initial *r*-process enrichment of the molecular cloud. These differences are reduced by increasing the number of thermal pulses. Indeed, $M_{AGB}^{ini} = 1.5 M_{\odot}$ models show negligible differences in $[hs/ls]$. The solar *r*-process contribution to Pb is $15\% (\pm 5)$, with negligible effects on $[Pb/Fe]$ for all initial mass models, due to the high *s*-process production of ^{208}Pb at low metallicities. In Fig. 5 *top and middle panels*, we show the theoretical predictions of AGB models with initial mass $M = 1.5 M_{\odot}$, a wide range of ^{13}C -pockets and $[r/Fe]^{ini} = 0$ and 2 , respectively.

To simulate large mixing between the *s*-rich AGB material accreted onto the convective envelope of an observed giant (after the FDU, Section 2), we show in Fig. 5 *bottom panel*, AGB models with $M_{AGB}^{ini} = 1.5 M_{\odot}$, $[r/Fe]^{ini} =$

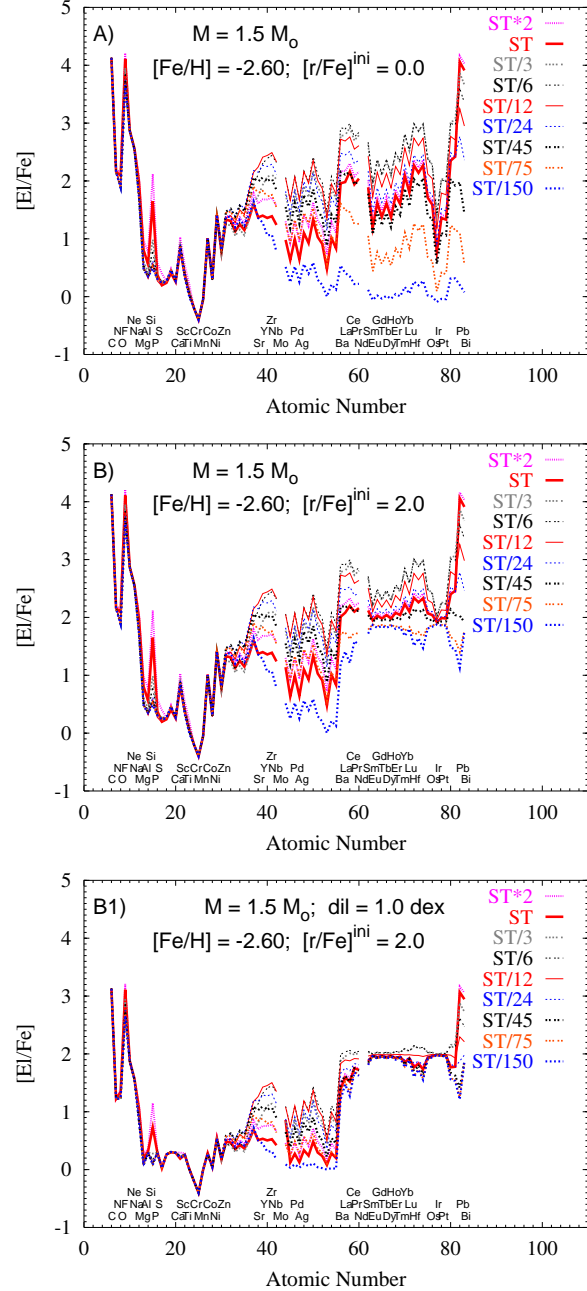


Figure 5. Theoretical predictions for AGB models of $M = 1.5 M_{\odot}$, $[Fe/H] = -2.6$, and a range of ^{13}C -pockets. While in *panel A* no initial *r*-enhancement is assumed, in *panel B* we adopt $[r/Fe]^{ini} = 2.0$. *Panel B1*: the same as panel B but with $dil = 1$ dex.

2 and a dilution of 1 dex. The dilution does not affect the initial $[El/Fe]$ enhancement assumed in the molecular cloud by *r*-process contributions, because both stars of the binary system are supposed to have the same initial chemical composition. Instead, the material transferred from the AGB is sensibly modified by large dilutions. Therefore, the initial *r*-contribution dominates the *s*-process material, thus affecting the $[hs/Fe]$ ratio.

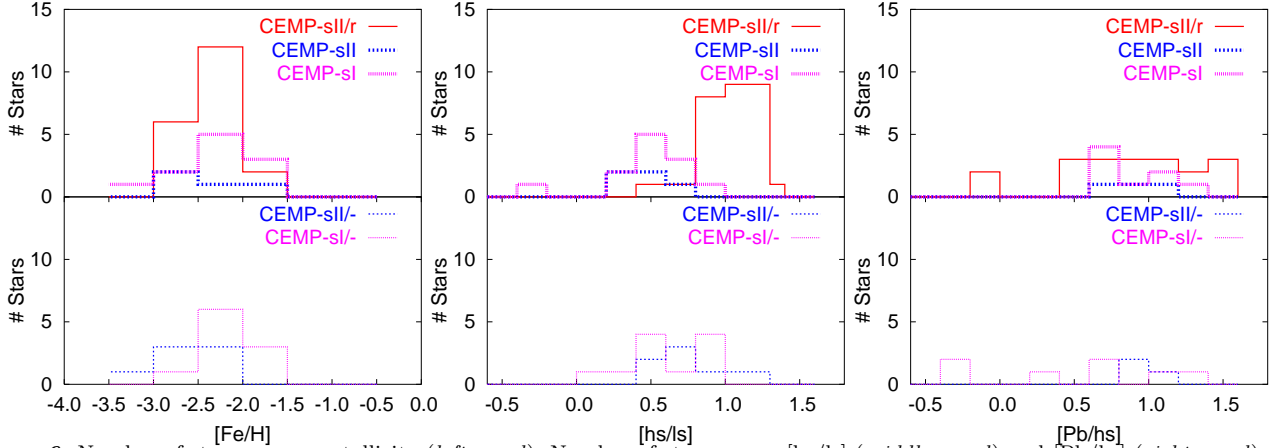


Figure 6. Number of stars versus metallicity (*left panel*). Number of stars versus $[\text{hs}/\text{ls}]$ (*middle panel*) and $[\text{Pb}/\text{hs}]$ (*right panel*). We present only the stars in Table 2 following the classification indicated in column 15: CEMP-sII/r, CEMP-sII and CEMP-sI are shown in the *top panels*, while stars with no Eu detection (CEMP-sII/- and CEMP-sI/-) in the *bottom panels*.

4 GENERAL COMPARISON BETWEEN THEORY AND OBSERVATIONS IN CEMP-s AND CEMP-s/r STARS: $[\text{La}/\text{Eu}]$, $[\text{hs}/\text{ls}]$ AND $[\text{Pb}/\text{hs}]$

In this Section, we compare spectroscopic observations of CEMP-s and CEMP-s/r stars listed in Table 2 with AGB predictions. Stars from Table 3 are excluded from this analysis owing to the limited number of detected s-process elements.

To examine the characteristics of the classes of stars indicated in Section 2, we show in Fig. 6 three histograms, with the number of stars versus $[\text{Fe}/\text{H}]$, $[\text{hs}/\text{ls}]$ and $[\text{Pb}/\text{hs}]$, respectively. CEMP-sII/r, CEMP-sII and CEMP-sI are displayed in the top panels, while stars without Eu measurement (CEMP-sII/- and CEMP-sI/-) are shown in the bottom panels. Note that no CEMP-sI/r are present in the sample. Most stars have metallicities between $-2.5 \lesssim [\text{Fe}/\text{H}] \lesssim -2.0$ (Fig. 6, left panel). On average, the same ranges are covered by CEMP-s/r and CEMP-s stars. A different behaviour appears in the middle panel for $[\text{hs}/\text{ls}]$: the majority of the stars lay between $0.5 \leq [\text{hs}/\text{ls}] \leq 1.2$, but CEMP-sII/r stars exhibit higher $[\text{hs}/\text{ls}]$ values than CEMP-sII and CEMP-sI stars. Instead, the $[\text{Pb}/\text{hs}]$ observed in CEMP-s and CEMP-s/r stars is equally distributed within the range $0.5 \leq [\text{Pb}/\text{hs}] \leq 1.3$ (right panel). To improve the analysis, we then exclude CEMP-sII/- and CEMP-sI/- from the following discussion to avoid possible medley between CEMP-s/r and CEMP-s stars. We start with the analysis of $[\text{La}/\text{Eu}]$ versus $[\text{Fe}/\text{H}]$ and $[\text{La}/\text{Fe}]$ versus $[\text{Eu}/\text{Fe}]$; then we discuss the behaviour of the two s-process indicators $[\text{hs}/\text{ls}]$ and $[\text{Pb}/\text{hs}]$ versus metallicity.

In Fig. 7, *top panel*, theoretical predictions of $[\text{La}/\text{Eu}]$ versus metallicity for AGB models with initial mass $M = 1.5 M_{\odot}$ and a range of ^{13}C -pockets are compared with observations of CEMP-s (little symbols) and CEMP-s/r (big symbols)

stars. Upper limits for Eu are represented by crosses with arrows. Diamonds represent stars before their FDU, while triangles denote giants having suffered the FDU (respectively ‘no’ and ‘yes’ in column 3 of Table 2). For simplicity, the five stars for which the occurrence of the FDU is uncertain (CS 31062–050, CS 22880–074, CS 29513–032, HE 0036+0113, HE 2232–0603, ‘no’ in column 3 of Table 2), are here included among the subgiants, which do not show FDU. For CS 22183–015, with uncertain atmospheric parameters (Cohen et al. 2006; Aoki et al. 2007; Johnson & Bolte 2002; Lai et al. 2007), the values obtained by different authors are connected by a (red) line. Typical error bars of $\Delta[\text{La}/\text{Eu}] = \pm 0.3$ dex and $\Delta[\text{Fe}/\text{H}] = \pm 0.2$ dex are shown. Theoretical predictions are normalised to the solar meteoritic abundances by Anders & Grevesse (1989). The differences between the solar normalisation adopted by different authors are negligible if compared with the typical error bars that are shown in the figures. For the most accurate analysis provided in Section 5 and in Paper III, both predictions and observations are normalised to the solar photospheric values by Lodders et al. (2009). As anticipated in Section 2, in general CEMP-s/r have $0.0 \leq [\text{La}/\text{Eu}] \leq 0.5$. AGB models with $[\text{r}/\text{Fe}]^{\text{ini}} = 0.5$ are shown in the *top panel*, in agreement with an average of the $[\text{Eu}/\text{Fe}]$ observed in field halo stars (Section 3.1). $[\text{La}/\text{Eu}]_{\text{th}}$ is definitely overestimated in CEMP-s/r. With an initial r-enrichment of $[\text{r}/\text{Fe}]^{\text{ini}} = 2$, *bottom panel*, an agreement between CEMP-s/r and theoretical predictions is reached except for two cases: the giant HD 209621 by Goswami & Aoki (2010) ($[\text{Fe}/\text{H}] = -1.93$ and $[\text{La}/\text{Eu}] \sim 1$) and the CEMP-s CS 29513–032 by Roederer et al. (2010a) ($[\text{Fe}/\text{H}] = -2.08$ and $[\text{La}/\text{Eu}] \sim 0$). HD 209621 has been classified as a CEMP-s/r because $[\text{r}/\text{Fe}]^{\text{ini}} = 1$ is needed to interpret the observed $[\text{hs}/\text{Eu}]$ ratio, even if $[\text{La}/\text{Fe}]$ is ~ 0.5 dex higher than the average for the hs elements. CS 29513–032 shows a mild s-process enhancement; then, the low $[\text{La}/\text{Eu}]$ observed has to be attributed to a

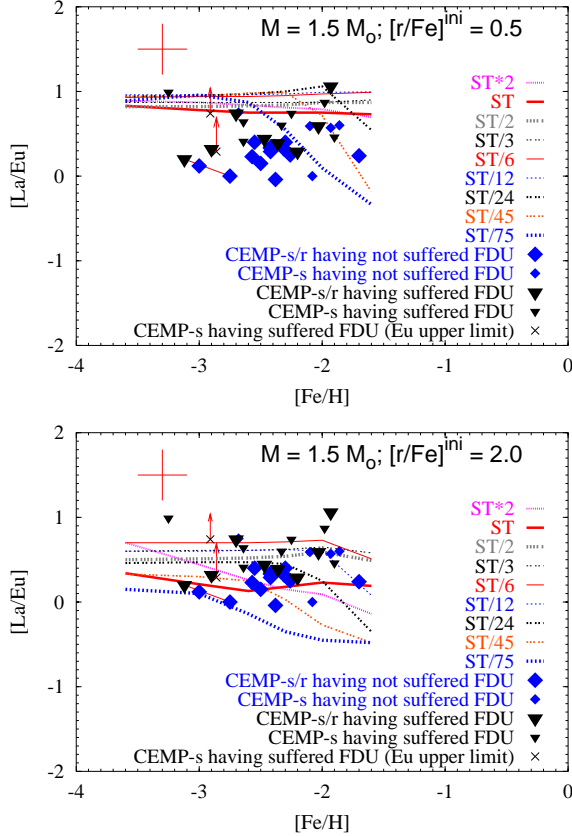


Figure 7. Theoretical predictions of $[La/Eu]$ versus metallicity for AGB models with initial mass $M = 1.5 M_{\odot}$ and a range of ^{13}C -pockets compared with observations of CEMP-*s* and CEMP-*s/r* stars listed in Table 2. In the *top panel* we adopt $[r/Fe]^{ini} = 0.5$, corresponding to an average of $[Eu/Fe]$ in unevolved halo stars (Section 3.1). *Bottom panel*: same as top panel but for $[r/Fe]^{ini} = 2$, taken as the highest value adopted to interpret CEMP-*s/r* stars. Diamonds are stars before the FDU, while triangles are stars having suffered the FDU. CEMP-*s/r* and CEMP-*s* stars are represented by big and little symbols, respectively. For the star CS 22183–015, having uncertain atmospheric parameters (Cohen et al. 2006; Aoki et al. 2007; Johnson & Bolte 2002; Lai et al. 2007), the values obtained by different authors are connected by a (red) line. Upper limits for Eu are represented by cross symbols. Note that HD 209621 ($[Fe/H] = -1.93$) is considered a CEMP-*s/r* despite its high $[La/Eu] \sim 1$, because an $[r/Fe]^{ini} = 1$ is needed to interpret $[hs/Eu]$; on the other side, CS 29513–032 ($[Fe/H] = -2.08$) is considered a CEMP-*s* despite the observed $[La/Eu] \sim 0$, because it has a low $[La/Fe]$ and not an enhanced $[Eu/Fe]$ ratio.

low *s*-process contribution to $[La/Fe]$ instead of an enhanced $[Eu/Fe]$ produced by the *r*-process.

In Fig. 8, $[La/Fe]$ is shown versus $[Eu/Fe]$. Symbols are the same as in Fig. 7. Spectroscopic observations are compared with AGB theoretical distributions assuming different initial *r*-process enrichments, $[r/Fe]^{ini} = 0.0, 0.5, 1.0, 1.5$ and 2.0 . The giant CS 30322–023 by Masseron et al. (2006) with a negative $[Eu/Fe]$, is matched with a subsolar initial enrichment of the molecular cloud (see Paper III).

In Figs. 9 – 12 we show the behaviour of $[hs/ls]$ (*top panels*) and $[Pb/hs]$ (*bottom panels*) versus metallicity for AGB models with $M_{AGB}^{ini} = 1.3$ and $1.5 M_{\odot}$ and a range of

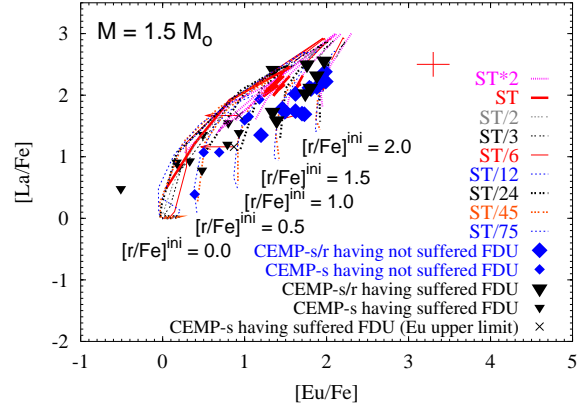


Figure 8. Theoretical predictions of $[La/Fe]$ versus $[Eu/Fe]$ for AGB models with initial mass $M = 1.5 M_{\odot}$ and a range of ^{13}C -pockets compared with observations of CEMP-*s* and CEMP-*s/r* stars. The different theoretical ranges correspond to the initial *r*-process enrichments $[r/Fe]^{ini} = 0.0, 0.5, 1.0, 1.5$ and 2.0 , adopted to interpret the spread observed in CEMP-*s* and CEMP-*s/r* stars. Symbols are the same as in Fig. 7. The star CS 30322–023 agrees with $[r/Fe]^{ini} = -1$ (see Paper III).

^{13}C -pockets, compared with the observations of stars listed in Table 2. Main-sequence/turnoff and subgiants having not suffered the FDU are compared with $M_{AGB}^{ini} = 1.3 M_{\odot}$ models (Figs. 9 – 10); subgiants/giants having suffered the FDU are compared with $M_{AGB}^{ini} = 1.5 M_{\odot}$ models (Figs. 11 – 12) and a $dil = 1.0$ dex to simulate the FDU mixing (Section 2). This distinction is made to simplify the discussion: indeed, the large dilution adopted for giants is still compatible with an observed high *s*-enhancement (e.g., $[hs/Fe] \sim 2$) if $M_{AGB}^{ini} = 1.5$ or $2 M_{\odot}$ models are adopted. $M_{AGB}^{ini} = 1.3 M_{\odot}$ models undergo a limited number of TDUs (at the 5th TDU the maximum $[hs/Fe]$ predicted is ~ 2.1 for cases close to ST/12, as shown in Fig. 8 of Paper I), and, in first approximation may be excluded during the analysis of CEMP-*s*II giants. However, this distinction has to be considered with caution: indeed, AGB models with different initial masses may plausibly interpret the spectroscopic observations of a given star (see e.g., Table 10). We defer to Paper III for a detailed analysis of individual stars. The star CS 22183–015, having uncertain atmospheric parameters is represented in both figures. Typical uncertainties are $\Delta[hs/ls] = \pm 0.3$ dex, $\Delta[Pb/hs] = \pm 0.3$ dex, and $\Delta[Fe/H] = \pm 0.2$ dex.

While no initial *r*-enhancement is assumed for CEMP-*s* stars (Figs. 9 and 11), CEMP-*s/r* stars are compared with AGB models with $[r/Fe]^{ini} = 2.0$ (Figs. 10 and 12). On average we confirm higher $[hs/ls]$ ratios for CEMP-*s/r* stars (big symbols) than for CEMP-*s* stars (little symbols) as shown in Fig. 6, middle panel. Preliminary results have been presented by Käppeler et al. 2010. This agrees with AGB model predictions if a very high initial *r*-process enhancement of the molecular cloud is adopted. As discussed in Section 3.3, an initial *r*-enhancement of $[r/Fe]^{ini} = 2.0$ may affect the final $[hs/Fe]$, because $\sim 30\%$ for solar La, $\sim 40\%$ for solar Nd, and $\sim 70\%$ for solar Sm are synthesised by the *r*-process. Indeed, with $[r/Fe]^{ini} = 2.0$, AGB models predict a maximum $[hs/ls]$ ratio ~ 0.3 dex higher than pure *s*-process nucleosynthesis models. In first approximation, this allows to reproduce the $[hs/ls]$ range covered by CEMP-*s/r* stars,

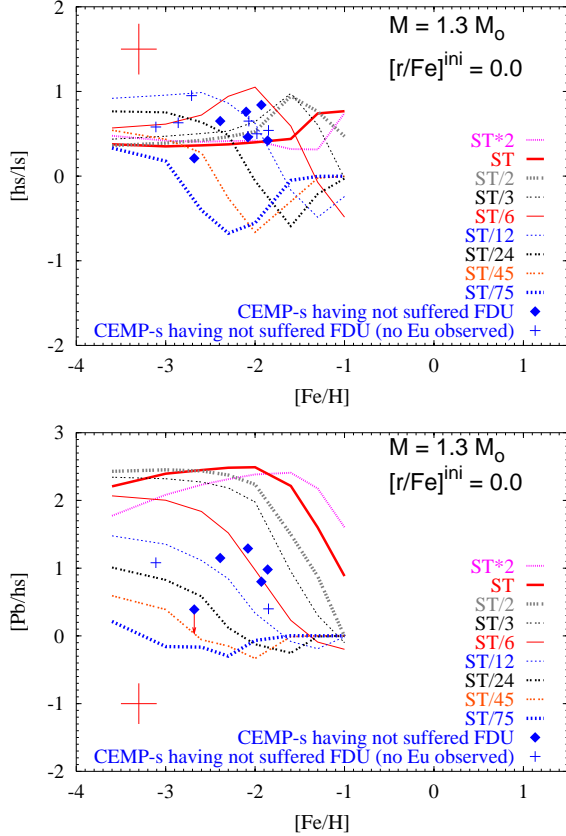


Figure 9. *Top Panel:* theoretical predictions of $[\text{hs}/\text{ls}]$ versus metallicity for AGB models with initial mass $M = 1.3 M_{\odot}$ and a range of ^{13}C -pockets compared with CEMP-s observations (little diamonds). No initial r -process enhancement is assumed. To simplify the discussion, we represent only main-sequence/turnoff/subgiant stars having not suffered the FDU (see text). CEMP-s without europium detection are indicated by plus symbols. *Bottom Panel:* the same as the top panel, but for $[\text{Pb}/\text{hs}]$ versus metallicity. Typical error bars are $\Delta[\text{hs}/\text{ls}] = \Delta[\text{Pb}/\text{hs}] = 0.3$; $\Delta[\text{Fe}/\text{H}] = 0.2$.

which are otherwise underestimated by pure s -process predictions. Note that, if lower $[\text{r}/\text{Fe}]^{\text{ini}}$ are assumed, the initial r -enhancement is dominated by the s -process contribution, and the maximum $[\text{hs}/\text{ls}]$ value is only marginally affected. No particular distinction between CEMP-s/ r and CEMP-s appears for $[\text{Pb}/\text{hs}]$, which lies within the theoretical predictions for a range of the ^{13}C -pockets between ST/2 and ST/45. Lead is largely produced at low metallicity (as ^{208}Pb) by the s -process, with a low r -process contribution ($\sim 15\%$ to solar Pb). Then, $[\text{Pb}/\text{Fe}]_{\text{s+r}}$ is not affected by high initial r -enrichments and possible variations in $[\text{Pb}/\text{hs}]$ are the consequence of the $[\text{hs}/\text{Fe}]_{\text{s+r}}$.

5 METHOD ADOPTED TO INTERPRET THE SPECTROSCOPIC DATA

In this Section we illustrate the method adopted to analyse the spectroscopic abundances of elements from C to Bi and to provide theoretical interpretations with AGB models. For this accurate investigation, we normalise both theoretical and spectroscopic abundances to the solar photo-

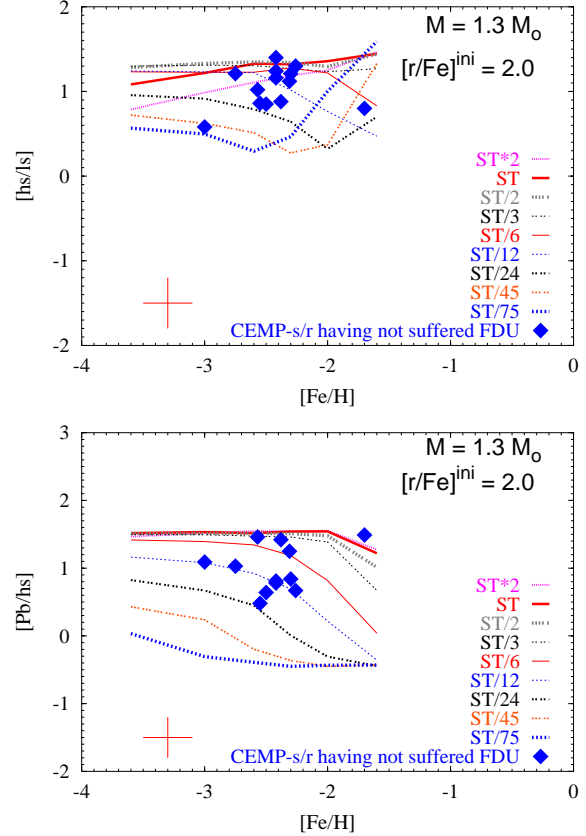


Figure 10. The same as Fig 9, but for AGB models with $[\text{r}/\text{Fe}]^{\text{ini}} = 2$, compared with observations of main-sequence/turnoff/subgiant CEMP-s/ r having not suffered the FDU (big diamonds).

spheric values by Lodders, Palme & Gail (2009). Differences higher than 0.05 dex between meteoritic solar abundances by Anders & Grevesse (1989) and photospheric solar abundances by Lodders, Palme & Gail (2009) are listed in the online material, Table A2 of Appendix A. We discuss here three stars with different characteristics taken as example: the giant CEMP-sI HD 196944, a second giant CEMP-sI without lead detection, HE 1135+0139 (Section 5.1), and the main-sequence CEMP-sII/ r HE 0338–3945 (Section 5.2). In Paper III, similar analyses will be provided for the stars listed in Tables 2 and 3.

5.1 How to fit CEMP-s stars

HD 196944 (Fig. 13, 14)

HD 196944 is a CEMP-sI giant (Aoki et al. 2002c,d, 2007, Van Eck et al. 2003, and Masseron et al. 2010), with observed $[\text{hs}/\text{ls}] = 0.3$ and $[\text{Pb}/\text{hs}] = 1.0$. At $[\text{Fe}/\text{H}] = -2.25$, these values correspond to a limited range of ^{13}C -pockets, depending on the initial AGB mass adopted (see e.g., Fig. 11). Once the ^{13}C -pocket efficiency that reproduces the s -process indicators $[\text{hs}/\text{ls}]$ and $[\text{Pb}/\text{hs}]$ is established, a proper dilution factor should be applied in order to fit the spectroscopic data. As described in Section 1, the dilution factor dil simulates the mixing between the s -rich material transferred from the AGB and the convective envelope of the

Table 8. χ_N^2 and distribution function $P(\chi_N^2)$ (obtained from the related tables) to test the goodness of the theoretical interpretation of the giant HD 196944. N is the number of elements considered. Case A: Y, Zr, La, Nd, Sm, Pb ($N = 6$). Case B: Case A with Na and Mg ($N = 8$). Case C: Na, Mg, Y, Zr, Ba, La, Ce, Nd, Sm, Eu, Dy, Er, Pb ($N = 13$). Case D: Y, Zr, Ba, La, Ce, Nd, Sm, Eu, Dy, Er, Pb ($N = 11$). Levels of confidence higher than 95% are obtained with an AGB model of initial mass $M = 1.5 M_\odot$ and case ST/5.

AGB Model	case	Case A ($N = 6$)		Case B ($N = 8$)		Case C ($N = 13$)		Case D ($N = 11$)	
(1)	(2)	χ_N^2	$P(\chi_N^2)$	χ_N^2	$P(\chi_N^2)$	χ_N^2	$P(\chi_N^2)$	χ_N^2	$P(\chi_N^2)$
$M = 1.3 M_\odot$	ST/12	4.7	58%	15.8	5%	18.2	15%	7.1	79%
	ST/15	3.7	72%	14.8	6%	17.5	18%	6.3	85%
	ST/18	4.9	56%	16.2	4%	19.6	11%	8.4	68%
$M = 1.5 M_\odot$	ST/3	3.0	81%	3.7	88%	6.7	92%	6.0	85%
	ST/5	1.7	95%	3.5	90%	5.5	96%	3.7	98%
	ST/6	2.0	92%	2.7	95%	6.1	94%	5.4	91%
$M = 2 M_\odot$	ST/6	2.6	86%	7.7	46%	11.2	59%	6.0	87%
	ST/9	2.1	91%	7.8	45%	10.9	62%	5.1	93%
	ST/12	3.1	80%	7.7	46%	11.6	56%	6.9	81%

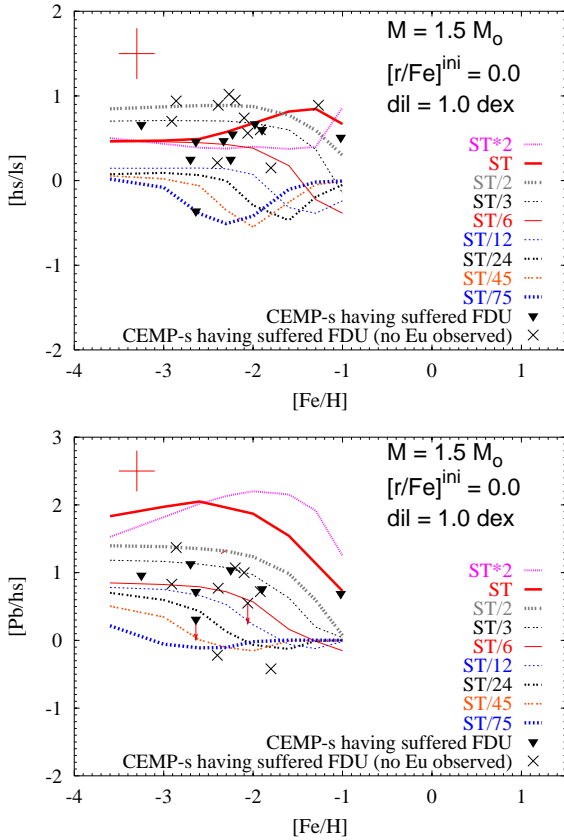


Figure 11. *Top Panel:* theoretical predictions of $[\text{hs}/\text{ls}]$ versus metallicity for AGB models with initial mass $M = 1.5 M_\odot$, a range of ^{13}C -pockets and $\text{dil} = 1.0$ dex, compared with CEMP-*s* observations (triangles). No initial *r*-process enhancement is assumed. To simplify the discussion, we represent only subgiants and giants having suffered the FDU (see text). CEMP-*s* stars without europium detection are indicated by crosses. *Bottom Panel:* the same as the top panel, but for $[\text{Pb}/\text{hs}]$ versus metallicity. Typical error bars are $\Delta[\text{hs}/\text{ls}] = \Delta[\text{Pb}/\text{hs}] = 0.3$; $\Delta[\text{Fe}/\text{H}] = 0.2$.

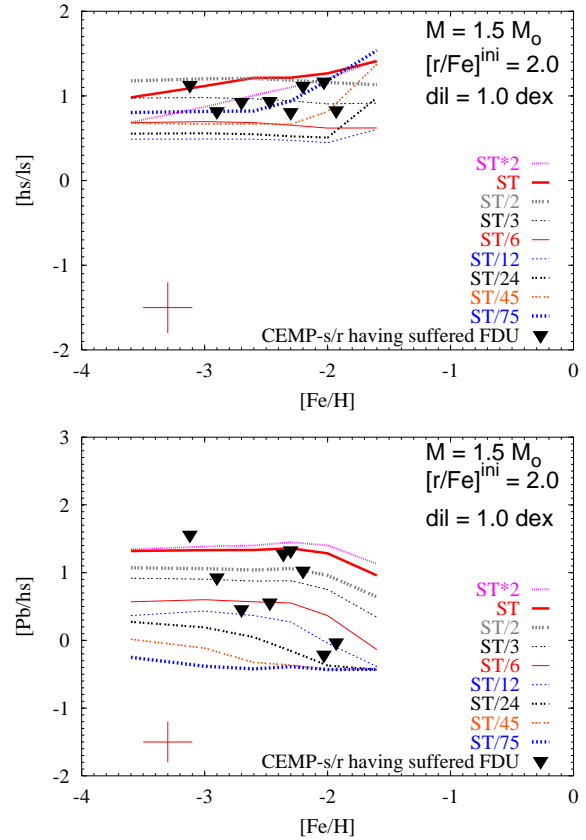


Figure 12. The same as Fig. 11, but for AGB models with $[\text{r}/\text{Fe}]_{\text{ini}} = 2$, as compared with CEMP-*s/r* stars having suffered the FDU (triangles).

observed star. HD 196944 is a giant having already suffered the FDU episode, requiring a dilution of the order of 1 dex or more. The difference between our predicted $[\text{La}/\text{Fe}]$ and the one observed in HD 196944 gives the first assessment of the dilution, afterward optimized with a more careful analysis of the uncertainties of the single species. An example is given in Fig. 13 for $M_{\text{ini}}^{\text{AGB}} = 1.5 M_\odot$, and cases from ST/3 down to ST/6. Here and in the following Figs. 13 to 16,

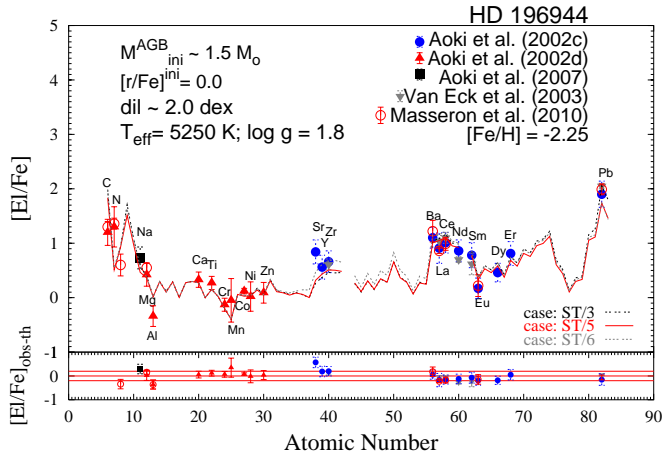


Figure 13. Spectroscopic $[\text{El}/\text{Fe}]$ abundances of the CEMP-sI giant HD 196944 compared with AGB models of initial mass $M = 1.5 M_{\odot}$, three ^{13}C -pockets (ST/3, ST/5, ST/9), and $\text{dil} \sim 2.0$ dex. Observations are from Aoki et al. (2002c,d, 2007), Van Eck et al. (2003) and Masseron et al. (2010). The lower panel displays the differences between observations and theoretical predictions (case ST/5), $[\text{El}/\text{Fe}]_{\text{obs-th}}$. The range between the two lines corresponds to an uncertainty of 0.2 dex. Here and in the following Figures $[\text{C}/\text{Fe}]$ and $[\text{N}/\text{Fe}]$ are not represented in bottom panel because they may be affected by extra-mixing (see Section 5.3).

the name of the star, its metallicity, the literature of the spectroscopic data, and the parameters of the AGB models adopted (i.e. initial mass, ^{13}C -pocket, dilution factor and initial r -process enhancement) are given in the inset. A solution is found for the case ST/5 (full line) with a dilution factor $\text{dil} = 2.0$ dex. This means that the material transferred from the AGB is 1% of the convective envelope of the observed star. The choice of the best fit is weighted on all the observed elements from carbon to lead, with particular attention to the three s -process peaks. AGB models of different initial masses, with proper choice of the dilution factor, may provide plausible solutions for the s -process elements: ST/15 and $\text{dil} = 1.1$ dex for $M_{\text{ini}}^{\text{AGB}} = 1.3 M_{\odot}$, ST/6 and $\text{dil} = 1.6$ dex for $M_{\text{ini}}^{\text{AGB}} = 1.4 M_{\odot}$ and ST/9 and $\text{dil} = 2.0$ dex for $M_{\text{ini}}^{\text{AGB}} = 2 M_{\odot}$ (Fig. 14). Significant differences between observed and predicted Na are found for $M_{\text{ini}}^{\text{AGB}} = 1.3$ and $2 M_{\odot}$ (~ 0.7 and 0.5 dex, respectively). The goodness of the fits is tested with a χ^2 distribution, by defining

$$\chi_N^2 = \sum_{i=1}^N \frac{(O_i - P_i)^2}{(\sigma_i)^2}, \quad (2)$$

where N is the number of elements considered, O_i is the observed abundance of the element i , P_i is the abundance predicted by the AGB model for the element i , σ_i is the uncertainty of the observed element i . Taking the number of elements N as degrees of freedom, we calculate the confidence level of the χ_N^2 test. The distribution function of χ_N^2 is $P(\chi_N^2)$, obtained from the related tables. The results for models presented in Figs. 13 and 14 are listed in Table 8. We considered different cases by changing the number of elements involved. In general, the theoretical interpretations are tested with the six s -elements Y, Zr, La, Nd, Sm and Pb (case A, columns 3 and 4). Note that the observed Na

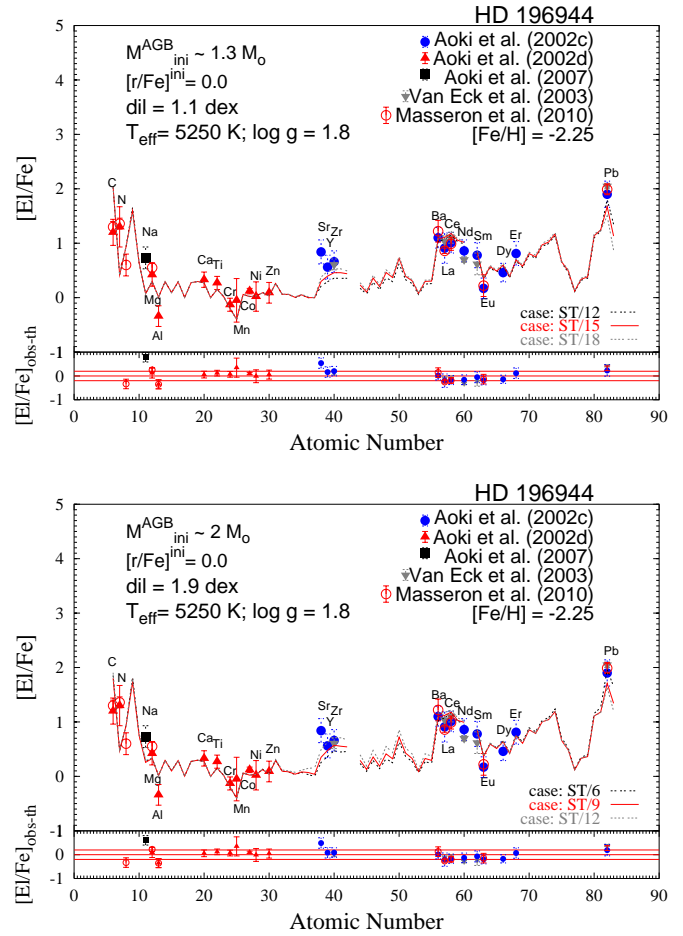


Figure 14. The same as Fig. 13, but for AGB models of initial mass $M = 1.3 M_{\odot}$, cases ST/12, ST/15, ST/18, $\text{dil} = 1.1$ dex (upper panel), and $M = 2 M_{\odot}$, cases ST/6, ST/9, ST/12, $\text{dil} = 1.9$ dex (bottom panel). The observed $[\text{Na}/\text{Fe}]$ is ~ 0.7 and 0.5 dex higher than the theoretical predictions, respectively. Differences between observations and theoretical predictions, $[\text{El}/\text{Fe}]_{\text{obs-th}}$, are shown for cases ST/15 and ST/9 (upper and bottom panels, respectively).

and Mg are important initial mass discriminators (case B, columns 5 and 6): levels of confidence higher than 95% are obtained only with AGB models of initial mass $M = 1.5 M_{\odot}$ and ^{13}C -pockets ST/5 - ST/6, even including other heavy elements as Ba, Ce, Eu, Dy, Er (cases C and D, last four columns).

Disagreements between predictions and observations remain for C, N, and Sr. A possibility to improve the C and N predictions is to hypothesise the occurrence of the Cool Bottom Processing (CBP, see Section 5.3), (Nollett et al. 2003; Busso et al. 2010).

Concerning Sr, all AGB models underestimate the observed $[\text{Sr}/\text{Fe}]$ ratio by about 0.4 dex. Note that the Sr abundance has been determined by using three lines, while Y and Zr seems to be more reliable with 7 and 6 lines detected, respectively.

For this star, the observed $[\text{La}/\text{Eu}]$ ratio is in agreement with a pure s -process contribution ($[\text{La}/\text{Eu}]_{\text{th}} = 0.74$, obtained with $[\text{r}/\text{Fe}]^{\text{ini}} = 0$).

AGB model of initial mass $M = 1.5 M_{\odot}$, case ST/5, dil

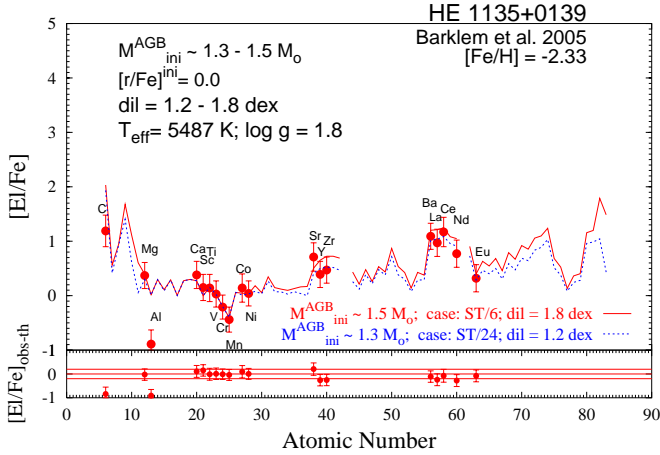


Figure 15. Spectroscopic $[El/Fe]$ abundances of the CEMP-sI giant HE 1135+0139 by Barklem et al. (2005), compared with two AGB stellar models of initial masses: $M_{\text{AGB}}^{\text{ini}} = 1.3 M_{\odot}$, case ST/24, $dil = 1.2$ dex (dashed line) and $M_{\text{AGB}}^{\text{ini}} = 1.5 M_{\odot}$, case ST/6, $dil = 1.8$ dex (solid line). We predict a $[Pb/Fe]_{\text{th}} \sim 1.0 - 1.8$. The observed $[Al/Fe]$ is ~ 1 dex lower than the solar value. The lower panel displays the differences between observations and theoretical predictions $[El/Fe]_{\text{obs-th}}$ for $M_{\text{AGB}}^{\text{ini}} = 1.5 M_{\odot}$ model. The range between the two lines corresponds to an uncertainty of 0.2 dex.

~ 2.0 dex and no initial *r*-process enhancement provide a theoretical interpretation for this giant.

HE 1135+0139 (Fig. 15)

Barklem et al. (2005) analysed a sample of 253 metal-poor halo stars during the HERES Survey (VLT/UVES), with a spectral resolution of $R \sim 20\,000$ ($S/N \sim 50$). One of them is the giant HE 1135+0139. No Pb has been detected in this star; however, many *s*-process elements are available: Sr, Y, Zr, Ba, La, Ce and Nd. Therefore, we can give a robust Pb prediction, within the range of the error bars. We evaluate the ^{13}C -pocket starting with the observed $[hs/ls] = 0.49$. Similarly to HD 196944, this CEMP-sI star has a low *hs* peak ($[hs/Fe] = 0.92$), requiring a high dilution factor depending on the AGB initial mass. In Fig. 15, we show two possible theoretical interpretations with $M_{\text{AGB}}^{\text{ini}} = 1.5 M_{\odot}$, $dil = 1.8$ dex, case ST/5 (full line) and $M_{\text{AGB}}^{\text{ini}} = 1.3 M_{\odot}$, $dil = 1.2$ dex, case ST/24 (dashed line). Solutions with a negligible dilution are discarded, in agreement with a giant after the FDU. We predict $[Pb/Fe]_{\text{th}} \sim 1.0 - 1.8$. The observed $[Al/Fe]$ is ~ 1 dex lower than the solar value, as observed in field metal-poor stars (Barklem et al. 2005).

5.2 How to fit CEMP-s/r stars

HE 0338-3945 (Fig. 16)

This CEMP-sII/r star was first analysed by Barklem et al. (2005). Subsequently, Jonsell et al. (2006) detected 33 species and provided upper limits for 6 elements, using a high-quality VLT-UVES spectra ($R = 30\,000 - 40\,000$; $S/N \sim 74$). This is a main-sequence star, with $T_{\text{eff}} = 6160 \pm 100$ K, $\log g = 4.13 \pm 0.33$ dex. The $[hs/ls]$ and $[Pb/hs]$ ratios determine the *s*-process distribution efficiency as described in Section 5.1 for the

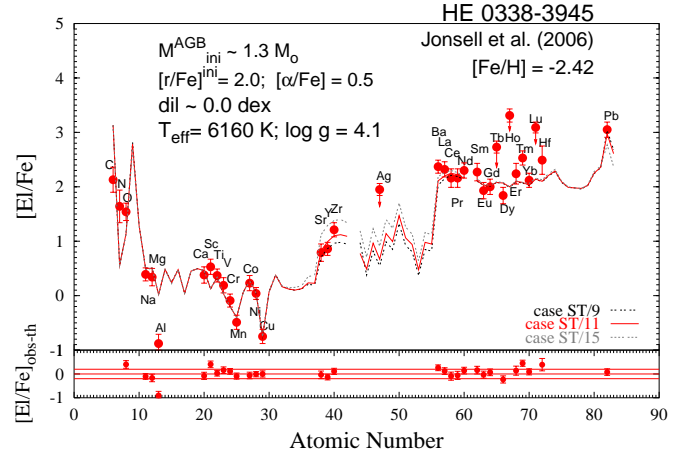


Figure 16. Spectroscopic $[El/Fe]$ abundances of the CEMP-sII/r main-sequence HE 0338-3945 by Jonsell et al. (2006), with AGB stellar models of $1.3 M_{\odot}$, cases ST/9, ST/11 and ST/15, and no dilution factor. Pure *s*-process AGB models predict $[Eu/Fe]_s = 1.2$, about 0.8 dex lower than that observed: an initial *r*-process enrichment of $[r/Fe]^{\text{ini}} = 2.0$ is needed. The lower panel displays the differences between observations and theoretical predictions (case ST/11), $[El/Fe]_{\text{obs-th}}$. The range between the two lines corresponds to an uncertainty of 0.2 dex. Four elements are not in agreement with the theoretical predictions (O, Al, Sc, Tm), while Ba, Dy, Hf lie within the uncertainties of the AGB models (see text).

giant HD 196944. In this case, no dilution is applied for low AGB initial masses, because of the high *s*-process enhancement observed in HE 0338-3945 ($[hs/Fe] \sim 2.3$). An interpretation of the observed abundances is obtained with AGB models of initial mass $1.3 M_{\odot}$, cases ST/9, ST/11, ST/15 and $dil = 0.0$ dex (see Fig. 16). Main-sequence/turnoff/subgiant stars have not suffered the FDU. Moreover, old main sequence stars of low mass ($M \sim 0.8 M_{\odot}$) have a very thin convective envelope and no large mixing between the *s*-rich material transferred from the AGB and the envelope of the observed star are expected contrary to the case of giants. As discussed in Section 2, the efficiency of mixing processes as thermohaline, gravitational settling and radiative levitation acting during the main-sequence phase is difficult to estimate. Then, for stars having not suffered the FDU we do not assume initial constraints on the dilution. If present, information about possible mixing provided by the dilution factor in main-sequence stars will be discussed in Section 6 and Paper III.

For a pure *s*-process prediction ($[r/Fe]^{\text{ini}} = 0$), we found a difference of about 0.7 dex between observed and predicted $[Eu/Fe]$. This is solved by adopting an initial *r*-enrichment of the interstellar cloud of $[r/Fe]^{\text{ini}} = 2.0$, which explains the observed $[La/Eu]$. The upper limit of Ag does not provide constraints for a possible initial *r*-enhancement of the elements lighter than Ba (see Section 3.1).

As discussed by Jonsell et al. (2006), C is uncertain due to the strong temperature sensitivity of CH molecule formation and 3D model calculations may add further uncertainties of about -0.5 to -0.3 dex (Asplund 2005). For N, a reasonable estimate of the NLTE and 3D effects may amount to -0.5 dex. The observed $[O/Fe]$ is slightly

underestimated by AGB models. [Al/Fe] is strongly subsolar, but NLTE effects may be important for Al (Asplund 2005; Baumüller & Gehren 1997; Andrievsky et al. 2008). [Sc/Fe] may be overestimated (Jonsell et al. 2006), indeed it appears enhanced compared to field halo stars. Note that AGBs do not synthesise copper: indeed [Cu/Fe] is negative, in accord with the observations of unevolved stars in the same range of metallicities (Bisterzo et al. 2004; Romano & Matteucci 2007). [Ba/Fe] is slightly higher than the AGB prediction; however, NLTE effects together with 3D models can decrease the abundances by about 0.3 dex Asplund (2004, 2005); Andrievsky et al. (2009). La could be underestimated, due to the incomplete hyperfine splitting (hfs) data. Dy and Tm are lower and higher by about 0.2 and 0.4 dex with respect to the case ST/11, respectively. For Pb an overionisation is possible, which would lead to a decrease of the observed abundance.

By increasing the number of TDUs (e.g. for AGB models of initial mass $1.5 M_{\odot}$; $dil \sim 0.8$ dex), the observed [Na/Fe]⁹ and [ls/Fe] are overestimated. Then, solution with AGB models of initial mass higher than $1.3 M_{\odot}$ are excluded for this star.

AGB model of initial mass $M = 1.3 M_{\odot}$, case ST/11, $dil = 0.0$ dex and $[r/Fe]^{ini} = 2.0$ provide a theoretical interpretation for this star.

5.3 Carbon and Nitrogen

For most CEMP-*s* and CEMP-*s/r* stars, the observed [C/Fe] and [N/Fe], as well as the carbon isotopic ratio $^{12}C/^{13}C$, are reproduced by AGB models. Spectroscopic observations of C and N in CEMP stars are affected by high uncertainties due to strong molecular bands, NLTE corrections or 3D hydrodynamical model atmospheres (Asplund 2005; Collet et al. 2007; Grevesse et al. 2007; Caffau et al. 2009). However, measurements in pre-solar grains of AGB origin (Zinner et al. 2006), which are more reliable than observations in CEMP-*s* stars, also show a disagreement from AGB predictions.

A large mixing, affecting C and N and decreasing the $^{12}C/^{13}C$ ratio, occurs during the red giant branch by the FDU¹⁰. However, it is not sufficient to explain the observed $^{12}C/^{13}C$ (e.g. see Abia et al. 2001 for disc C stars). Further extra-mixing has to be hypothesised during the following AGB phase to interpret the observations. To solve this problem, it was proposed that some material could be transported from the fully convective envelope into the underlying radiative region, down to the outer zone of the hydrogen shell, where partial H burning occurs. CBP is pre-

dicted to occur in low-mass AGB stars (see Nollett et al. 2003; Domínguez et al. 2004; Wasserburg et al. 1995, 2006; Busso et al. 2010), and may decrease ^{12}C in the envelope while ^{14}N increases (Wasserburg et al. 1995); consequently, [C/Fe] and $^{12}C/^{13}C$ also decrease, together with an increase of [N/Fe].

CBP is the most plausible hypothesis to reproduce the observations, although its efficiency is difficult to estimate because it may be affected by many physical processes (e.g., rotation, magnetic fields, thermohaline mixing).

5.3.1 $^{12}C/^{13}C$

In Table 9, we collected the isotopic ratio $^{12}C/^{13}C$ as well as [C/Fe], [N/Fe] and [O/Fe] for the CEMP-*s* and CEMP-*s/r* stars listed in Tables 2 (first group) and 3 (second group). The same references and labels are adopted here in columns 2, 5 and 11. When AGB models predict higher [C/Fe] ratio than the observed value, we simulate the occurrence of CBP by applying the method used for HD 196944 and HE 0338–3945. In column 12, comments about the hypothesis of extra-mixing are listed. The label ‘CBP’ means that CBP may explain the observed [C/Fe] and [N/Fe]. Most stars need the occurrence of a ‘CBP’. Only in four stars the observed [C/Fe] ratios agree with AGB predictions without involving extra-mixing: CS 22880–074, CS 30315–91, HE 0507–1653 and HE 1429–0551. The first two show also relatively high lower limits for $^{12}C/^{13}C$ ($> 40 - 60$). If a CBP overestimates the observed [N/Fe], we adopt the label “low [N/Fe]_{obs}”. Five stars have [N/Fe] higher than [C/Fe], but only two of them are incompatible with the hypothesis of a CBP (label “high [N/Fe]_{obs}”; CS 30322–023, HE 1031–0020).

Several stars show $^{12}C/^{13}C \sim 10$ in agreement with Early-Type CH stars (see e.g., Van Eck et al. 2003). An exception is V Ari, a giant for which Beers et al. (2007a) detected $^{12}C/^{13}C = 90 \pm 10$. $^{12}C/^{13}C$ lower limits are measured for CS 29497–030 (> 10), HE 0143–0441, HE 0012–1441 and HE 1410–0004 ($\gtrsim 3$), HE 2232–0603 (> 6), CS 22967–07 (> 60), as well as CS 22880–074 and CS 30315–91. Theoretical AGB predictions are strongly enhanced: $(^{12}C/^{13}C)_{th} \sim 2 - 3 \times 10^4$ for AGB models of initial mass $M = 1.3 M_{\odot}$ and 2×10^5 for $M = 1.5 M_{\odot}$. This confirms that an extra-mixing must be assumed to reduce the ^{12}C observed in the envelope of CEMP-*s* stars.

Another mechanism may affect the C and N ratios during the AGB phase. Low mass stars with [Fe/H] < -2.5 may experience a huge thermal pulse (Hollowell et al. 1990; Iwamoto et al. 2004; Cristallo et al. 2009; Campbell & Lattanzio 2008; Lau et al. 2009; Suda & Fujimoto 2010; Straniero et al. 2010). When the CNO abundances in the envelope are low, the entropy barrier provided by the H-burning shell may vanish and protons are ingested from the envelope down to the He-intershell during the first fully developed thermal pulse resulting in a violent H-burning. During this episode large amount of ^{13}C and ^{14}N are produced, which are mixed to the surface by an extremely deep TDU, thus decreasing the $^{12}C/^{13}C$ ratio sensibly, while [N/Fe] increases. Note that the mass and metallicity limits for the occurrence of this deep TP would be decreased if an initial O enhancement is adopted. However, different models may provide contrasting

⁹ Note that NLTE effects further decrease the observed [Na/Fe] (Baumüller et al. 1998; Andrievsky et al. 2007).

¹⁰ As anticipated in Section 2, during the FDU, the material processed in the hydrogen shell is brought to the surface, changing the CNO isotopic composition of the envelope. The main isotopes involved are ^{13}C , ^{14}N and ^{17}O which increase, while ^{12}C , ^{15}N and ^{18}O decrease (the observed isotopic ratio $^{14}N/^{15}N$ increases by a factor of 6). From the point of view of the observations, since ^{12}C decreases of 30% and ^{13}C increases of a factor of 2 ~ 3 , the evidence of the FDU is confirmed by the reduction of the $^{12}C/^{13}C$ ratio to about 20 (Boothroyd & Sackmann 1988; Busso et al. 1999).

Table 9. $^{12}\text{C}/^{13}\text{C}$, $[\text{C}/\text{Fe}]$, $[\text{N}/\text{Fe}]$ and $[\text{O}/\text{Fe}]$ observed in CEMP-*s* and CEMP-*s/r* stars listed in Tables 2 (first group) and 3 (second group). References and labels are the same as in Tables 2 and 3. Goswami et al. 2005, G05, using low resolution spectra detected $^{12}\text{C}/^{13}\text{C}$ in several CEMP-*s*. For $^{12}\text{C}/^{13}\text{C}$ measured by C06 (Cohen et al. 2006), the first value is detected by using the C₂ band, the second by using the CH band.

Stars (1)	Ref.s (2)	T_{eff} (3)	$\log g$ (4)	FDU (5)	$[\text{Fe}/\text{H}]$ (6)	$^{12}\text{C}/^{13}\text{C}$ (7)	$[\text{C}/\text{Fe}]$ (8)	$[\text{N}/\text{Fe}]$ (9)	$[\text{O}/\text{Fe}]$ (10)	Type (11)
BD +04°2466	P09	5100	1.8	yes	-1.92	15^{+5}_{-3}	1.17	1.1	0.3	sI/-
CS 22183-015	C06	5620	3.4	no?	-2.75	8-10	1.92	1.77	-	sII/rII
CS 22880-074	A02,A07	5850	3.8	no?	-1.93	>40	1.3	-0.1	-	sI
CS 22881-036	PS01	6200	4.0	no	-2.06	40	1.96	1	-	sII
CS 22898-027	A02,A07	6250	3.7	no	-2.26	15 ± 5	2.2	0.9	-	sII/rII
CS 22942-019	A02	5000	2.4	yes	-2.64	8 ± 2	2	0.8	-	sI
"	M10	5100	2.5	"	-2.43	12 ± 1	2.14	1.15	0.97	"
CS 22948-27	BB05	4800	1.8	yes	-2.47	-	2.43	1.75	-	sII/rII
"	A07	5000	1.9	"	-2.21	10 ± 3	2.12	2.43	-	"
CS 29497-030	I05	7000	4.1	no	-2.57	>10(S04)	2.3	2.12	1.48	sII/rII
CS 29497-34	BB05	4800	1.8	yes	-2.9	-	2.63	2.38	-	sII/rII
"	A07	4900	1.5	"	-2.91	12 ± 4	2.72	2.63	-	"
CS 30301-015	A02,A07	4750	0.8	yes	-2.64	6 ± 2	1.6	1.7	-	sI
CS 30322-023	M06	4100	-0.3	yes	-3.5	4 ± 1	0.6	2.81	0.63	sI
"	M10	4100	-0.3	yes	-3.39	4 ± 1	0.8	2.91	0.63	"
CS 31062-012	A02,A07,A08	6250	4.5	no	-2.55	15 ± 5	2.1	1.2	-	sII/rII
CS 31062-050	A02	5600	3	no?	-2.42	8 ± 2	2	1.2	-	sII/rII
HD 26	VE03	5170	2.2	yes	-1.25	$\sim 6(\text{G05})$	-	-	-	sII
"	M10	4900	1.5	yes	-1.02	9 ± 2	0.68	0.94	0.36	"
HD 5223	G06	4500	1.0	yes	-2.06	$\sim 6(\text{G05})$	1.57	-	-	sII/-
HD 187861	VE03	5320	2.4	yes	-2.30	-	-	-	-	sII/rI
"	M10	4600	1.7	"	-2.36	10 ± 1	2.02	2.18	1.40	"
HD 196944	A02,A07	5250	1.8	yes	-2.25	5 ± 1	1.2	0.04	-	sI
"	M10	5250	1.7	"	-2.19	"	1.30	1.41	0.63	"
HD 206983	M10	4200	0.6	yes	-0.99	$5\pm 3; 9(\text{DP08})$	0.50	1.21	<0.23	sI
HD 209621	GA10	4500	2.0	yes	-1.93	$\sim 9(\text{G05})$	1.25	-	-	sII/rI
HD 224959	M10	4900	2.0	yes	-2.06	4 ± 2	1.77	1.88	1.10	sII/rII
HE 0143-0441	C06	6240	3.7	no	-2.31	>4	1.98	1.73	-	sII/rI
HE 0212-0557	C06	5075	2.15	yes	-2.27	4.0 ± 1.3	1.74	1.09	-	sII/-
HE 0336+0113	C06	5700	3.5	no?	-2.68	$2.5\pm 1; 7.5^a$	2.25	1.6	-	sII
HE 0338-3945	J06	6160	4.13	no	-2.42	~ 10	2.13	1.55	1.4	sII/rII
HE 1031-0020	C06	5080	2.2	yes	-2.86	5 ± 1.5	1.63	2.48	-	sI/-
HE 1305+0007	G06	4750	2.0	yes	-2.03	10	1.84	-	-	sII/rII
"	Beers07	4560	1.0	"	-2.5	9 ± 2	2.4	1.9	0.8	"
HE 1434-1442	C06	5420	3.15	yes	-2.39	5 ± 1.5	1.95	1.4	-	sI/-
HE 1509-0806	C06	5185	2.5	yes	-2.91	4 ± 1.3	1.98	2.23	-	sII(/-)
HE 2148-1247	C03	6380	3.9	no	-2.3	10	1.91	1.65	-	sII/rII
HE 2158-0348	C06	5215	2.5	yes	-2.7	$6\pm 1.8; 3-5^a$	1.87	1.52	-	sII
HE 2232-0603	C06	5750	3.5	no?	-1.85	>6	1.22	0.47	-	sI/-
LP 625-44	A02,A06	5500	2.5	yes	-2.7	$\sim 20(\text{A01})$	2.25	0.95	1.85:	sII/rII
V Ari	VE03	3580	-0.2	yes	-2.4	-	-	-	-	sI/-
"	Beers07	3500	0.5	"	-2.5	90 ± 10	1.5	1.5	0.2	"
CS 22891-171	M10	5100	1.6	yes	-2.25	6 ± 2	1.56	1.67	<0.79	sII/rII
CS 22956-28	M10	6700	3.5	no	-2.33	5 ± 2	1.84	1.85	<2.47	sI/-
"	S03	6900	3.9	"	-2.08	-	1.34	-	0.5:	"
CS 22967-07	L04	6479	4.2	no	-1.81	>60	1.8	0.9	0.85	sII(/-)
CS 29495-42	L04	5544	3.4	no?	-1.88	7 ± 2	1.3	1.3	0.64	sI
CS 30315-91	L04	5536	3.4	no?	-1.68	>60	1.3	0.4	0.51	sI(/-)
CS 30323-107	L04	6126	4.4	no	-1.75	9 ± 2	1.1	0.8	0.84	sII(/-)
CS 30338-089	A07	5000	2.1	yes	-2.45	12 ± 4	2.06	1.27	-	sII(/rII) (L04)
HE 0012-1441	C06	5730	3.5	no?	-2.52	>3	1.59	0.64	-	sI/-
HE 0024-2523	L03,C04	6625	4.3	no	-2.72	$6\pm 1; \sim 7(\text{C04})$	2.6	2.1	0.4	sII(/-)
HE 0206-1916	A07	5200	2.7	yes	-2.09	15 ± 5	2.1	1.61	-	sII/-
HE 0322-1504	Beers07	4460	0.8	yes	-2	6 ± 2	2.3	2.2	-	s/-
HE 0507-1430	Beers07	4560	1.2	yes	-2.4	9 ± 2	2.6	1.7	1.1	s/-
HE 0507-1653	A07	5000	2.4	yes	-1.38	$40^{+20}_{-12}; \sim 7(\text{G05})$	1.29	0.8	-	sII/-
HE 1001-0243	M10	5000	2.0	yes	-2.88	30 ± 5	1.59	1.20	<1.92	sI
HE 1045-1434	Beers07	4950	1.8	yes	-2.5	20 ± 2	3.2	2.8	1.8	s/-
HE 1157-0518	A07	4900	2	yes	-2.34	15 ± 5	2.15	1.56	-	sII/-
HE 1319-1935	A07	4600	1.1	yes	-1.74	8 ± 3	1.45	0.46	-	sII/-
HE 1410-0004	C06	5605	3.5	no?	-3.02	>3	1.99	-	1.18	sI/-
HE 1419-1324	M10	4900	1.8	yes	-3.05	12 ± 2	1.76	1.47	<1.19	sI
HE 1429-0551	A07	4700	1.5	yes	-2.47	$30^{+20}_{-10}; \sim 2(\text{G05})$	2.28	1.39	-	sII/-
HE 1443+0113	C06	4945	1.95	yes	-2.7	5 ± 1.5	1.84	-	-	sI/-
HE 1447+0102	A07	5100	1.7	yes	-2.47	25 ± 10	2.8	1.39	-	sII/-
HE 1523-1155	A07	4800	1.6	yes	-2.15	$\sim 2.5(\text{G05})$	1.86	1.67	-	sII/-
HE 1528-0409	A07	5000	1.8	yes	-2.61	$12\pm 5; \sim 2.4(\text{G05})$	2.42	2.03	-	sII/-
HE 2221-0453	A07	4400	0.4	yes	-2.22	$10\pm 4; \sim 13(\text{G05})$	1.83	0.84	-	sII/-
HE 2228-0706	A07	5100	2.6	yes	-2.41	15^{+5}_{-3}	2.32	1.13	-	sII/-

^a The first value estimated using the C₂ band, the second using the CH band.

results because different prescriptions are adopted. For instance, Lau et al. (2009) find an enhancement in C, but only a marginal enrichment in N. Similar behaviours are obtained for low mass models by Campbell & Lattanzio (2008) and Suda & Fujimoto (2010).

In intermediate mass stars ($3 < M/M_{\odot} \lesssim 8$), the Hot Bottom Burning (HBB) also modifies the final C and N abundances (Sugimoto 1971, Iben 1973, Karakas & Lattanzio 2003, Ventura & D’Antona 2005), destroying C and producing a large amount of N (NEMPs, nitrogen-enhanced metal-poor stars Johnson et al. 2007). Moreover, AGB models of intermediate mass and halo metallicity seem to be affected by extreme mixing, as hot TDU (when the envelope penetrates burning protons at its base), which may modify the stellar structure of the star and its evolution (Herwig 2004; Goriely & Siess 2004; Campbell & Lattanzio 2008; Lau et al. 2009). However, the mass of the He-intershell is smaller than low mass AGBs and also the ^{13}C -pocket and the TDU efficiency are reduced. Moreover, the maximum temperature reached during the TP is high enough to efficiently activate the $^{22}\text{Ne}(\alpha, n)^{25}\text{Mg}$ reaction. Consequently, the production of the first s -peak should be favoured, while the contribution of the ^{13}C -pocket to the s -process elements is marginal in these stars. Because there are no information about the consequences of hot TDU on the s -process distribution so far, these models are not considered in the present discussion.

In this paper, AGB models with specific range of initial masses ($M \sim 1.3 \div 2 M_{\odot}$) were considered. Further studies would be necessary to establish the contribution by AGB stars with initial mass out of this range. Low metallicity AGB models with initial mass below the adopted range would help to understand the effects of the proton ingestion episode on C and N, as well as on the s -process elements distribution. The need of stars with low initial mass has also been invoked by Izzard et al. (2009) to explain the high fraction of carbon enhanced stars among very metal-poor stars. However, additional sources of carbon, besides the nucleosynthesis of AGB stars in binary systems, may be hypothesised (see e.g., Carollo et al. 2011).

6 SUMMARY OF THE RESULTS

The results are summarised in Tables 10 and 11. In Table 10, 55 CEMP- s and CEMP- s/r stars with a great number of observations among the s -elements are listed, and in Table 11 we report 36 CEMP- s and CEMP- s/r stars for which a limited number of ls and hs elements is detected (in several cases only Sr and Ba). All the stars lie in a metallicity range $-3 \lesssim [\text{Fe}/\text{H}] \lesssim -1.7$. The only exceptions are five CH stars with $[\text{Fe}/\text{H}] \sim -1.2$ (CS 29503–010, HD 26, HD 206983, HE 0507–1653 and HE 1152–0355), which may be considered as a link between CEMP- s and Ba stars of nearly solar metallicity, because their C and s -enrichment are due to the same physical reasons (Paper III). In columns 1 to 3 in Tables 10 and 11, the name of the stars, their references and metallicities are listed. In column 4 we distinguish between main-sequence/turnoff or subgiants before and giants after the FDU (labeled ‘no’ and ‘yes’, respectively). The class of each star is specified in column 5. In columns 6 to 9,

AGB models that best reproduce the spectroscopic observations are listed: the AGB initial mass (in solar masses), the ^{13}C -pocket, the dilution factor, and the initial r -process enhancement.

Robust predictions for s -process elements are provided for stars in Table 10, while a degeneracy of solutions may equally interpret the limited number of observations for stars in Table 11. In column 10 of Table 10, $[\text{Pb}/\text{Fe}]_{\text{th}}$ predictions are given within ± 0.3 dex of uncertainties. In general, reasonable solutions are obtained by using AGB models with initial masses in the range $1.3 \leq M/M_{\odot} \leq 2$. Otherwise, in column 11 of Table 10 and in column 10 of Table 11, we report the elements that provide a constraint on AGB models. The label ‘FDU’ means that the only constraint is given by the occurrence of the FDU, in agreement with a high dilution. For instance, CEMP- s II giants need high AGB initial mass, because high s -process enhancements ($[\text{hs}/\text{Fe}] = 2$) are obtained together with a large dilution factor ($\text{dil} \sim 1$ dex) only if $M_{\text{ini}}^{\text{AGB}} = 1.5 - 2 M_{\odot}$ are adopted. Indeed, AGB models with $M_{\text{ini}}^{\text{AGB}} = 1.3 M_{\odot}$ underwent 5 TDUs, with a maximum $[\text{hs}/\text{Fe}] \sim 2$.

A range of s -process efficiencies was adopted by Busso et al. (2001) in order to interpret the observed $[\text{hs}/\text{ls}]$ and $[\text{Pb}/\text{hs}]$ ratios of disc stars; Käppeler et al. (2010) included in their analysis recent spectroscopic observations of different stellar populations (Ba stars, CH stars, Post-AGB, CEMP- s and CEMP- s/r stars) sustaining this hypothesis. We confirm the need of a spread of ^{13}C -pocket efficiencies. In Fig. 17, we display the number of stars (taken from Table 10) as a function of the strength of the ^{13}C -pocket, for AGB models of initial mass $M = 1.3$ and $1.35 M_{\odot}$ (left panel) and $M = 1.4, 1.5$ and $2 M_{\odot}$ (right panel). The most common ^{13}C -pockets are close to ST/12 for $M_{\text{ini}}^{\text{AGB}} = 1.3 - 1.35 M_{\odot}$ and ST/4 for $M_{\text{ini}}^{\text{AGB}} = 1.4 - 2 M_{\odot}$. One finds that s -process efficiencies below $\sim \text{ST}/24$ are rare (CS 22942–019, CS 31062–012, HE 0336+0113, V Ari, HE 1135+0139, HD 189711, as well as CS 22891–171, CS 22956–28, for which $[\text{Pb}/\text{hs}] \sim 0$ are observed).

In Table 10, seventeen stars lie on the main-sequence, and ten of them can be only interpreted with AGB models of low initial mass and negligible dilutions. Note that, in several stars, the main constraint of the initial mass model is given by Na. This seems to indicate that no efficient mixing takes place in main-sequence stars, in agreement with model calculations by Thompson et al. (2008), (see also Vauclair 2004; Richard et al. 2002), who showed that gravitational settling can confine the efficiency of thermohaline mixing in these low mass metal-poor stars. Two stars showing a low s -process enhancement, BS 16080–175 and CS 22964–161, may only be interpreted with AGB models with $\text{dil} = 0.5 - 1.0$ dex. Three other stars do not show any dilution constraints.

7 CONCLUSIONS

We have compared spectroscopic observations of 94 CEMP- s and CEMP- s/r stars collected from the literature with AGB models of different initial masses and metallicities presented in Paper I.

All CEMP- s stars are old halo main-sequence/turnoff or giants of low initial mass ($M < 0.9 M_{\odot}$). The most plausible

Table 10. Summary of theoretical interpretations for the stars listed in Table 2. AGB initial mass, ^{13}C -pocket, dilution factor, and initial r -enhancement are shown. For stars, where Pb is not observed yet, we provide theoretical predictions. The elements used for constraining the AGB models are listed in column 11 (values in brackets are very uncertain). If Eu is not detected we add the symbol (*) in column 9. In these cases, an average value of $[\text{r}/\text{Fe}]^{\text{ini}} = 0.5$ is adopted (see text).

Stars (1)	Ref. (2)	[Fe/H] (3)	FDU (4)	Type (5)	$M_{\text{ini}}^{\text{AGB}}$ (6)	pocket (7)	dil (8)	$[\text{r}/\text{Fe}]^{\text{ini}}$ (9)	[Pb/Fe] _{th} (10)	NOTE (11)
BD +04°2466	P09,I10,Z09	-1.92,-2.10	yes	sI/-	1.3	ST/9	0.9	0.5*	-	Na ([Fe/H] _{th} = -2)
"	"	"	"	"	1.5;2	ST/3	1.8	0.5*	-	C, ([Fe/H] _{th} = -1.8)
BS 16080-175	T05	-1.86	no	sII	1.5	ST/3	1.2	0.7	-	-
"	"	"	"	"	1.35	ST/9	0.6	"	-	"
"	"	"	"	"	2	ST/6	1.2	"	-	"
BS 17436-058	T05	-1.90	yes	sI	1.5	ST/5	1.6	0.7	-	-
"	"	"	"	"	1.4	ST/9	1.2	-	-	-
"	"	"	"	"	1.3	ST/12	0.7	-	-	-
"	"	"	"	"	2	ST/8	1.5	-	-	-
CS 22183-015	A07,C06	-2.75	no?	sII/rII	1.3	ST/12	0.0	1.5	-	Na, Sr, Y
"	JB02,T05,Lai07	-3.17	yes	"	1.5	ST/2	1.2	-	-	FDU
"	"	"	"	"	2	ST/3	1.2	-	-	FDU
CS 22880-074	A07,A02c,d	-1.93	no?	sI	1.3	ST/6	0.9	0.0	-	Na, Y
"	"	"	"	"	1.2	ST/6	0.4	-	-	"
CS 22881-036	PS01	-2.06	no	sII	1.3	ST/8	0.0	0.5	2.7	Na
CS 22887-048	T05	-1.70	no	sII/rI	1.4	ST/2	0.0	1.0	-	-
"	"	"	"	"	1.5;2	ST×1.2	0.3	"	-	-
CS 22898-027	A07,A02c,d	-2.26	no	sII/rII	1.3	ST/12	0.0	2.0	-	Na, ls
CS 22942-019	A02c,d,PS01,Sch08,M10	-2.64,-2.43	yes	sI	2	ST/50	0.7	0.5	-	Na, FDU
CS 22948-27	BB05,A07	-2.47,-2.21	yes	sII/rII	1.5	ST/9	0.8	1.5	-	FDU ([Na,ls/Fe] _{obs} low)
"	"	"	"	"	(1.35)	(ST/15)	(0.4)	-	-	Na (FDU)
"	"	"	"	"	2	ST/18	0.7	-	-	FDU ([Na,ls/Fe] _{obs} low)
CS 22964-161A/B	T08	-2.39	no	sI	1.3	ST/12	0.9	0.5	-	Na
"	"	"	"	"	1.2	ST/15	0.4	-	-	-
CS 29497-030	I05	-2.57	no	sII/rII	1.35	ST/9	0.0	2.0	-	Na,Mg; (hs high)
CS 29497-34	BB05,A07	-2.90	yes	sII/rII	2	ST/9	1.0	1.5	-	FDU, Na
CS 29513-032	R10	-2.08	no?	sI	1.2	ST/9	0.3	0.3	-	-
"	"	"	"	"	1.3	ST/9	1.4	-	-	-
"	"	"	"	"	1.5;2	ST/3	2.4	-	-	-
CS 29526-110	A07,A02c,d,A08	-2.38,-2.06	no	sII/rII	1.3	ST/6	0.0	1.5	-	Na, Mg
CS 29528-028	A07	-2.86	no	sII/-	2	ST/12	0.0	0.5*	3.8	Na, high [ls,hs/Fe] _{obs}
CS 30301-015	A07,A02c,d	-2.64	yes	sI	1.5	ST/9	1.8	0.0	-	Na, Mg
CS 30322-023	M06,A07,M10	-3.50,-3.25	yes	sI	1.5;2	ST/3	2.5	-1.0	-	Na
CS 31062-012	A07,A02c,d,A08	-2.55	no	sII/rII	1.3	ST/30	0.0	1.5	-	Na, ([ls/Fe] _{obs} low)
CS 31062-050	JB04,A07,A06,A02c,d	-2.42	no?	sII/rII	1.3	ST/12	0.2	1.6	-	Na
HD 26	VE03,M10	-1.25,-1.02	yes	disc (sII)	1.5;2	ST/2	1.0	0.0	-	FDU
HD 5223	G06	-2.06	yes	sII/-	2	ST/15	1.2	0.5*	-	Na, FDU
HD 187861	(VE03)*,M10	-2.36	yes	sII/rI	1.4	ST/5	1.0	1.3	-	Mg
HD 189711	VE03	-1.80	yes	sI/-	1.5;2	ST/24	0.9	0.5*	-	FDU
HD 196944	A07,A02c,d,VE03,M10	-2.25	yes	sI	1.5	ST/5	2.0	0.0	-	Na
HD 198269	VE03	-2.20	yes	sI/-	1.5;2	ST/2	1.5	0.5*	-	FDU
HD 201626	VE03	-2.10	yes	sII/-	1.5;2	ST/3	1.3	0.5*	-	FDU
HD 206983	M10, JP01	-0.99,-1.43	yes	disc (sI)	1.3	~ ST	0.7	0.5	-	-
"	"	"	"	"	1.5;2	~ ST	1.6	"	-	-
HD 209621	GA10	-1.93	yes	sII/rI	2	ST/15	0.9	1.0	-	FDU; ([Na/Fe] _{obs} low)
HD 224959	VE03,M10	-2.20,-2.06	yes	sII/rII	1.5;2	ST/3	1.0	1.6	-	FDU
HE 0143-0441	C06	-2.31	no	sII/rI	1.3	ST/9	0.0	1.0	-	-
"	"	"	"	"	1.5	ST/3	0.6	-	-	"
"	"	"	"	"	2	ST/5	1	-	-	"
HE 0202-2204	B05	-1.98	yes	sI	1.3	ST/9	0.7	0.0	2.0	-
"	"	"	"	"	1.5	ST/3	1.6	-	-	Mg
"	"	"	"	"	2	ST/6	1.7	-	-	-
HE 0212-0557	C06	-2.27	yes	sII/-	2	ST/8	0.8	0.5*	3.0	FDU; ([Na,ls/Fe] _{obs} low)
HE 0231-4016	B05	-2.08	no	sI/-	1.2	ST/12	0.2	0.5*	-	-
"	"	"	"	"	1.3	ST/15	0.7	"	-	-
"	"	"	"	"	1.5;2	ST/5	1.6	-	-	-
HE 0336+0113	C06	-2.68	no?	sII	1.4	ST/55	0.0	0.5	-	Mg
"	"	"	"	"	1.5	ST/45	0.2	-	-	-
"	"	"	"	"	2	ST/45	0.3	-	-	-
HE 0338-3945	J06	-2.42	no	sII/rII	1.3	ST/11	0.0	2.0	-	Na,Mg,ls
HE 0430-4404	B05	-2.07	no	sI/-	1.2	ST/9	0.0	0.5*	-	-
"	"	"	"	"	1.3	ST/15	0.7	"	-	-
"	"	"	"	"	1.5;2	ST/3	1.5	"	-	-
HE 1031-0020	C06	-2.86	yes	sI/-	1.3	ST/15	0.8	0.5*	-	FDU
"	"	"	"	"	1.4	ST/5	1.2	"	-	FDU, (Mg)
"	"	"	"	"	2	ST/5	1.6	"	-	FDU, (Mg)
HE 1105+0027	B05	-2.42	no	sII/rII	1.3	ST/9	0.0	1.8	3.0	(Mg)
"	"	"	"	"	2	ST/3	0.6	-	-	-
HE 1135+0139	B05	-2.33	yes	sI	1.3	ST/24	1.2	0.0	1.0	-
"	"	"	"	"	1.5;2	ST/6	1.8	-	1.8	-
HE 1152-0355	G06	-1.27	yes	disc (sI/-)	1.5;2	ST/2	1.0;1.2	0.0*	2.0	FDU
HE 1305+0007	G06	-2.03	yes	sII/rII	2	ST/15	0.4	2.0	-	(FDU)
HE 1430-1123	B05	-2.71	no	sII/-	1.3	ST/12	0.2	0.5*	-	Mg
"	"	"	"	"	2	ST/5	1	"	-	(Mg)
HE 1434-1442	C06	-2.39	yes	sI/-	1.3	ST/15	0.8	0.5*	-	Na
"	"	"	"	"	1.4	ST/12	1.2	-	-	Na
HE 1509-0806	C06	-2.91	yes	sII(/-)* ^a	1.4	ST/18	0.7	(0.5*) ^b	-	FDU; (Mg)
"	"	"	"	"	2	ST/12	1.2	-	-	-
HE 2148-1247	C03	-2.30	no	sII/rII	1.35	ST/9	0.0	2.0	-	Mg,ls
"	"	"	"	"	(2)	(ST/6)	(0.7)	-	-	(Mg)
HE 2150-0825	B05	-1.98	no	sI/-	1.2	ST/15	0.2	0.5*	-	-
"	"	"	"	"	1.3	ST/15	0.7	-	-	-
"	"	"	"	"	1.5;2	ST/5	1.5	-	-	-
HE 2158-0348	C06	-2.70	yes	sII	1.5	ST/5	1.4	0.5	-	FDU
"	"	"	"	"	2	ST/9	1.4	-	-	-
HE 2232-0603	C06	-1.85	no?	sI/-	1.2	ST/12	0.4	0.5*	-	ls
"	"	"	"	"	1.3	ST/12	1.0	-	-	-
HKII 17435-00532	R08	-2.23	yes	sI	1.5	ST/12	1.8	0.3	1.4	Na
"	"	"	"	"	"	ST/5	2.1	"	1.7	Y
LP 625-44	A02,A06	-2.70	yes	sII/rII	1.5	ST/8	0.8	1.5	-	Na,Mg
V Ari	VE03	-2.40	yes	sI/-	1.5	ST/30	0.9	0.5*	-	FDU
SDSS 0126+06	A08	-3.11	no	sII/-	1.4	ST/12	0.0	0.5*	-	high [ls,hs/Fe], ([Na/Fe] _{obs} low)
"	"	"	"	"	1.5;2	ST/6;ST/12	0.4	-	-	(Na,Mg low)
SDSSJ 0912+0216	B10	-2.50	no	sII/rI	1.3	ST/18	0.6	1.0	-	Na
SDSSJ 1349-0229	B10	-3.00	no	sII/rII	1.35	ST/15	0	1.5	-	Na,Mg

^a The solution provided here interprets the spectroscopic observations by Masseron et al. (2010). The abundances by Van Eck et al. (2003) are more uncertain due to the presence of molecular band contaminations in the spectra.

^b For this star a low upper limit is measured for Eu.

Table 11. The same as Table 10, but for the CEMP-*s* and CEMP-*s/r* stars listed in Table 3. The symbol \oplus indicates that all the solutions with AGB initial masses in the range $1.3 \leq M/M_{\odot} \leq 2$ are accepted. ^{13}C -pockets between brackets indicate very uncertain solutions due to the limited number of spectroscopic observations.

Star (1)	Ref. (2)	[Fe/H] (3)	FDU (4)	Type (5)	$M_{\text{ini}}^{\text{AGB}}$ (6)	Pocket (7)	dil (8)	[r/Fe] ⁱⁿⁱ (9)	NOTE (10)
CS 22891–171	M10	-2.25	yes	sII/rII	2	ST/45	0.3	1.8	(FDU)
CS 22956–28	M10,S03	-2.33,-2.08	no	sI/–	1.3	ST/80	0.0	0.5*	[hs/lr] \sim -0.6
CS 22960–053	A07	-3.14	yes	sI/–	1.5 ^c	(ST/30)	(1.7)	0.5*	-
CS 22967–07	L04	-1.81	no	sII(/–)	1.3	ST/9	0.0	(0.0*)	Na
CS 29495–42	L04	-1.88	yes	sI	1.3	ST/18	0.9	0.5	Na, Sr
CS 29503–010	A07	-1.06	no	disc (sII(/–))	1.3 ^c	ST/2 - ST/3	0.0	0.5*	Na
CS 29509–027	S03	-2.02	no	sI/–	1.5 ^c	ST - ST/18	0.0 - 1.5	0.5*	-
CS 30315–91	L04	-1.68	no?	sI/–	1.5 ^c	ST/3	1.6	(0.0*)	-
CS 30323–107	L04	-1.75	no	sII(/–)	1.3	ST/3	0.3	(0.0*)	(Na)
CS 30338–089	A07	-2.45	yes	sII/–	1.5 – 2	ST/2	\sim 0.5	0.5*	FDU (Na)
"	L04	-1.75	"	sII(/rII)	"	ST/2 - ST/3	\sim 0.5	1.8	FDU (Na)
G 18–24 ^a	I10	-1.62	no	(sI/–) ^a	1.3 ^c	ST/6	1.0	0.5*	-
HE 0012–1441	C06	-2.52	no?	sI/–	1.4 – 2	(ST/60)	0.0 – 1.0	0.5*	Mg
HE 0024–2523	L03	-2.70	no	sII(/–)	1.3	ST/9	0.0	(0.0*)	(Na),Mg
HE 0131–3953	B05	-2.71	no	sII/rII	1.3	ST/12	0.0	1.5	(Mg)
HE 0206–1916	A07	-2.09	yes	sII/–	1.5; 2	(ST/5)	1.0	0.5*	FDU (Na)
HE 0400–2030	A07	-1.73	no?	sII/–	1.5 ^c	(ST/6)	1.9	0.5*	-
HE 0441–0652	A07	-2.47	yes	sI/–	1.5 ^c	(ST/5)	(2.0)	0.5*	-
HE 0507–1653	A07	-1.38	yes	disc (sII/–)	1.5; 2	(ST/2)	0.7	0.5*	FDU
HE 1001–0243	M10	-2.88	yes	sI	1.3 – 2	\leq ST/30	1.3-2.1	0.0	-
HE 1005–1439	A07	-3.17	yes	sI/–	1.5 ^c	(ST/6)	(1.5)	0.5*	-
HE 1157–0518	A07	-2.34	yes	sII/–	1.5; 2	(ST/2 - ST/12)	\sim 1.0	0.5*	FDU (Na)
HE 1305+0132	Sch08	-1.92	yes	sI/–	1.5 ^c	(ST)	(1.2)	0.5*	-
HE 1319–1935	A07	-1.74	yes	sII/–	1.5; 2	(ST/2)	\sim 0.7	0.5*	FDU
HE 1410–0004	C06	-3.02	no?	sI/–	1.2;1.4	ST/24	0.2;1.5	0.5*	Na
HE 1419–1324	M10	-3.05	yes	sI	1.5;2	ST/2	\sim 2.0	0.5	Mg
HE 1429–0551	A07	-2.47	yes	sII/–	1.4 – 2	(ST/5)	1.0 - 1.5	0.5*	FDU
HE 1443+0113	C06	-2.07	yes	sI/–	1.5 ^c	ST/12	1.5	0.5*	FDU, (high Ba)
HE 1447+0102	A07	-2.47	yes	sII/–	1.5; 2	(ST/6)	\sim 0.5	0.5*	(FDU, Na)
HE 1523–1155	A07	-2.15	yes	sII/–	1.5; 2	(ST/2)	1.2	0.5*	FDU
HE 1528–0409	A07	-2.61	yes	sII/–	1.5; 2	(ST/2)	\sim 1.0	0.5*	FDU (Na, Mg)
HE 2221–0453	A07	-2.22	yes	sII/–	1.5 ^c	ST/2 - ST/24	\sim 0.9	0.5*	-
HE 2227–4044	B05	-2.32	no?	sI/–	1.2 – 2	ST/12 - ST/6	0.0 – 1.5	0.5*	-
HE 2228–0706	A07	-2.41	yes	sII/–	1.5; 2	ST/15	0.8	0.5*	FDU
HE 2240–0412	B05	-2.20	no	sI/–	1.2 – 2	ST/12 - ST/6	0.0 – 1.5	0.5*	-
HE 2330–0555	A07	-2.78	yes	sI/–	1.5 ^c	(ST/5)	(1.5)	0.5*	-
(SDSS 0817+26) ^b	A08	-3.16	no	(sI/–)	-	-	-	-	-
SDSS 0924+40	A08	-2.51	no	sII/–	1.35 - 2	ST/9 - ST/5	0.4 - 1.0	0.5*	Na Mg
SDSS 1707+58	A08	-2.52	no	sII/–	2	ST/18	0.0	0.5*	high s
SDSS 2047+00	A08	-2.05	no	sII/–	1.2; 1.3; 2	ST/12 - ST/5	0.0 - 1.4	0.5*	Na

^a We suggest caution in the interpretation of this star because no carbon and Eu have been detected.^b This star is excluded from CEMP-*s* stars because no clear excess of carbon and *s*-process elements have been detected.^c Solutions with AGB initial masses in the range $1.3 \leq M/M_{\odot} \leq 2$ are acceptable with a proper choice of the ^{13}C -pocket and dilution.

explanation of their *s*-enhancement is the pollution by stellar winds diffused by a more massive AGB companion during their thermally pulsing phase, which evolved to a white dwarf afterwards.

Particularly debated is the interpretation of those CEMP-*s* stars showing an enhancement in *r*-processes elements, incompatible with a pure *s*-process nucleosynthesis: among 45 stars with measured Eu, 23 are CEMP-*s/r*. Even if the astrophysical site of the *r*-process is not well known, it is associated to explosive conditions in massive stars, in environments separated by the *s*-process. Several hypotheses have been advanced to interpret the CEMP-*s/r* stars (Jonsell et al. 2006 and references therein). We suggest that a supernova exploded in the neighborhood of the molecular cloud from which the binary system was formed, polluting it with *r*-process elements. The more massive companion of the binary system evolved as AGB star, synthesising *s*-elements, which are detected in the envelope of the observed star af-

ter the mass transfer. The initial *r*-enhancement $[\text{r/Fe}]^{\text{ini}}$ is evaluated by using the residual method, $N_{\text{r}} = N_{\odot} - N_{\text{s}}$, where the *s*-process solar contributions are obtained as in Arlandini et al. (1999) (updated in Table 5). This is an approximation, adopted because of the poor knowledge of the primary *r*-process nucleosyntheses. We apply an initial *r*-process distribution $[\text{r/Fe}]^{\text{ini}}$ scaled to the Eu observed in the CEMP-*s/r* stars, to the isotopes between Ba and Bi. Indeed, observations of *r*-II stars sustain the hypothesis of the existence of multiple *r*-process components: a light-*r* component for $Z < 56$, a heavy-*r* component for $56 < Z < 83$ (see review by Sneden et al. 2008), as well as an additional third component invoked to explain a subsolar Th and U component (Roederer et al. 2009). For neutron capture elements below Ba, we did not apply any initial *r*-process enhancement. Spectroscopic observations in this region are extremely limited: only one star has Pd detected, CS 31062–050 (Johnson & Bolte 2004), and upper limit for Ag have

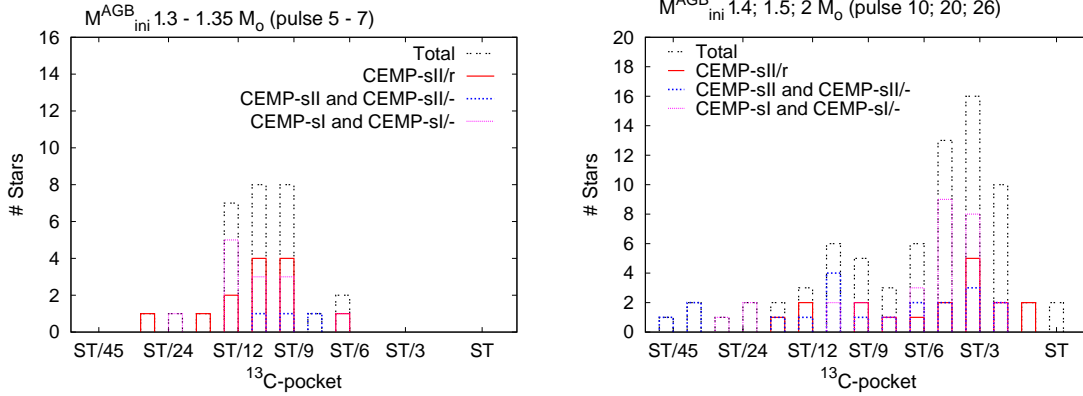


Figure 17. Number of stars versus the size of the ^{13}C -pocket, for AGB models with initial masses $M = 1.3$ and $1.35 M_{\odot}$ (left panel), $M = 1.4, 1.5$ and $2 M_{\odot}$ (right panel). We only consider stars from Table 10, following the classification indicated in column 5. All solutions listed in Table 10 are shown.

been obtained for CS 29497–030 (Ivans et al. 2005) and HE 0338–3945 (Jonsell et al. 2006).

In general, the $[\text{La}/\text{Eu}]$ ratio (where La and Eu are typical *s* and *r* elements) provides an important discriminator between CEMP-*s/r* and CEMP-*s* stars. For $[\text{Fe}/\text{H}] < -2$, an observed $[\text{La}/\text{Eu}] \sim 0.0 - 0.5$ dex (together with a high *s*-enhancement) can not be explained by a pure *s*-process contribution. The range of the initial *r*-enhancement adopted to interpret the observed Eu is a consequence of the inhomogeneity of the Galactic interstellar medium, and it is independent of AGB models. Starting from the spread observed in the $[\text{Eu}/\text{Fe}]$ ratios in field stars with $[\text{Fe}/\text{H}] \lesssim -2$, we hypothesise a similar range of initial *r*-process enrichments in order to interpret observations in CEMP-*s/r* stars ($[\text{r}/\text{Fe}]^{\text{ini}}$ up to 2.0). We classify as CEMP-*s/r* those stars that need an $[\text{r}/\text{Fe}]^{\text{ini}}$ from 1.0 to 2.0. Five stars show an observed $[\text{La}/\text{Eu}] \sim 0$, together with $[\text{La}/\text{Fe}] \sim 2$: CS 22898–027, CS 29497–030, HE 0338–3945, HE 1305+0007, HE 2148–1247. Their interpretation requires the highest *r*-enhancement $[\text{r}/\text{Fe}]^{\text{ini}} = 2.0$. Note that stars with $[\text{r}/\text{Fe}]^{\text{ini}} = 1.0$ lie at the limit between normal CEMP-*s* and CEMP-*s/r* (CS 22887–048, HD 209621, HE 0143–0441, SDSS J1349–0229).

The initial *r*-process enhancements do not affect in any way the nucleosynthesis of the *s*-process. However, we have to consider that also the isotopes mainly produced by the *s*-process receive a partial *r* contribution for the hs elements, e.g. $\sim 30\%$ of solar La, $\sim 40\%$ of solar Nd, and $\sim 70\%$ of solar Sm. In case of high initial *r*-enhancements as $[\text{r}/\text{Fe}]^{\text{ini}} = 2.0$, this implies an increase of the maximum $[\text{hs}/\text{ls}]$ up to 0.3 dex. In this regard, we discuss the behaviour of the two *s*-process indicators, $[\text{hs}/\text{ls}]$ and $[\text{Pb}/\text{hs}]$ versus metallicity. On average, the $[\text{hs}/\text{ls}]$ observed in CEMP-*s/r* stars shows higher values than that in CEMP-*s*. From a general analysis, $[\text{hs}/\text{ls}]$ in CEMP-*s/r* stars seems to be better reproduced by models with very high initial *r*-enhancement. However, a detailed analysis of individual stars is needed (Paper III). No particular distinction between CEMP-*s/r* and CEMP-*s* appears for $[\text{Pb}/\text{hs}]$.

We have focused our attention on three stars taken as example to explain the method adopted to interpret the observations. All the elements are considered, with particular

attention to C, N, Na, Mg, ls, hs, Pb, as well as Eu, which is fundamental to evaluate possible *r*-process contributions. The $[\text{hs}/\text{ls}]$ and $[\text{Pb}/\text{hs}]$ ratios provide informations about the ^{13}C -pocket, while the first assessment of the dilution factor is based on the observed $[\text{hs}/\text{Fe}]$. The occurrence of the FDU provides the first constraint on the AGB models: during the FDU subgiants or giants undergo a large mixing involving about 80% of the mass of the star, which dilutes the C and *s*-rich material previously transferred from the AGB companion, implying solutions with $\text{dil} \gtrsim 1$ dex. The choice of the AGB models reproducing the observations are based on the analysis of single species including their uncertainties and the number of detected lines, in particular within the three *s*-peaks.

We have presented a general description of the sample, and the main results obtained by this study. However, discussions of individual stars are necessary to underline possible discrepancies between AGB models and observations and to suggest possible points of debate for unsolved problems. This will be the topic of Paper III.

To simplify the analysis we divided the stars in different classes, according to the observed abundance pattern of the *s*-elements and of Eu. Stars with $[\text{hs}/\text{Fe}] \gtrsim 1.5$ are called CEMP-sII (or CEMP-sII/*r* if they show also an *r*-enhancement), while stars with $[\text{hs}/\text{Fe}] < 1.5$ are CEMP-sI (or CEMP-sI/*r*). The level of *s*-enhancement, ‘II’ or ‘I’, depends on different factors: the *s*-process nucleosynthesis of the primary AGB, the efficiency of mass transfer by stellar winds, the distance between the two stars, and the mixing of the transferred material with the envelope of the observed star.

The range covered by the observed $[\text{hs}/\text{ls}]$ and $[\text{Pb}/\text{hs}]$ requires the assumption of different ^{13}C -pocket efficiencies. This may be related to the uncertainty affecting the formation of the ^{13}C -pocket, the hydrogen profile and, then, the amount of ^{13}C and ^{14}N in the pocket. A clear answer to the properties of the mixing processes at radiative/convective interfaces during TDU episodes, which lead to the formation of the ^{13}C -pocket, has not been reached yet. Moreover, models including rotation, gravity waves or magnetic fields, may influence the formation of the ^{13}C -

pocket (Langer et al. 1999; Herwig et al. 2003; Siess et al. 2004; Denissenkov & Tout 2003). This translates into different *s*-process distributions. Further investigations are desirable.

AGB models with $M_{\text{ini}}^{\text{AGB}} = 1.4 - 2 M_{\odot}$ an asymptotic trend beyond the 10th TDU (Paper I). Consequently, negligible differences are observed in the *s*-process distribution at the last TDUs when the envelope is affected by efficient stellar winds. Instead, $M_{\text{ini}}^{\text{AGB}} = 1.3 - 1.35 M_{\odot}$ models undergo 5 to 7 thermal pulses with TDU, without reaching an asymptotic trend. Deeper investigations are in project for $M_{\text{ini}}^{\text{AGB}} \sim 1.3 M_{\odot}$ models, which provide theoretical interpretations for several CEMP-*s* and CEMP-*s/r* stars.

In general, AGB models with different initial masses in the range $1.3 \leq M/M_{\odot} \leq 2$ and a proper choice of ^{13}C -pocket may equally interpret the *s*-process observations. On average, possible fits with $M_{\text{ini}}^{\text{AGB}} \sim 1.3 - 1.35 M_{\odot}$ models require ^{13}C -pockets close to case ST/12, while case ST/4 are achieved for $M_{\text{ini}}^{\text{AGB}} = 1.4 - 2 M_{\odot}$ models. A restricted number of stars need *s*-process efficiencies below $\sim \text{ST}/24$ (CS 22942–019, CS 31062–012, HE 0336+0113, V Ari, HE 1135+0139, HD 189711, as well as CS 22891–171, CS 22956–28). The ^{13}C -pocket spread observed seems larger than that suggested by Bončić Marinović et al. (2007) in their population synthesis study. A detailed investigation of individual stars will be presented in Paper III.

[Na/Fe] may provide indications on the AGB initial mass. In CEMP-*s*II or CEMP-*s*II/*r* before the FDU, an observed ratio $[\text{Na}/\text{Fe}] \leq 0.5$ is only interpreted by $M_{\text{ini}}^{\text{AGB}} \sim 1.3 M_{\odot}$ models, because a large *s*-enhancement together with a low [Na/Fe] may be reached only after a limited number of thermal pulses. Nine stars among the sample show a high Na abundances ($[\text{Na}/\text{Fe}] \geq 1$): CS 22942–019 (Preston & Sneden 2001), CS 29497–34, CS 29528–028 and CS 30301–015 (Aoki et al. 2007, 2008), CS 30322–023 (Masseron et al. 2006; Aoki et al. 2007), LP 625–44 (Aoki et al. 2002a), SDSS J1349–0229 (Behara et al. 2010), SDSS 0924+40, and SDSS 1707+58 (Aoki et al. 2008). The maximum values observed are for CS 29528–028 with $[\text{Na}/\text{Fe}] = 2.33$ and SDSS 1707+58 with $[\text{Na}/\text{Fe}] = 2.71$. For these stars, $M_{\text{ini}}^{\text{AGB}} \sim 1.5 M_{\odot}$ models are adopted.

Apart from the information on the *s*-process efficiency, the ls peak may also represent an indicator for the AGB initial mass. In particular, in CEMP-*s*II stars with low Sr-Y-Zr (with respect to [hs/Fe]), AGB models with low initial mass are adopted ($M_{\text{ini}}^{\text{AGB}} \leq 1.4 M_{\odot}$, e.g., CS 22183–015, CS 22880–074, CS 22898–027, CS 31062–012, HE 0338–3945, HE 2232–0603).

Despite the uncertainty of C and N in very metal-poor stars (due to strong molecular bands, 3D model atmospheres and non-LTE corrections), the observed [C/Fe] and [N/Fe] values and the low $^{12}\text{C}/^{13}\text{C}$ ratio in most stars indicate that the CBP is needed during the AGB phase. However, its efficiency is difficult to estimate because several physical processes may concur in this mixing (e.g., magnetic fields, rotation, thermohaline). We are planning a detailed study about the discrepancy between observed and predicted carbon in a forthcoming paper.

Several mixing processes may occur in the envelope of the star during the main-sequence phase (e.g., thermohaline, gravitational settlings, radiative levitation). Their efficiency is different from star to star, depending on its age, initial

metallicity, initial mass, on the amount of material accreted from the AGB companion, and the time at which this material was accreted. These additional effects have not been included in the present study, but the comparison between models and observations may provide important clues for these aspects.

ACKNOWLEDGMENTS

We are deeply grateful to W. Aoki, T. C. Beers, J. J. Cowan, I. I. Ivans, C. Pereira, G. W. Preston, I. U. Roederer, C. Sneden, I. B. Thompson, S. Van Eck, for enlightening discussions about CEMP-*s* and CEMP-*s/r* stars. This work has been supported by MIUR and by KIT (Karlsruhe Institute of Technology, Karlsruhe).

REFERENCES

- Abia C., Busso M., Gallino R., Domínguez I., Straniero O., Isern J., 2001, *ApJ*, 559, 1117
- Abia C. et al., 2002, *ApJ*, 579, 817
- Allen D. M., Barbuy B., 2006, *A&A*, 454, 895
- Allen D. M., Ryan S. G., Rossi S., Tsangarides S. A., 2010, *Proceedings IAU Symposium N. 265*, 118
- Anders E., Grevesse N., 1989, *GCA*, 53, 197
- Andrievsky S. M., Spite M., Korotin S. A., Spite F., Bonifacio P., Cayrel R., Hill V., François P., 2007, *A&A*, 464, 1081
- Andrievsky S. M., Spite M., Korotin S. A., Spite F., Bonifacio P., Cayrel R., Hill V., François P., 2008, *A&A*, 481, 481
- Andrievsky S. M., Spite M., Korotin S. A., Spite F., François P., Bonifacio P., Cayrel R., Hill V., 2009, *A&A*, 494, 1083
- Andrievsky S. M., Spite M., Korotin S. A., Spite F., Bonifacio P., Cayrel R., François P., Hill V., 2010, *A&A*, 509, 88
- Andrievsky S. M., Spite F., Korotin S. A., François P., Spite M., Bonifacio P., Cayrel R., Hill V., 2011, *A&A*, 530, 105
- Angelou G. C., Church R. P., Stancliffe R. J., Lattanzio J. C., Smith G. H., 2011, *ApJ*, 728, 79
- Angulo C. et al., 1999, *Nucl. Phys. A*, 656, 3
- Aoki W., Norris J. E., Ryan S. G., Beers T. C., Ando H., 2000, *ApJ*, 536, 97
- Aoki W. et al., 2001, *ApJ*, 561, 346
- Aoki W. et al., 2002a, *PASJ*, 54, 427
- Aoki W., Norris J. E., Ryan S. G., Beers T. C., Ando H., 2002b, *ApJ*, 576, L141
- Aoki W., Norris J. E., Ryan S. G., Beers T. C., Ando H., 2002c, *PASJ*, 54, 933
- Aoki W., Ryan S. G., Norris J. E., Beers T. C., Ando H., Tsangarides S., 2002d, *ApJ*, 580, 1149
- Aoki W. et al., 2003, *ApJ*, 592, 67
- Aoki W., Norris J. E., Ryan S. G., Beers T. C., Christlieb N., Tsangarides S., Ando H., 2004, *ApJ*, 608, 971
- Aoki W. et al., 2005, *ApJ*, 632, 611
- Aoki W., Bisterzo S., Gallino R., Beers T. C., Norris J. E., Ryan S. G., Tsangarides S., 2006, *ApJ*, 650, 127

- Aoki W., Beers T., Christlieb N., Norris J. E., Ryan S. G., Tsangarides S., 2007, *ApJ*, 655, 492
- Aoki W., Honda S., 2008, *PASJ*, 60, L7
- Aoki W. et al., 2008, *ApJ*, 678, 1351
- Aoki W., Beers T. C., Honda S., Carollo D., 2010, *ApJ*, 723, L201
- Arlandini C., Käppeler F., Wisshak K., Gallino R., Lugaro M., Busso M., Straniero O., 1999, *ApJ*, 525, 886
- Asplund M., 2004, *Mem. Soc. Astron. It.*, 75, 300
- Asplund M., 2005, *ARA&A*, 43, 481
- Barbuy B., Cayrel R., Spite M., Beers T. C., Spite F., Nordstroem B., Nissen P. E., 1997, *A&A*, 317, 63
- Barbuy B., Spite M., Spite F., Hill V., Cayrel R., Plez B., Petitjean, P., 2005, *A&A*, 429, 1031
- Barklem P. S. et al., 2005, *A&A*, 439, 129
- Baumüller D., Gehren T., 1997, *A&A*, 325, 1088
- Baumüller D., Butler K., Gehren T., 1998, *A&A*, 338, 637
- Beers T. C., Preston G. W., Shectman S. A., 1992, *AJ*, 103, 1987
- Beers T. C., Christlieb N., 2005, *ARA&A*, 43, 531
- Beers T. C., Sivarani T., Marsteller B., Lee Y., Rossi S., Plez B., 2007a, *AJ*, 133, 1193
- Beers T. C., 2007b, *AIP Conf. Proc.*, 1057, 59
- Behara N. T., Bonifacio P., Ludwig H.-G., Sbordone L., González Hernández J. I., Caffau E., 2010, *A&A*, 513, A72
- Bisterzo S., Gallino R., Pignatari M., Pompeia L., Cunha K., Smith V., 2004, *Mem. Soc. Astron. It.*, 75, 741
- Bisterzo S., Gallino R., Straniero O., Aoki W., 2009, *PASA*, 26, 314
- Bisterzo, S., Gallino, R., Straniero, O., Cristallo, S., 2010, *MNRAS*, 404, 1529 (Paper I)
- Boothroyd A. I., Sackmann I.-J., 1988, *ApJ*, 328, 653
- Bončić Marinović A., Izzard R. G., Lugaro M., Pols O. R., 2007, *A&A* 469, 1013
- Burbidge E. M., Burbidge G. R., Fowler W. A., Hoyle F., 1957, *Rev. Mod. Phys.*, 29, 4
- Busso M., Lambert D. L., Beglio L., Gallino R., Raiteri C. M., Smith V. V., 1995, *ApJ*, 446, 775
- Busso M., Gallino R., Wasserburg G. J., 1999, *ARA&A*, 37, 239
- Busso M., Gallino R., Lambert D. L., Travaglio C., Smith V.V., 2001, *ApJ*, 557, 802
- Busso M., Palmerini S., Maiorca E., Cristallo S., Straniero O., Abia C., Gallino R., La Cognata M., 2010, *ApJ*, 717, L47
- Caffau E., Maiorca E., Bonifacio P., Faraggiana R., Steffen M., Ludwig H.-G., Kamp I., Busso M., 2009, *A&A*, 498, 877
- Campbell S. W., Lattanzio J. C., 2008, *A&A*, 490, 769
- Cantiello M., Langer N., 2010, *A&A*, 521, 9
- Cayrel R. et al., 2004, *A&A*, 416, 1117
- Carollo D. et al., 2007, *Nature*, 450, 1020
- Carollo D. et al., 2010, *ApJ*, 712, 692
- Carollo D., Beers T. C., Bovy J., Sivarani T., Norris J. E., Freeman K. C., Aoki W., Lee Y. S., 2011, *ApJ*, submitted (arXiv:1103.3067)
- Cassisi S., Castellani M., Caputo F., Castellani V., 2004, *A&A*, 426, 641
- Charbonnel C., Zahn J.-P., 2007, *A&A*, 467, L15
- Charbonnel C., Lagarde N., 2010, *A&A*, 522, 10
- Chieffi A., Straniero O., 1989, *ApJS*, 71, 47
- Christlieb N., 2003, *Rev. Mod. Astron.*, 16, 191
- Christlieb N. et al., 2004, *A&A*, 428, 1027
- Cohen J. G., Christlieb N., Qian Y. Z., Wasserburg G. J., 2003, *ApJ*, 588, 1082
- Cohen J. G. et al. 2004, *ApJ*, 612, 1107
- Cohen J. G. et al., 2005, *ApJ*, 633, L109
- Cohen J. G. et al., 2006, *AJ*, 132, 137
- Collet R., Asplund M., Trampedach R., 2007, *A&A*, 469, 687
- Cowan J. J. et al., 2002, *ApJ*, 572, 861
- Cristallo S., Straniero O., Lederer M. T., Aringer B., 2007, *ApJ*, 667, 489
- Cristallo S., Piersanti L., Straniero O., Gallino R., Domínguez I., Käppeler F., 2009, *PASA*, 26, 139
- Denissenkov P. A., Tout C. A., 2003, *MNRAS*, 340, 722
- Denissenkov P. A., Pinsonneault M., 2008, *ApJ*, 679, 1541
- Denissenkov P. A., Pinsonneault M., MacGregor K. B., 2009, *ApJ*, 696, 1823
- Denissenkov P. A., 2010, *ApJ*, 723, 563
- Depagne E. et al., 2002, *A&A*, 390, 187
- Dillmann I., Heil M., Käppeler F., Plag R., Rauscher T., Thielemann F.-K., 2006, *AIP Conf. Proc.*, 819, 123
- Domínguez I., Abia C., Straniero O., Cristallo S., Pavlenko Ya. V., 2004, *A&A*, 422, 1045
- Drake M. A., Pereira C. B., 2008, *ApJ*, 135, 1070
- Eggleton P. P., Dearborn D. S. P., Lattanzio J. C., 2006, *Sci.*, 314, 1580
- Farouqi K., Kratz K.-L., Pfeiffer B., Rauscher T., Thielemann F.-K., Truran J., 2010, *ApJ*, 712, 1359.
- François P. et al., 2007, *A&A*, 476, 935
- Frebel A., Christlieb N., Norris J. E., Thom C., Beers T. C., Rhee J., 2007, *ApJ*, 660, 117
- Gallino R., Arlandini C., Busso M., Lugaro M., Travaglio C., Straniero O., Chieffi A., Limongi M., 1998, *ApJ*, 497, 388
- Gallino R., Delaude D., Husti L., Cristallo S., Straniero O., Ryan S., 2005, *Nucl. Phys. A*, 758, 485
- Gallino R., Bisterzo S., Husti L., Käppeler F., Cristallo S., Straniero O., 2006, *Nuclei in the Cosmos - IX, Proceedings of Science (PoS)*, 100
- Gallino R., Bisterzo S., Husti L., 2008, *AIP Conf. Proc.*, 1001, 123
- Gehren T., Shi J. R., Zhang H. W., Zhao G., Korn A. J., 2006, *A&A*, 451, 1065
- Goriely S., Mowlavi N., 2000, *A&A*, 362, 599
- Goriely S., Siess L., 2004, *A&A*, 421, 25
- Goswami A., 2005, *MNRAS*, 359, 531
- Goswami A., Aoki W., Beers T. C., Christlieb N., Norris J. E., Ryan S. G., Tsangarides S., 2006, *MNRAS*, 372, 343
- Goswami A., Aoki W., 2010, *MNRAS*, 404, 253
- Grevesse N., Asplund M., Sauval A. J., 2007, *Sp. Sci. Rev.*, 130, 105
- Hayek W. et al., 2009, *A&A*, 504, 511
- Herwig F., Langer N., Lugaro M., 2003, *ApJ*, 593, 1056
- Herwig F., 2004, *ApJS*, 155, 651
- Hill V. et al., 2000, *A&A*, 353, 557
- Hill V. et al., 2002, *A&A*, 387, 560
- Hollowell D., Iben I. I., Fujimoto M. Y., 1990, *ApJ*, 351, 245
- Honda S., Aoki W., Kajino T., Ando H., Beers T. C., Izu-miura H., Sadakane K., Takada-Hidai M., 2004, *ApJ*, 607, 474

- Husti L., Gallino R., Bisterzo S., Cristallo S., Straniero O., 2007, *Mem. Soc. Astron. It.*, 78, 523
- Husti L., Gallino R., Bisterzo S., Straniero O., Cristallo S., 2009, *PASA*, 26, 176
- Iben I. Jr., 1973, *ApJ*, 185, 209
- Iben I. Jr., Renzini A., 1983, *ARA&A*, 21, 271
- Ivans I. I., Sneden C., Gallino R., Cowan J. J., Preston G. W., 2005, *ApJ*, 627, 145
- Ivans I. I., Simmerer J., Sneden C., Lawler J. E., Cowan J. J., Gallino R., Bisterzo S., 2006, *ApJ*, 645, 613
- Ishigaki M., Chiba M., 2010, *PASJ*, 62, 143
- Ishimaru I., Wanajo S., 1999, *ApJ*, 511, L33
- Israelian G., Rebolo R., Garcia Lopez R. J., Bonifacio P., Molaro P., Basri G., Shchukina N., 2001, *ApJ*, 551, 833
- Iwamoto N., Kajino T., Mathews G. J., Fujimoto M. Y., Aoki W., 2004, *ApJ*, 602, 377
- Izzard R. G., Glebbeek E., Stancliffe R. J., Pols O. R., 2009, *A&A*, 508, 1359
- Jonsell K., Barklem P. S., Gustafsson B., Christlieb N., Hill V., Beers T. C., Holmberg J., 2006, *A&A*, 451, 651
- Jonsell K., Edvardsson B., Gustafsson B., Magain P., Nissen P. E., Asplund M., 2005, *A&A*, 440, 321
- Johnson, J. A., & Bolte, M. 2001, *ApJ*, 554, 888
- Johnson J. A., Bolte M., 2002, *ApJ*, 579, 87
- Johnson J. A., Bolte M., 2004, *ApJ*, 605, 462
- Johnson J. A., Herwig F., Beers T. C., Christlieb N., 2007, *ApJ*, 658, 1203
- Jorissen A., Zacs L., Uldry S., Lindgren H., Musaev F. A., 2007, *A&A*, 441, 1135
- Junqueira S., Pereira C. B., 2001, *A&A*, 122, 360
- Käppeler F., Beer H., Wisshak K., Clayton D. D., Macklin R. L., Ward R. A., 1982, *ApJ*, 257, 821
- Käppeler F., Beer F. H., Wisshak K., 1989, *Rep. Prog. Phys.*, 52, 945.
- Käppeler F., Gallino R., Bisterzo S., Aoki W., 2011, *Rev. Mod. Phys.*, 83, 157
- Karakas A., Lattanzio J., 2003, *PASA*, 20, 279
- Kim Y.-C., Demarque P., Sukyoung K. Y., Alexander D. R., 2002, *ApJS*, 143, 499
- Kipper T., Jørgensen U. G., 1994, *A&A*, 290, 148
- Kratz K.-L., Farouqi K., Pfeiffer B., Truran J. W., Sneden C., Cowan J. J., 2007, *ApJ*, 662, 39
- Lai D. K., Bolte M., Johnson J. A., Lucatello S., 2004, *AJ*, 128, 2402
- Lai D. K., Johnson J. A., Bolte M., Lucatello S., 2007, *ApJ*, 667, 1185
- Lai D. K., Bolte M., Johnson J. A., Lucatello S., Heger A., Woosley S. E., 2008, *ApJ*, 681, 1524
- Langer N., Heger A., Wellstein S., Herwig F., 1999, *A&A*, 346, L37
- Lau H. H. B., Stancliffe R. J., Tout C. A., 2009, *MNRAS*, 396, 1046
- Lee Y. S. et al., 2008a, *AJ*, 136, 2022
- Lee Y. S. et al., 2008b, *AJ*, 136, 2050
- Lodders K., 2003, *ApJ*, 591, 1220
- Lodders K., Palme H., Gail H.-P., 2009, *Landolt-Börnstein - Group VI Astronomy and Astrophysics Numerical Data and Functional Relationships in Science and Technology*, Edited by J.E. Trümper, 4B: Solar System, 4.4
- Lucatello S., Gratton R., Cohen J. G., Beers T. C., Christlieb N., Carretta E., Ramírez S., 2003, *ApJ*, 125, 875
- Lucatello S., 2004, Ph.D. Thesis, “C-enhanced metal poor stars”, Università di Padova, Italy
- Lucatello S., Tsangarides S., Beers T. C., Carretta E., Gratton R. G., Ryan S. G., 2005, *ApJ*, 625, 825
- Lucatello S., Masseron T., Johnson J. A., 2009, *PASA*, 26, 303
- Mashonkina L., Gehren T., Travaglio C., Borkova T., 2003, *A&A* 397, 275
- Mashonkina L. et al., 2008, *A&A*, 478, 529
- Mashonkina L., Christlieb N., Barklem P. S., Hill V., Beers T. C., Velichko A., 2010, *A&A*, 516, 46
- Masseron T. et al., 2006, *A&A*, 455, 1059
- Masseron T., Johnson J. A., Plez B., Van Eck S., Primas F., Goriely S., Jorissen A., 2010, *A&A*, 509, A93
- McClure R. D., Woodsworth A. W., 1990, *ApJ*, 352, 709
- McWilliam A., Preston G. W., Sneden C., Searle L., 1995, *AJ*, 109, 2527
- Mishenina T., Kovtyukh V., 2001, *A&A*, 370, 951.
- Montes F. et al., 2007, *ApJ*, 671, 1685
- Mowlavi N., 1999, *A&A*, 350, 73
- Nollett K. M., Busso M., Wasserburg G. J., 2003, *ApJ*, 582, 1036
- Norris J. E., Ryan .G., Beers T. C., 1997, *ApJ*, 488, 350
- Norris J. E., Ryan .G., Beers T. C., 2001, *ApJ*, 561, 1034
- Pereira C. B., Drake N. A., 2009, *A&A*, 496, 791
- Plez B. et al., 2004, *A&A* 428, L9
- Preston G. W., Sneden C., 2000, *AJ*, 120, 1014
- Preston G. W., Sneden C., 2001, *AJ*, 122, 1545
- Preston G. W., 2009, *PASA*, 26, 372
- Qian Y.-Z., Wasserburg G., 2007, *Phys. Rep.*, 442, 237.
- Qian Y.-Z., Wasserburg G. J., 2008, *ApJ*, 687, 272
- Ramsey L. W. et al., 1998, *Proc. SPIE*, 3352, 34
- Richard O., Michaud G., Richer J., Turcotte S., Turck-Chièze S., Vandenberg D. A., 2002, *ApJ*, 568, 979
- Roederer I. U. et al., 2008, *ApJ*, 679, 1549
- Roederer I. U. et al., 2008a, *ApJ*, 675, 723
- Roederer I. U., Kratz K.-L., Frebel A., Norbert C., Pfeiffer B., Cowan J. J., Sneden C., 2009, *ApJ*, 698, 1963
- Roederer, I. U., Sneden, C., Thompson, I. B., Preston, G. W., Shectman, S. A., 2010a, *ApJ*, 7119, 573
- Roederer I. U., Sneden C., Lawler J. E., Cowan J. J., 2010b, *ApJ*, 714, L123
- Roederer I. U., Cowan J. J., Karakas A. I., Kratz K.-L., Lugaro M., Simmerer J., Farouqi K., Sneden C., 2010c, *ApJ*, 724, 975
- Romano D., Matteucci F., 2007, *MNRAS*, 378, L59
- Rossi S., Beers T. C., Sneden C., Seavastyanenko T., Rhee J., Marsteller B., 2005, *AJ*, 130, 2804
- Schatz H., Toenjes R., Pfeiffer B., Beers T. C., Cowan J. J., Hill V., Kratz K.-L., 2002, *ApJ*, 579, 626
- Schuler S. C., Cunha K., Smith V. V., Sivarani T., Beers T. C., Sun Lee Y., 2007, *AJ*, 667, L81
- Schuler S. C., Margheim S. J., Sivarani T., Asplund M., Smith V. V., Cunha K., Beers T. C., 2008, *AJ*, 136, 2244
- Serminato A., Gallino R., Travaglio C., Bisterzo S., Straniero O., *PASA*, 26, 153
- Short C. I., Hauschildt P. H., 2006, *ApJ*, 641, 494
- Siess L., Goriely S., Langer N., 2004, *A&A*, 415, 1089
- Simmerer J., Sneden C., Cowan J. J., Collier J., Woolf V. M., Lawler J. E., 2004, *ApJ*, 617, 1091.
- Sivarani T. et al., 2004, *A&A*, 413, 1073
- Sivarani T. et al., 2006, *A&A*, 459, 125

- Sneden C., Preston G. W., McWilliam A., Searle L., 1994, *ApJ*, 431, L27
- Sneden C. et al. 2003a, *ApJ*, 591, 936
- Sneden C., Preston G. W., Cowan J. J., 2003b, *ApJ*, 592, 504
- Sneden C., Cowan J. J., Gallino R., 2008, *ARA&A*, 46, 241
- Stancliffe R. J., Glebbeek E., Izzard R. G., Pols O. R., 2007, *A&A*, 464, 57
- Stancliffe R. J., Glebbeek E., 2008, *MNRAS*, 389, 1828
- Stancliffe R. J., 2010, *MNRAS*, 403, 505
- Straniero O., Gallino R., Busso M., Chieffi A., Raiteri C. M., Limongi M., Salaris M., 1995, *ApJ*, 440, 85
- Straniero O., Domínguez I., Cristallo S., Gallino R., 2003, *PASA*, 20, 389
- Straniero O., Gallino R., Cristallo S., 2006, *Nucl. Phys. A*, 777, 311
- Straniero O. et al., 2010, *ASP Conf. Ser.*, in press
- Suda T. et al., 2008, *PASJ*, 60, 1159
- Suda T., Fujimoto M. Y., 2010, *MNRAS*, 405, 177
- Suda T., Yamada S., Katsuta Y., Komiya Y., Ishizuka C., Aoki W., Fujimoto M. Y., 2011, *MNRAS*, 412, 843
- Sugimoto D., 1971, *Progress of Theoretical Physics*, 45, 761
- Takeda Y., Zhao G., Takada-Hidai M., Chen Y.-Q., Saito Y.-J., Zhang H.-W., 2003, *Chinese J. Astron. Astrophys.*, 3, 316
- Thompson I. B. et al., 2008, *ApJ*, 677, 556
- Travaglio C., Galli D., Gallino R., Busso M., Ferrini F., Straniero O., 1999, *ApJ*, 521, 691
- Travaglio C., Galli D., Burkert A., 2001b, *ApJ*, 547, 217
- Travaglio C., Gallino R., Arnone E., Cowan J., Jordan F., Sneden C., 2004, *ApJ*, 601, 684
- Tsangarides S. A., 2005, Ph.D. Thesis, Open University (United Kingdom), DAI-C 66/04
- Van Eck S., Goriely S., Jorissen A., Plez B., 2003, *A&A*, 404, 291
- Vanhala H. A. T., Cameron A. G. W., 1998, *ApJ*, 508, 291
- Vauclair S., 2004, *ApJ*, 605, 874
- Ventura P., D'Antona F., 2005, *A&A*, 431, 279
- Wanajo S., Ishimaru Y., 2006, *Nucl. Phys. A*, 777, 676
- Wasserburg G. J., Boothroyd A. I., Sackmann I.-J., 1995, *ApJ*, 447, L37
- Wasserburg G. J., Busso M., Gallino R., Nollett K. M., 2006, *Nucl. Phys. A*, 777, 5
- Westin J., Sneden C., Gustafsson B., Cowan J. J., 2000, *ApJ*, 530, 783
- Winckler N., Dababneh S., Heil M., Käppeler F., Gallino R., Pignatari M., 2006, *ApJ*, 647, 685
- York D. G. et al., 2000, *AJ*, 120, 1579
- Zhang L., Ishigaki M., Aoki W., Zhao G., Chiba M., 2009, *ApJ*, 706, 1095
- Zijlstra A. A., 2004, *MNRAS*, 348, L23
- Zinner E., Nittler L. R., Gallino R., Karakas A. I., Lugaro M., Straniero O., Lattanzio J. C., 2006, *ApJ*, 650, 350

APPENDIX A. SEE SUPPLEMENTARY MATERIAL

This paper has been typeset from a \LaTeX file prepared by the author.